# SAR Image Statistical Modeling Part I: Single-Pixel Statistical Models



| | |
|---|---|
| Journal: | *IEEE Geoscience and Remote Sensing Magazine* |
| Manuscript ID | GRSM-2020-00007.R1 |
| Manuscript Type: | Review Paper |
| Date Submitted by the Author: | 24-Apr-2020 |
| Complete List of Authors: | Yue, Dong-Xiao; Fudan University, Key Lab for Information Science of Electromagnetic Waves (MoE)<br>Xu, Feng; Fudan University, Key Lab for Information Science of Electromagnetic Waves (MoE)<br>Frery, Alejandro; Universidade Federal de Alagoas, Laboratório de Computação Científica e Análise Numérica<br>Jin, Yaqiu; Fudan University, Key Lab of EMW Information |
| Keywords: | Synthetic aperture radar, Statistical distributions, Image texture |
| | |

# Responses to Reviewers' Comments

We appreciate very much the constructive comments from the reviewers, which have had helped us to revise and improve the paper greatly. One-to-one responses and corresponding revisions are given below.

## Associate Editor:

Comments to the Author:
Both reviews were quite positive about the quality and importance of this paper. However, they did recommend some changes, which could require significant re-writing. Therefore, I recommend a "major revision". Please revise addressing the comments from the reviewers, including the addition of more references, particularly more recent ones, and consider inclusion of new topics such as Quantum Synthetic Aperture Radars. Reviewer 2 suggested some re-organization of the paper.

A: Thanks for the comments on this work. Following the reviewers' suggestions, more references have been supplemented including recent ones and technologies such as polarimetric SAR, interferometric SAR, bistatic SAR, constellation SAR and quantum radar. For details, please find the corresponding answers A1 and A9 to reviewer 1, A6 to reviewer 2. Also, this paper has been reorganized and please refer to the A2 to reviewer 2 for details.

## Reviewer 1:

Comments to the Author
This paper reviews the major development of SAR image statistical modeling since the beginning, including more than 20 statistical distributions of 8 statistical models, and gives their derivations and expressions, which can be used as a basic reference for statistical modeling of SAR images.

Q1. Introduction: Please refer also to Quantum synthetic Aperture radars and potential application of quantum entanglement.

A1. We thank the reviewer for this suggestion which enriches the content of the paper by adding the latest Quantum radar technology. As the latest advanced technology, the introduction of quantum radar is supplemented in Section 5.2, Page 23, Left-column, Lines 17-26, and Right-column, Lines 7-38:

*"…The rapid development of radar system technologies lead to the emergence of new types of SAR images, including polarimetric SAR (PolSAR) [2], interferometric SAR [107], bistatic and multistatic constellation SAR [108-112] and quantum radar [113]. For example, the advanced non-interrupted synchronization scheme for spaceborne bistatic SAR in [108] demonstrates superiority over techniques of existing systems such as TanDEM-X and is promising in the future spaceborne bistatic and multistatic systems. Another example is quantum radar which may greatly enhance receiver sensitivity. These new types of SAR data have brought higher requirements and more opportunities to the task of image interpretation.*

*…*

*(5) Quantum technology [135] may bring change to both radar systems and image interpretation.*

*On the one hand, the development of quantum device in quantum radar [113] is based on the mechanisms of quantum physics. Quantum radar has been proved to have the potential to break the limit of conventional radar detection performance such as system sensitivity [136] and target detection capability [137]. Several quantum radar concepts such as quantum radar equation, quantum radar cross section (QRCS) and quantum detection theory have been* *researched recently [137-139]. Quantum entanglement is a quantum phenomenon where multiple particles are linked together in a way such that the measurement of one particle's quantum state determines the possible quantum states of the other particles [113]. It leads to correlations between observable physical properties of the systems [113, 136]. It has been shown the resolution of quantum radar systems using entangled photons is higher then that of non-entangled quantum radar [140]. As the further development of quantum radar theory and core techniques, the corresponding statistical modeling should be a studied.*

*On the other hand, the principles of quantum computing [135], such as uncertainty, superposition, interference and implicit parallelism, make it have better diversity and better trade-off between the exploration and the exploitation than common evolutionary algorithms [141]. These principles have inspired many evolutionary computing algorithms to solve the optimization problem in SAR image segmentation, such as quantum clonal selection clustering (QCSC) algorithm [142], quantum immune fast spectral clustering (QIFSC) approach [143] and quantum-inspired multiobjective evolutionary clustering (QMEC) algorithm [141]. These research results demonstrate the application value of quantum computing in the field of SAR image modeling and data processing."*

Q2. This comment refers to both Figure 6 and Figure 7, which are a bit complicate to understand. For example explain better what the small box linked by the letter "A" stands for.

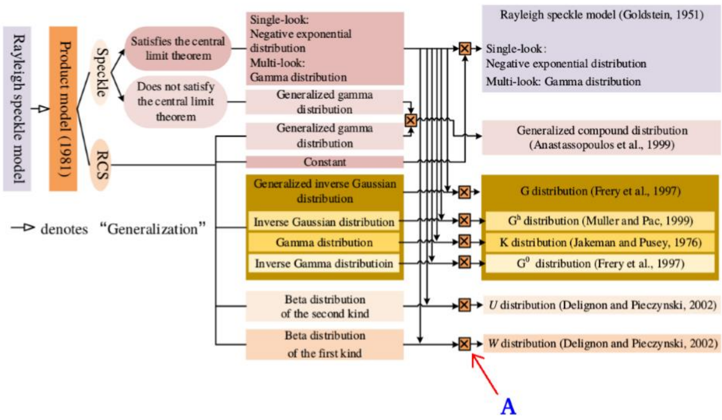


Figure6

A2. Thanks for pointing out this issue and it helps to improve the presentation of the figures. Following the reviewer's suggestion, the "Yellow shading box with embedded product operator" in Figure 6 linked by the letter "A" denotes the "Product model". It has two inputs i.e. the statistical distribution of speckle and RCS, and outputs the distribution of SAR image intensity. Now this is explained in Page 5 Right-column Line 1-4:

*"The "Yellow shading box with embedded product operator" in Figure 6 denotes the "Product model" which has two inputs, i.e. the statistical distribution of speckle and RCS, and outputs the distribution of SAR image intensity."*

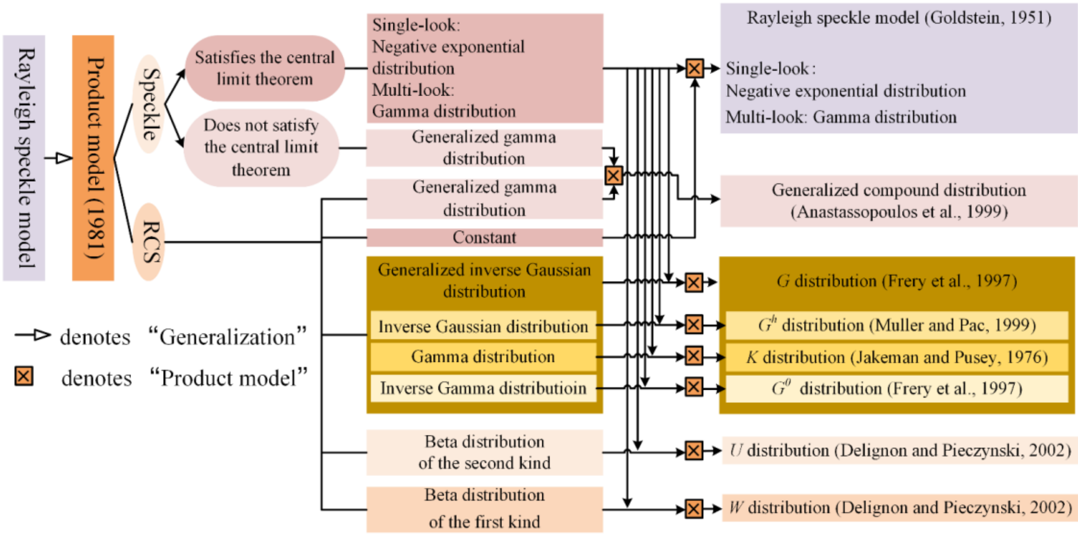


*Figure 1: Statistical distributions of scattered intensity based on product model*

Similarity, the Figure 7 is revised and explained in Page 10 Right-column Line 48-52, Figure 9 is revised and explained in Page 14 Right-column Line 11-15, Figure 10 is revised and explained in Page 15 Right-column Line 6-9.

*"The "Yellow shading box with embedded 'NR'" in Figure 7 denotes the "non-Rayleigh speckle model" which inputs the statistical distribution of the number of scatterers and the amplitude of the scatterers, and outputs the distribution of SAR image intensity."…*

*"As shown in Figure 9, the "Yellow shading box with embedded 'GCL'" denotes the "Generalized central limit theorem model" which inputs the statistical distribution of the real and imaginary components, and outputs the distribution of SAR image intensity."…*

*"As shown in Figure 10, the "Yellow shading box with embedded 'ISS'" denotes the "Incoherent scatterer model" which inputs the statistical distribution of the number of scatterers, and outputs the distribution of SAR image intensity."*

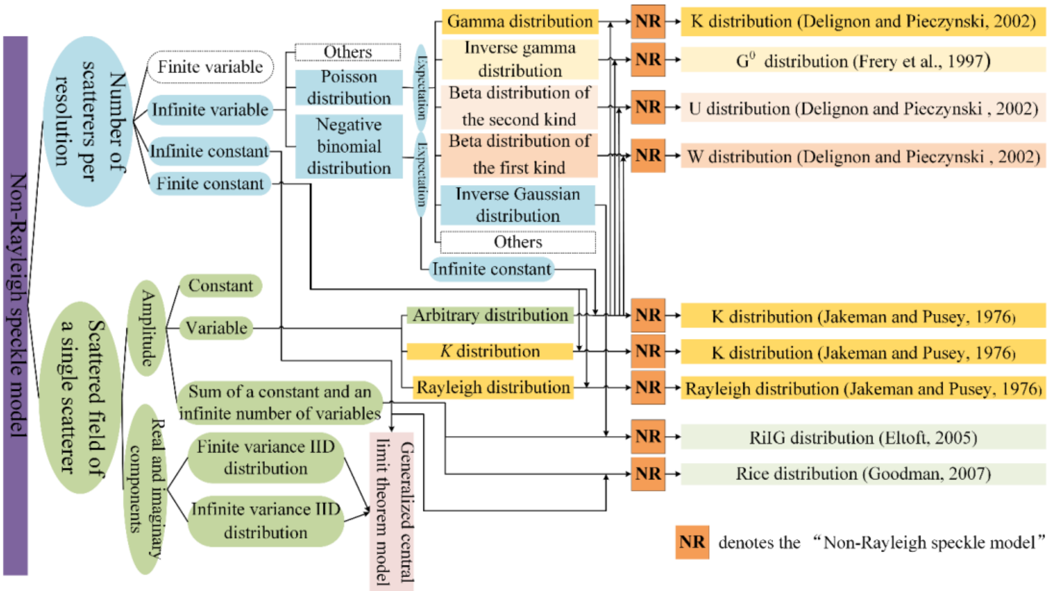


*Figure 2 Statistical distributions of scattered intensity based on non-Rayleigh speckle model*

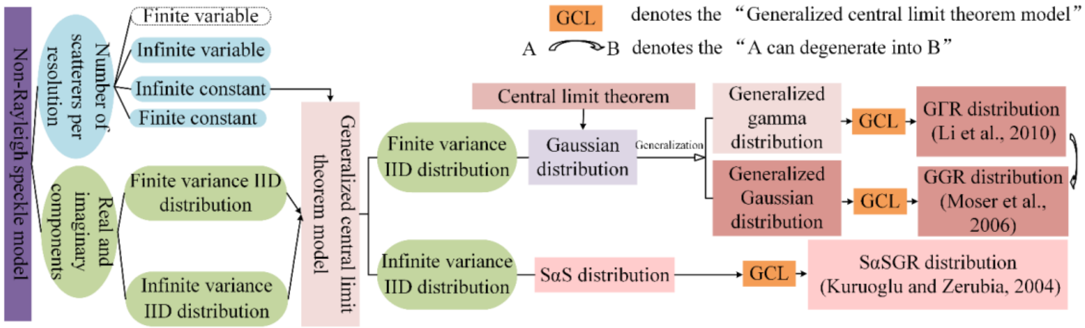


*Figure 3 Statistical distributions of scattered intensity based on generalized central limit theorem model*

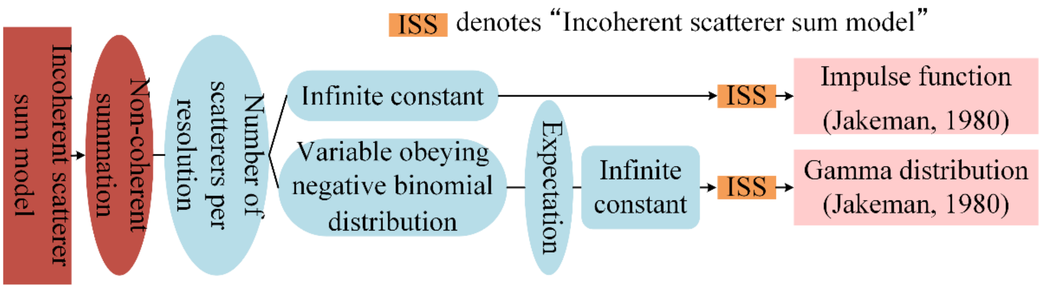


*Figure 4 Statistical distributions of scattered intensity based on incoherent scatterer sum model*

Q3. Table 1 and table 2 are not synchronized in the style of representation and then, in my opinion, they are a bit too complicated. For example, table 1 is interrupted from the end of the page, then, always in table 1 there are things defined in bold where you can't see them in table 2. In my opinion the graphic of table 2 needs to be redone, it seems to be a bit heavy.

A3. We thank the reviewer for pointing out these problems. Now Table 1 is adjusted to avoid interruption shown in Page 5 Line 43. Table 1 describes two statistical distributions under the Rayleigh speckle model including its statistical characteristics. Table 2 is relatively complicated because it expresses the modeling idea of the product model. It gives the corresponding probability density function (PDF) of RCS and speckle while the intensity distribution of SAR images. The $r$-order moments in Table 2 shows the statistical characteristics of distributions. To make the Table 2 clearer and less heavy, we have changed its expressions as shown in Page 7 Line 1:

“

*Table 1: Statistical distribution and characteristics of product model for intensity data*

| Distribution type | PDF of RCS $p(X_\sigma = x)$ | PDF of Speckle $p(Y_\sigma = y)$ | PDF of SAR image $p(Z_\sigma = z)$ | $r$ – order moment $E\{Z_\sigma^r\}$ |
|---|---|---|---|---|
| Gamma distribution [1] | $p_C$ | $p_\Gamma$ | $p_{\mathrm{Gamma}_\sigma}(Z_\sigma = z; n, \sigma) = \frac{1}{\Gamma(n)}\left(\frac{n}{\sigma}\right)^n z^{n-1} \exp\left(-\frac{nz}{\sigma}\right)$ | $E\{Z_\sigma^r\} = \frac{\Gamma(n+r)}{\Gamma(n)}\left(\frac{\sigma}{n}\right)^r$ |
| *G* distribution [43,44] | $p_{GIG}$ | | $p_{G_\sigma}(Z_\sigma = z; \beta, \gamma, \alpha, n) = \frac{n^n (\beta/\gamma)^{\alpha/2} z^{(n-1)}}{\Gamma(n) K_\alpha(2\sqrt{\beta\gamma})}\left(\frac{\gamma + nz}{\beta}\right)^{\frac{\alpha-n}{2}} K_{\alpha-n}\left(2\sqrt{\beta(\gamma+nz)}\right)$ | $E\{Z_\sigma^r\} = \left(\frac{\gamma}{n^2\beta}\right)^{\frac{r}{2}} \frac{K_{\alpha+r}(2\sqrt{\beta\gamma})\Gamma(n+r)}{K_\alpha(2\sqrt{\beta\gamma})\Gamma(n)}$ |
| *K* distribution [2,43] | $p_{\mathrm{Gamma}}$ | | $p_{K_\sigma}(Z_\sigma = z; \beta, \alpha, n) = \frac{2\beta n}{\Gamma(n)\Gamma(\alpha)}(\beta n z)^{\frac{\alpha+n}{2}-1} K_{\alpha-n}(2\sqrt{\beta n z})$ | $E\{Z_\sigma^r\} = (n\beta)^{-r}\frac{\Gamma(n+r)\Gamma(\alpha+r)}{\Gamma(n)\Gamma(\alpha)}$ |
| $G^0$ distribution [43] | $p_{\mathrm{Gamma}^{-1}}$ | | $p_{G_\sigma^0}(Z_\sigma = z; \gamma, -\alpha, n) = \frac{n^n \Gamma(n-\alpha)\gamma^{-\alpha} z^{n-1}}{\Gamma(n)\Gamma(-\alpha)(\gamma+nz)^{n-\alpha}}$ | $E\{Z_\sigma^r\} = (\gamma/n)^r \frac{\Gamma(n+r)\Gamma(-\alpha-r)}{\Gamma(n)\Gamma(-\alpha)}$ |
| $G^h$ distribution [43,45] | $p_{\mathrm{IG}}$ | | $p_{G_\sigma^h}(Z_\sigma = z; \lambda, \mu) = \sqrt{\frac{2\lambda}{\pi}} e^{\sqrt{\frac{\lambda^2}{\mu}}} \frac{n^n z^{n-1}}{\Gamma(n)}\left(\frac{(\lambda+2nz)\mu}{\lambda}\right)^{\frac{-1-2n}{4}} \times K_{n+\frac{1}{2}}\left(\frac{(\lambda+2nz)\lambda}{\mu}\right)$ | $E\{Z_\sigma^r\} = \sqrt{\frac{2\lambda}{\pi}}\left(\frac{\mu}{n^2}\right)^{\frac{r}{2}} e^{\sqrt{\frac{\lambda^2}{\mu}}}\mu^{-\frac{1}{4}} \times \frac{K_{r-1/2}(\lambda/\sqrt{\mu})\Gamma(n+r)}{\Gamma(n)}$ |
| GC distribution [38] | $p_{G\Gamma}$ | $p_{G\Gamma}$ | $p_{GC_\sigma}(Z_\sigma = z; a, b_1, v_1, b_2, v_2) = \frac{b_1 b_2}{2z\Gamma(v_1)\Gamma(v_2)} \frac{\sqrt{z}^{b_1 v_1}}{a^{b_2 v_2}} \int_0^\infty x^{b_2 v_2 - b_1 v_1 - 1} \times \exp\left[-\left(\frac{x}{a}\right)^{b_2} - \left(\frac{\sqrt{z}}{x}\right)^{b_1}\right] dx$ | $E\{Z_\sigma^r\} = a^{2r}\frac{\Gamma(\frac{2r}{b_1}+v_1)\Gamma(\frac{2r}{b_2}+v_2)}{\Gamma(v_1)\Gamma(v_2)}$ |

**Notes and Supplements**

Without special explanation, the symbols in this table above are defined as follows: $n$ is the number of look, the special function $K_n(\cdot)$ is the second type of modified Bessel function, $\Gamma(\cdot)$ is the gamma function, $X_\sigma$ denotes the RCS, and $Y_\sigma$ denotes the speckle. $Z_\sigma = X_\sigma \cdot Y_\sigma$ denotes the SAR intensity image.

(1) The detailed expressions in the second column, i.e. Probability density function (PDF) of RCS, are:

$$p_C(X_\sigma = x; \sigma) = \begin{cases} 1, x = \sigma \\ 0, \text{others} \end{cases}; \ \sigma > 0,$$

$$p_{GIG}(X_\sigma = x; \beta, \gamma, \alpha) = \frac{\left(\frac{\beta}{\gamma}\right)^{\frac{\alpha}{2}}}{2K_\alpha(2\sqrt{\beta\gamma})} x^{(\alpha-1)} \times e^{-\left(\beta x + \frac{\gamma}{x}\right)}; \alpha \in R, (\beta, \gamma) \in \Theta_\alpha; \Theta_\alpha = \begin{cases} \{(\beta,\gamma): \beta > 0, \gamma \ge 0\} & if \ \ \alpha > 0 \\ \{(\beta,\gamma): \beta > 0, \gamma > 0\} & if \ \ \alpha = 0, \\ \{(\beta,\gamma): \beta \ge 0, \gamma > 0\} & if \ \ \alpha < 0 \end{cases}$$

$$p_{\mathrm{Gamma}}(X_\sigma = x; \beta, \alpha) = \frac{\beta^\alpha}{\Gamma(\alpha)} x^{(\alpha-1)} e^{-\beta x}; \beta, \alpha > 0,$$

$$p_{\mathrm{Gamma}^{-1}}(X_\sigma = x; \alpha, \gamma) = \frac{\gamma^{-\alpha}}{\Gamma(-\alpha)} x^{\alpha-1} e^{-\gamma/x}; -\alpha, \gamma > 0,$$

$$p_{\mathrm{IG}}(X_\sigma = x; \mu, \lambda) = \left[\frac{\lambda}{2\pi x^3}\right]^{1/2} \times \exp\left[-\lambda\left(\frac{x}{2\mu} + \frac{1}{2x}\right)\right]; \mu \ge 0, \lambda > 0,$$

$$p_{G\Gamma}(X_\sigma = x; a, b_2, v_2) = \frac{b_2}{2\sqrt{x} a \Gamma(v_2)}\left(\frac{\sqrt{x}}{a}\right)^{b_2 v_2 - 1} \times \exp\left[-\left(\frac{\sqrt{x}}{a}\right)^{b_2}\right]; a, b_2, v_2 > 0.$$

(2) The detailed expressions in the third column, i.e. PDF of Speckle, are gamma distributed speckle $Y_\sigma \sim \mathrm{Gamma}(n, n)$, which is

$$p_\Gamma(Y_\sigma = y) = \frac{2n^n}{\Gamma(n)} y^{2n-1} \exp(-ny^2), y, n > 0,$$

and generalized gamma distributed speckle $Y_\sigma \sim G\Gamma(b_1, v_1)$, which is:

$$p_{G\Gamma}(Y_\sigma = y) = \frac{b_1}{2\Gamma(v_1)} y^{\frac{b_1 v_1}{2} - 1} \exp\left[-y^{\frac{b_1}{2}}\right]; b_1, v_1 > 0$$

”

Q4. I take as an example the Page 8 line 2, left column: is it possible to cite references from the title of subsections?

A4. Thanks for pointing out this issue. To make it more appropriate, we move the references in the title of subsections to the main text including Section 2.3.2(a-f), Section 2.4.2(b-f) and Section 2.5.2(a-c) in the revised version.

Q5. Formula 35: Probably Sum_i(m_i)=n instead Sum(m_1)=n?

A5. Yes, it should be $\sum m_i = n$ and this confusion may be caused by the small font. We have checked it and, to make it more clear, we use $\sum_{i=1}^{N} m_i = n$ instead of $\sum m_i = n$ in Page 10 Right-column Line 14 & 19:

Q6. Figure 9 is too small;

A6. We thank the suggestion and the font of Figure 9 is enlarged now shown in Page 14 Line 31.

Q7. You have inserted a comma and then you have inserted a capital letter.

where $\langle\cdot\rangle$ denotes the expectation.
If $\bar{N} \to \infty$, the limit form of Eq. (94) is:

$$\lim_{\bar{N}\to\infty} Q_{\bar{N}}(s) = (1 + s\langle\sigma\rangle/\alpha)^{-\alpha}, \tag{95}$$

Then the gamma distributed scattered intensity can be obtained using the inverse transform on Eq. (95):

$$p(\sigma) = \left(\frac{\alpha}{\langle\sigma\rangle}\right)^{\alpha} \frac{\sigma^{\alpha-1}}{\Gamma(\alpha)} \exp\left(-\frac{\alpha\sigma}{\langle\sigma\rangle}\right). \tag{96}$$

A7. We thank the reviewer for pointing out this issue. Now it is corrected by using “then” instead of ‘Then in Page 15 Right-column Line 57.

Q8. Tab. 4 and Tab. 5: please refere to previous comments.

A8. Following the reviewer’s suggestion, Table 3 in Page 17 Line 1、Table 4 in Page 17 Line 24 and Table 5 in Page 18 Line1 are re-drawn in the same style as the Table 1 and Table 2:

“Table 2: Statistical distribution and characteristics of single empirical distribution model

| Distribution type | Probability density function (PDF) | Mean | Variance | r-order moment |
|---|---|---|---|---|
| Log-normal distribution | $p_{LN}(z;\beta,V) = \frac{1}{z\sqrt{2\pi V}} exp\left[-\frac{(\ln z-\beta)^2}{2V}\right]$ | $exp\left[\beta+\frac{V}{2}\right]$ | $exp(2\beta+V)\,(exp(V)-1)$ | $E\{Z^r\} = exp\left[r\beta+\frac{r^2V}{2}\right]$ |
| Weibull distribution | $p_{WB}(z;c,b) = \frac{cz^{c-1}}{b^c} exp\left[-\left(\frac{z}{b}\right)^c\right]$ | $b\Gamma\left(1+\frac{1}{c}\right)$ | $b^2\left[\Gamma\left(\frac{2}{c}+1\right)-\Gamma^2(\frac{1}{c}+1)\right]$ | $E\{Z^r\} = b^r\Gamma(\frac{r}{c}+1)$ |
| Fisher distribution | $p_F(z;L,M,\mu) = \frac{\Gamma(L+M)}{\Gamma(L)\Gamma(M)}\frac{L}{M\mu}\frac{\left(\frac{Lz}{M\mu}\right)^{L-1}}{\left(1+\frac{Lz}{M\mu}\right)^{L+M}}$, $L>0, M>0$ | $\frac{M}{M-1}\mu$ | $\frac{M^2\mu^2(L+M-1)}{L(M-1)^2(M-2)}$ | —— |
| Generalized gamma distribution ($G\Gamma D-1$) | $p_{G\Gamma D1}(z;a,b,v) = \frac{b}{a\Gamma(v)}\left(\frac{z}{a}\right)^{bv-1} exp\left[-\left(\frac{z}{a}\right)^b\right]$ | $a\frac{\Gamma(\frac{1}{b}+v)}{\Gamma(v)}$ | $\frac{a^2}{\Gamma^2(v)}\left[\Gamma\left(\frac{2}{b}+v\right)\Gamma(v) - \Gamma^2\left(\frac{1}{b}+v\right)\right]$ | $E\{x^r\} = a^r\frac{\Gamma(\frac{r}{b}+v)}{\Gamma(v)}$ |
| Generalized gamma distribution ($G\Gamma D-2$) | $p_{G\Gamma D2}(z;v,\kappa,\eta) = \frac{\lvert v\rvert\kappa^\kappa}{\eta\Gamma(\kappa)}\left(\frac{z}{\eta}\right)^{\kappa v-1} exp\left[-\kappa\left(\frac{z}{\eta}\right)^v\right]$, $v\neq 0, \kappa>0, \eta>0$ | $\begin{cases}\frac{\eta}{\kappa^{1/v}}\frac{\Gamma(\kappa+\frac{1}{v})}{\Gamma(\kappa)}, \frac{1}{v} > -\kappa \\ \infty, \ otherwise\end{cases}$ | $\frac{\eta^2}{\Gamma^2(\kappa)\kappa^{\frac{2}{v}}}[\Gamma\left(\kappa+\frac{2}{v}\right)\Gamma(\kappa) -\Gamma^2\left(\kappa+\frac{1}{v}\right)]$, $\frac{1}{v}>-\kappa$, $\frac{2}{v}>-\kappa$ | $E\{x^r\} = \begin{cases}\frac{\eta^r}{\kappa^{r/v}}\frac{\Gamma(\kappa+\frac{r}{v})}{\Gamma(\kappa)}, \frac{r}{v} > -\kappa \\ \infty, \ otherwise\end{cases}$ |

Table 3: Parameter estimation formulas of MoLC method for amplitude distributions

| Distribution type | Probability density function (PDF) | Parameters | Estimation formula of MoLC |
|---|---|---|---|
| **Rayleigh distribution** | $p(A)=\frac{2A}{\sigma}e^{-\frac{A^2}{\sigma}}$ | $\sigma$ | $k_1=\frac{(\ln\sigma+\Psi(1))}{2}$ |
| **Square root gamma distribution** | $p(A)=\frac{2}{\Gamma(n)}\left(\frac{n}{\sigma}\right)^n A^{2n-1}e^{-nA^2/\sigma}$ | $n$, $\sigma$ | $2k_1=\ln\sigma+\Psi(n)-\ln n$ <br> $4k_2=\Psi(1,L)$ |
| **K distribution** | $p(A;\beta,\alpha,n)=\frac{4\beta nA}{\Gamma(n)\Gamma(\alpha)}(\beta nA^2)^{(\alpha+n)/2-1}K_{\alpha-n}(2A\sqrt{\beta n})$ | $\beta$, $\alpha$, $n$ | $2k_1=\ln\beta+\Psi(n)-\ln n+\Psi(\alpha)$ <br> $4k_2=\Psi(1,n)+\Psi(1,\alpha)$ <br> $8k_3=\Psi(2,n)+\Psi(2,\alpha)$ |
| **SαSGR distribution** | $p_A(A;\gamma,\alpha)=A\int_0^{\infty}s\,exp(-\gamma s^{\alpha})J_0(sA)ds$ | $\gamma$, $\alpha$ | $\alpha k_1=\Psi(1)(\alpha-1)+\alpha\ln 2+\ln\gamma$ <br> $k_2=\Psi(1,1)\alpha^{-2}$ |
| **GGR distribution** | $p_A(A;\gamma,c)=\frac{\gamma^2c^2A}{\Gamma^2(\frac{1}{c})}\int_0^{\frac{\pi}{2}}exp\{-(\gamma A)^c(\lvert\cos\theta\rvert^c+\lvert\sin\theta\rvert^c)\}d\theta$ | $\gamma$, $c$ | $k_1=\frac{1}{c}\Psi\left(\frac{2}{c}\right)-\ln\gamma-\frac{1}{c}G_1\left(\frac{1}{c}\right)G_0\left(\frac{1}{c}\right)^{-1}$ <br> $k_2=\frac{1}{c^2}\Psi\left(1,\frac{2}{c}\right)+\frac{1}{c^2}G_2\left(\frac{1}{c}\right)G_0\left(\frac{1}{c}\right)^{-1}-\frac{1}{c^2}G_1\left(\frac{1}{c}\right)^2G_0\left(\frac{1}{c}\right)^{-2}$ |
| **GΓR distribution** | $p_A(A;\nu,\eta,\kappa)=\left[\frac{\nu}{\eta^{\kappa\nu}\Gamma(\kappa)}\right]^2A^{2\kappa\nu-1}\cdot\int_0^{\frac{\pi}{2}}\lvert\cos\theta\sin\theta\rvert^{\kappa\nu-1}exp\left\{-\left(\frac{A}{\eta}\right)^{\nu}(\lvert\cos\theta\rvert^{\nu}+\lvert\sin\theta\rvert^{\nu})\right\}d\theta,\nu=\frac{1}{\varpi}$ | $\nu$, $\eta$, $\kappa$ | $k_1=\ln\eta+\varpi\Psi(2\kappa)-\varpi\frac{G_1(\kappa,\varpi)}{G_0(\kappa,\varpi)}$ <br> $k_2=\varpi^2\left[\Psi(1,2\kappa)+\frac{G_2(\kappa,\varpi)}{G_0(\kappa,\varpi)}-\frac{G_1^2(\kappa,\varpi)}{G_0^2(\kappa,\varpi)}\right]$ <br> $k_3=\varpi^3\left[\Psi(2,2\kappa)-\frac{G_3(\kappa,\varpi)}{G_0(\kappa,\varpi)}+3\frac{G_2(\kappa,\varpi)G_1(\kappa,\varpi)}{G_0^2(\kappa,\varpi)}-2\frac{G_1^3(\kappa,\varpi)}{G_0^3(\kappa,\varpi)}\right]$ |
| **Log-normal distribution** | $p(A;V,\beta)=\frac{1}{A\sqrt{2\pi V}}exp\left[-\frac{(\ln A-\beta)^2}{2V}\right]$ | $V$, $\beta$ | $k_1=\beta$ <br> $k_2=V$ |
| **Weibull distribution** | $p(A;b,c)=\frac{cA^{c-1}}{b^c}exp\left[-\left(\frac{A}{b}\right)^c\right]$ | $b$, $c$ | $k_1=\ln b+\Psi(1)c^{-1}$ <br> $k_2=\Psi(1,1)c^{-2}$ |
| **Fisher distribution** | $p(A;L,M,\mu)=\frac{\Gamma(L+M)}{\Gamma(L)\Gamma(M)}\frac{L}{M\mu}\frac{\left(\frac{LA}{M\mu}\right)^{L-1}}{\left(1+\frac{LA}{M\mu}\right)^{L+M}}$ | $L$, $M$, $\mu$ | $k_1=\ln\mu+(\Psi(L)-\ln L)-(\Psi(M)-\ln M)$ <br> $k_2=\Psi(1,L)+\Psi(1,M)$ <br> $k_3=\Psi(2,L)-\Psi(2,M)$ |
| **Generalized gamma distribution** | $f(A;a,b,v)=\frac{b}{a\Gamma(v)}\left(\frac{A}{a}\right)^{bv-1}exp\left[-\left(\frac{A}{a}\right)^b\right]$ | $a$, $b$, $v$ | $k_1=\Psi(v)/b+\ln a$ <br> $k_2=\Psi(1,v)/b^2$ <br> $k_3=\Psi(2,v)/b^3$ |

**Note:** $\mathbf{K_v}(\cdot)$ is the second type of modified Bessel function, $\mathbf{\Psi}(\cdot)$ denotes the digamma function, $\mathbf{\Psi}(\mathbf{i},\cdot)$ represents the $\mathbf{i}$-order polygamma function, $\mathbf{G_v}(\boldsymbol{\lambda})$ is an integral function introduced in [20]:

$$G_v(\lambda)=\int_0^{\pi/2}\frac{\ln^v A(\theta,\lambda)}{A(\theta,\lambda)^{2\lambda}}d\theta,v=0,1,2;\ A(\theta,\lambda)=\lvert\cos\theta\rvert^{1/\lambda}+\lvert\sin\theta\rvert^{1/\lambda}$$

$\mathbf{G_i}(\mathbf{k},\boldsymbol{\varpi})$ is an integral function introduced in [21]:

$$G_i(k,\varpi)=\int_0^{\pi/2}\lvert\cos\theta\sin\theta\rvert^{\frac{k}{\varpi}-1}\frac{\log^i A(\theta,\lambda)}{A(\theta,\lambda)^{2k}}d\theta;\ A(\theta,\lambda)=\lvert\cos\theta\rvert^{1/\lambda}+\lvert\sin\theta\rvert^{1/\lambda}$$

Table 4: Summary of single-pixel statistical modeling

| Models | Model complexity & physical meaning | Distributions | Existence of analytical PDF | Application scope |
|---|---|---|---|---|
| **Rayleigh speckle model** | Low model complexity & weak physical meaning | Negative exponential distribution | Yes | Widely used in single-look intensity image of homogenous area |
| | | Rayleigh distribution | Yes | Widely used in single-look amplitude image of homogenous area |
| | | Gamma distribution | Yes | Widely used in multi-look intensity image of homogenous area |
| | | Square root gamma distribution | Yes | Widely used in multi-look amplitude image of homogenous area |
| **Product model** | Less high model complexity & Less strong physical meaning | G distribution | Yes | Used in homogenous, inhomogeneous, extremely inhomogeneous areas; suitable for single/multi-look intensity or amplitude image |
| | | $G^h$ distribution | Yes | Used in extremely inhomogeneous urban areas and mixed terrain areas; |
| | | GC distribution | Yes | Used in sea and land areas of medium-resolution ($15m^2$/$30\ m^2$) |
| **Non-Rayleigh speckle model** | High model complexity & strong physical significance | $G^0$ distribution | Yes | Used in homogenous, inhomogeneous, extremely inhomogeneous areas; suitable for single/multi-look intensity or amplitude image |
| | | K distribution | Yes | Widely used in medium inhomogeneous area; suitable for single/multi-look intensity or amplitude image |
| | | W distribution | Yes | Used in medium inhomogeneous area; suitable for single/multi-look intensity or amplitude image |
| | | U distribution | Yes | Used in medium inhomogeneous area; suitable for single/multi-look intensity or amplitude image |
| | | Rice distribution | Yes | Used in low-resolution images with targets in weak clutter |
| | | RiIG distribution | Yes | Used in SAR amplitude image or ultrasound image |
| **Generalized central limit theorem model** | Less high model complexity & Less strong physical meaning | GGR distribution | No | Used for multiple types of terrains (such as urban areas, farmland, lakes, mountains) in multi-polarized channels |
| | | GΓR distribution | No | Used for homogenous or inhomogeneous SAR amplitude image with multiple types of terrains (such as urban areas, farmland, and mountains) |
| | | SαSGR distribution | No | Used for Long-tailed amplitude image of urban area |
| **Single empirical distribution model** | Low model complexity & no clear physical meaning | Log-normal distribution | Yes | Used for medium-resolution amplitude images for sea clutter and homogenous urban |
| | | Weibull distribution | Yes | Used for medium-resolution amplitude or intensity images |
| | | Fisher distribution | Yes | Used in homogenous, inhomogeneous, extremely inhomogeneous areas; suitable for single/multi-look intensity or amplitude image |
| | | Generalized gamma distribution | Yes | Used for homogenous or inhomogeneous SAR amplitude/intensity image with multiple types of terrains (such as urban areas, farmland, and mountains) |
| **Finite mixture statistical model** | High model complexity & weak physical significance | Mixed K-distribution or mixed log-normal distribution | Yes | Used for homogenous or inhomogeneous high-resolution SAR images |
| | | Dictionary-based mixture distribution model | Yes | Used for complex scenes composed by multiple types of terrains with medium, high or ultra-high resolution. |
| **Non-parametric statistical model** | High model complexity & no clear physical meaning | Parzen-window method | No | Used for complex scenes composed by multiple types of terrains |
| | | SVM method | No | Used for complex scenes composed by multiple types of terrains |
| | | Neural network method | No | Used for complex scenes composed by multiple types of terrains |

”

Q9. Please consider to insert into bibliography the following works:

V. Akbari, S. N. Anfinsen, A. P. Doulgeris, T. Eltoft, G. Moser and S. B. Serpico, "Polarimetric SAR Change Detection With the Complex Hotelling–Lawley Trace Statistic," in IEEE Transactions on Geoscience and Remote Sensing, vol. 54, no. 7, pp. 3953-3966, July 2016. doi: 10.1109/TGRS.2016.2532320

W. B. Silva, C. C. Freitas, S. J. S. Sant'Anna and A. C. Frery, "Classification of Segments in PolSAR Imagery by Minimum Stochastic Distances Between Wishart Distributions," in IEEE Journal of Selected Topics in Applied Earth Observations and Remote Sensing, vol. 6, no. 3, pp. 1263-1273, June 2013. doi: 10.1109/JSTARS.2013.2248132

A. C. Frery, R. J. Cintra and A. D. C. Nascimento, "Entropy-Based Statistical Analysis of PolSAR Data," in IEEE Transactions on Geoscience and Remote Sensing, vol. 51, no. 6, pp. 3733-3743, June 2013. doi: 10.1109/TGRS.2012.2222029

S. N. Anfinsen, A. P. Doulgeris and T. Eltoft, "Goodness-of-Fit Tests for Multilook Polarimetric Radar Data Based on the Mellin Transform," in IEEE Transactions on Geoscience and Remote Sensing, vol. 49, no. 7, pp. 2764-2781, July 2011. doi: 10.1109/TGRS.2010.2104158

Biondi, F. (2019). Multi-chromatic analysis polarimetric interferometric synthetic aperture radar (MCA-PolInSAR) for urban classification. International journal of remote sensing, 40(10), 37213750.

A9. Thanks for sharing these excellent works. These works mainly focus on the polarimteric statistical modeling for SAR images which is an important extension of single-channel statistical modeling introduced in this paper. These works as well as the references are now referred in the outlook of this paper, which is in Section 5.2 in Page 23 Left-column Line 50- Right-column Line 7:

*"…(4) PolSAR images contain richer scene information compared with the single-channel SAR data [2]. The statistical analysis [114, 115] of PolSAR images plays an important role for its interpretation such as image segmentation [116, 117] and classification [118-122], change detection [123-128], target detection [129, 130] and despeckling [131-134]. Many statistical distributions for PolSAR data can be seen as an extension of single-channel statistical modeling reviewed in this paper. The scaled complex Wishart distribution is employed as a statistical model for homogeneous regions in PolSAR images [115]. And the product model has developed many statistical distributions to describe the nonhomogeneous regions in PolSAR images such as the polarimetric G_P distribution, K_P distribution, G_P^0 distribution, U distribution and so on [114, 120]. The expansion from single-channel statistical modeling to polarimetric statistical modeling and the study of polarimetric statistical modeling will provide an important research foundation for the wide application of PolSAR images. …"*

with the corresponding references:

*"…**[115] A. C. Frery, R. J. Cintra, A. D. C. Nascimento, "Entropy-based Statistical Analysis of PolSAR Data,"[J] IEEE Transactions on Geoscience & Remote Sensing, vol. 51, pp. 3733-3743, 2012.***

*[116] F. Lang, J. Yang, D. Li, L. Zhao, L. Shi, "Polarimetric SAR image segmentation using statistical region merging,"[J] IEEE geoscience and remote sensing letters, vol. 11, pp. 509-513, 2013.*

*[117] N. Bouhlel, S. Méric, "Unsupervised Segmentation of Multilook Polarimetric Synthetic Aperture Radar Images,"[J] IEEE Transactions on Geoscience and Remote Sensing, vol. 57, pp. 6104-6118, 2019.*

*[118] S.-W. Chen, C.-S. Tao, "PolSAR image classification using polarimetric-feature-driven deep convolutional neural network,"[J] IEEE Geoscience and Remote Sensing Letters, vol. 15, pp. 627-631, 2018.*

*[119] A. Masjedi, M. J. V. Zoej, Y. Maghsoudi, "Classification of polarimetric SAR images based on modeling contextual information and using texture features,"[J] IEEE Transactions on Geoscience and Remote Sensing, vol. 54, pp. 932-943, 2015.*

***[120] W. B. Silva, C. C. Freitas, S. J. Sant'Anna, A. C. Frery, "Classification of segments in PolSAR imagery by minimum stochastic distances between Wishart distributions,"[J] IEEE Journal of Selected Topics in Applied Earth Observations and Remote Sensing, vol. 6, pp. 1263-1273, 2013.***

***[121] N. Anfinsen, A. P. Doulgeris, T. Eltoft, "Goodness-of-Fit Tests for Multilook Polarimetric Radar Data Based on the Mellin Transform,"[J] IEEE Transactions on Geoscience and Remote Sensing, vol. 49, pp. 2764-2781, 2011.***

***[122] F. Biondi, "Multi-chromatic analysis polarimetric interferometric synthetic aperture radar (MCA-PolInSAR) for urban classification,"[J] International journal of remote sensing, vol. 40, pp. 3721-3750, 2019.***

***[123] V. Akbari, S. N. Anfinsen, A. P. Doulgeris, G. M. T. Eltoft, S. B. Serpico, "Polarimetric SAR Change Detection With the Complex Hotelling–Lawley Trace Statistic,"[J] IEEE Transactions on Geoscience and Remote Sensing, vol. 54, pp. 3953-3966, 2016.***

*[124] J. Prendes, M. Chabert, F. Pascal, A. Giros, J.-Y. Tourneret, "A new multivariate statistical model for change*

*detection in images acquired by homogeneous and heterogeneous sensors,"[J] IEEE Transactions on Image Processing, vol. 24, pp. 799-812, 2014.*

*[125] N. Bouhlel, S. Méric, "Multilook Polarimetric SAR Change Detection Using Stochastic Distances Between Matrix-Variate Gd $^0$ Distributions,"[J] IEEE Transactions on Geoscience and Remote Sensing, 2020.*

*[126] T. Liu, Z. Yang, A. Marino, G. Gao, J. Yang, "Robust CFAR Detector Based on Truncated Statistics for Polarimetric Synthetic Aperture Radar,"[J] IEEE Transactions on Geoscience and Remote Sensing, 2020.*

*[127] A. D. Nascimento, A. C. Frery, R. J. Cintra, "Detecting changes in fully polarimetric SAR imagery with statistical information theory,"[J] IEEE Transactions on Geoscience and Remote Sensing, vol. 57, pp. 1380-1392, 2018.*

*[128] W. Yang, X. Yang, T. Yan, H. Song, G.-S. Xia, "Region-based change detection for polarimetric SAR images using Wishart mixture models,"[J] IEEE Transactions on Geoscience and Remote Sensing, vol. 54, pp. 6746-6756, 2016.*

*[129] A. Marino, I. Hajnsek, "Statistical Tests for a Ship Detector Based on the Polarimetric Notch Filter,"[J] IEEE Transactions on Geoscience and Remote Sensing, vol. 53, pp. 4578-4595, 2015.*

*[130] D. Tao, A. P. Doulgeris, C. Brekke, "A Segmentation-Based CFAR Detection Algorithm Using Truncated Statistics,"[J] IEEE Transactions on Geoscience and Remote Sensing, vol. 54, pp. 2887-2898, 2016.*

*[131] P. A. A. Penna, N. D. A. Mascarenhas, "SAR Speckle Nonlocal Filtering With Statistical Modeling of Haar Wavelet Coefficients and Stochastic Distances,"[J] IEEE Transactions on Geoscience and Remote Sensing, vol. 57, pp. 7194-7208, 2019.*

*[132] L. Torres, S. J. S. Sant'Anna, C. C. Freitas, A. C. Frery, "Speckle Reduction in Polarimetric {SAR} Imagery with Stochastic Distances and Nonlocal Means,"[J] Pattern Recognition, vol. 47, pp. 141--157, 2014.*

*[133] J.-S. Lee, T. L. Ainsworth, Y. Wang, K.-S. Chen, "Polarimetric SAR Speckle Filtering and the Extended Sigma Filter,"[J] Transactions on Geoscience and Remote Sensing, vol. 53, pp. 1150--1160, 2015.*

*[134] H. Zhong, J. Zhang, G. Liu, "Robust Polarimetric SAR Despeckling Based on Nonlocal Means and Distributed Lee Filter,"[J] IEEE Transactions on Geoscience and Remote Sensing, vol. 52, pp. 4198 - 4210 2014.... "*

Q10. Thank you and good work!

A10. We appreciate the encouragement from the reviewer.

## Reviewer 2:

Comments to the Author

SAR image statistical modeling is one of the theoretical foundations for SAR image interpretation. This paper presents an overview of SAR image single-pixel statistical modeling, including more than 20 statistical distributions of 8 statistical models, gives their derivations and expressions, and introduces the application situation of each model and distribution. It can be used as an important reference for SAR image statistical modeling research, and will provide guidelines for researchers to further enhance the development of SAR image statistical modeling. The remarks are as follows:

Q1: The title is suggested to be changed to "SAR Image Statistical Modeling Part I: Single-Pixel Statistical Modeling".

A1: Following the reviewer's suggestion, the title of the paper is changed to "SAR Image Statistical Modeling Part I: Single-Pixel Statistical Models".

Q2: It is suggested that the structure of the paper be divided into five sections: Introduction, Statistical modeling based on coherent scatterer models, Statistical modeling based on empirical models, Model selection and parameter estimation, and Conclusion.

A2: We thank the reviewer for this suggestion. It makes a clearer description for the categories of statistical models. Now the structure of the paper is divided into five sections as suggested. To make the whole paper consistent, the Figure 4 as well as its description is moved to Section 1.1 Page 3 Left-column Line 3.

Q3: The fonts of many figures and tables are a little small, so it is recommended to change them a little larger.

A3: Thanks for this suggestion and the fonts of Figures 7, 9, 10, 13 and Tables 1-5 are enlarged now.

Q4: Some terminologies are a little confusing. For example, three different terms, "non-Rayleigh model", "non-Rayleigh speckle model" and "non-Rayleigh speckle", appear in the paper, but they seem to have the same meaning. There are similar situations such as "single-pixel statistical modeling", "single-pixel statistical models", "single-pixel model" and "single-pixel distribution models".

A4: We apologize for the confusing terminologies. "non-Rayleigh model" and "non-Rayleigh speckle model" have the same meaning and they are unified as "non-Rayleigh speckle model" now. The "non-Rayleigh speckle model" introduced in Section 2.4 is a statistical modeling which brings K distribution, Rice distribution, RiIG distribution, $G^0$ distribution, W distribution and U distribution. However, as shown in Figure 4, the "non-Rayleigh speckle" does not refer to a certain model, but covers the statistical modeling developed from the coherent scatterer model whose amplitude does not follow the Rayleigh distribution. "non-Rayleigh speckle" includes the product model, non-Rayleigh speckle model, generalized central limit theorem model and incoherent scatterer sum model. This is explained in Page 2 Right-column Line 29-33.

*"…non-Rayleigh speckle covers the statistical modeling developed from the coherent scatterer model whose amplitude does not follow the Rayleigh distribution including the product model, non-Rayleigh speckle model, generalized central limit theorem model and incoherent scatterer sum model…."*

"single-pixel statistical modeling", "single-pixel statistical models", "single-pixel model" and "single-pixel distribution models" have the same meaning, and they are all unified by "single-pixel statistical modeling" now.

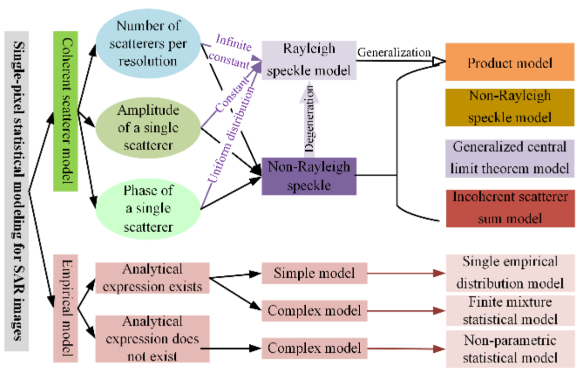


*Figure 5: The framework of single-pixel statistical modeling*

Q5: There seems to be something wrong with equation (9). According to my personal derivation, it should be

$$p_{R,I} = \frac{1}{\pi\sigma^2} e^{-\frac{R^2+I^2}{\sigma^2}}$$

Equation (49) may have the same problem. In addition, the intensity and standard deviation in the paper are expressed by the same symbol $\sigma$, is it easy to cause confusion?

A5: We thank the reviewer for pointing out this problem and apologize for the incorrect expression in Eq. (9). In following we give the detailed derivation of Eq. (9). The standard deviation is denoted by $\sqrt{\sigma/2}$.

The $\Re$ and $\Im$ are Gaussian distributed random variables with zero mean and the same variance $\sigma/2$. Note that the variance "$\sigma^2/2$" in original paper is revised by "$\sigma/2$" in the revised version in Page 4 Right-column Line 14-15:

*"$\Re$ and $\Im$ are Gaussian distributed random variables with zero mean and the same variance $\sigma/2$".*

Then we write the distribution of $\Re$ and $\Im$ as:

$$p_{\Re}(\Re) = \frac{1}{\sqrt{\pi\sigma}} e^{-\frac{\Re^2}{\sigma}}, \qquad p_{\Im}(\Im) = \frac{1}{\sqrt{\pi\sigma}} e^{-\frac{\Im^2}{\sigma}},$$

and therefore:

$$p_{\Re,\Im}(\Re,\Im) = p_{\Re}(\Re)p_{\Im}(\Im) = \frac{1}{\pi\sigma} e^{-\frac{\Re^2+\Im^2}{\sigma}}.$$

The Eq. (9) is now corrected using above equation in Page 4 Right-column Line 17:

"

$$p_{\Re,\Im}(\Re,\Im) = \frac{1}{\pi\sigma} e^{-\frac{\Re^2+\Im^2}{\sigma}}. \tag{1}$$

"

The joint probability distribution of amplitude $A = \sqrt{\Re^2 + \Im^2}$ and phase $\theta = \arctan(\Im/\Re)$ then can be obtained using variable substitution:

$$p_{A,\theta}(A,\theta) = \frac{A}{\pi\sigma} \exp\left[-\frac{A^2}{\sigma}\right].$$

The probability distribution of $A$ is obtained by integrating $\theta$, which is Rayleigh distribution:

$$p_A(A) = \frac{2A}{\sigma} \exp\left[-\frac{A^2}{\sigma}\right]$$

Take $\sigma$ as a random variable denoted by symbol $z$, we obtain the Eq. (49) in Page 11 Right-column Line 51 :

"

$$p(A|z) = \frac{2A}{z} e^{-\frac{A^2}{z}}. \tag{2}$$

".

Besides, what we need to explain is that the intensity in the paper are expressed by the same symbol $\sigma$ or $I$ which has been illustrated in the original paper in Section 1.2 Page 3 Left-column Line 30-33:

"*$\sigma$: for the model not taking into account the imaging function, it denotes the intensity of scattered field $\sigma = A^2$; but for the model taking into account imaging function, it denotes the radar cross section (RCS), while the intensity is denoted by $I$;*".

The standard deviation is denoted by $\sqrt{\sigma/2}$, and please note that "σ" and "$\sigma$" are two different symbols.

Q6: It is suggested to cite more literatures published in the past 5 years.

A6: Thanks for the good suggestion to improve this paper. We have supplemented more recent literatures by looking into the important and forefront SAR technologies especially for the polarimetric SAR and quantum radar, more detailed information can be found in the A1 and A9 to reviewer 1. The supplemented literatures are:

"...

*[94] X. Y. Hou, W. Ao, Q. Song, J. Lai, H. P. Wang, F. Xu, "FUSAR-Ship: building a high-resolution SAR-AIS matchup dataset of Gaofen-3 for ship detection and recognition,"[J] Sci China Inf Sci, vol. 63, p. 140303,* ***2020****.*

*....*

*[97] F. Xu, C. Hu, J. Li, A. Plaza, M. Datcu, "Special focus on deep learning in remote sensing image processing,"[J] Sci China Inf Sci, vol. 63, p. 140300, **2020**.*

*...*

*[107] S. R. Cloude, K. P. Papathanassiou, "Polarimetric SAR interferometry,"[J] IEEE Transactions on Geoscience and Remote Sensing, vol. 36, pp. 1551-1565, 1998.*

*[108] D. Liang, K. Liu, H. Yue, Y. Chen, Y. Deng, H. Zhang, G. J. C. Li, R. Wang, "An Advanced Non-Interrupted Synchronization Scheme for Bistatic Synthetic Aperture Radar," in 2019 IEEE International Geoscience and Remote Sensing Symposium Yokohama, Japan, **2019**, pp. 1116-1119.*

*[109] H. Zhang, Y. Deng, R. Wang, N. Li, S. Zhao, F. Hong, L. Wu, O. Lofeld, "Spaceborne/Stationary Bistatic SAR Imaging With TerraSAR-X as an Illuminator in Staring-Spotlight Mode,"[J] IEEE Transactions on Geoscience and Remote Sensing, vol. 54, pp. 5203-5216, **2016**.*

*[110] M. Zhang, R. Wang, Y. Deng, L. Wu, Z. Zhang, H. Zhang, N. Li, Y. Liu, X. Luo, "A Synchronization Algorithm for Spaceborne/Stationary BiSAR Imaging Based on Contrast Optimization With Direct Signal From Radar Satellite,"[J] IEEE Transactions on Geoscience and Remote Sensing, vol. 54, pp. 1977-1989, **2016**.*

*[111] R. Wang, W. Wang, Y. Shao, F. Hong, P. Wang, Y. Deng, Z. Zhang, O. Loffeld, "First Bistatic Demonstration of Digital Beamforming in Elevation With TerraSAR-X as an Illuminator,"[J] IEEE Transactions on Geoscience and Remote Sensing, vol. 54, pp. 842-849, **2016**.*

*[112] Z. Li, Z. Bao, H. Wang, G. Liao, "Performance improvement for constellation SAR using signal processing techniques,"[J] IEEE Transactions on Aerospace and Electronic Systems, vol. 42, pp. 436-452, 2006.*

*[113] M. Lanzagorta, "Quantum Radar,"[M]: Morgan & Claypool, 2011.*

*[114] X. Deng, C. López-Martínez, J. Chen, P. Han, "Statistical modeling of polarimetric SAR data: A survey and challenges,"[J] Remote Sensing, vol. 9, p. 348, **2017**.*

*[115] A. C. Frery, R. J. Cintra, A. D. C. Nascimento, "Entropy-based Statistical Analysis of PolSAR Data,"[J] IEEE Transactions on Geoscience & Remote Sensing, vol. 51, pp. 3733-3743, 2012.*

*[116] F. Lang, J. Yang, D. Li, L. Zhao, L. Shi, "Polarimetric SAR image segmentation using statistical region merging,"[J] IEEE geoscience and remote sensing letters, vol. 11, pp. 509-513, 2013.*

*[117] N. Bouhlel, S. Méric, "Unsupervised Segmentation of Multilook Polarimetric Synthetic Aperture Radar Images,"[J] IEEE Transactions on Geoscience and Remote Sensing, vol. 57, pp. 6104-6118, **2019**.*

*[118] S.-W. Chen, C.-S. Tao, "PolSAR image classification using polarimetric-feature-driven deep convolutional neural network,"[J] IEEE Geoscience and Remote Sensing Letters, vol. 15, pp. 627-631, **2018**.*

*[119] A. Masjedi, M. J. V. Zoej, Y. Maghsoudi, "Classification of polarimetric SAR images based on modeling contextual information and using texture features,"[J] IEEE Transactions on Geoscience and Remote Sensing, vol. 54, pp. 932-943, **2015**.*

*[120] W. B. Silva, C. C. Freitas, S. J. Sant'Anna, A. C. Frery, "Classification of segments in PolSAR imagery by minimum stochastic distances between Wishart distributions,"[J] IEEE Journal of Selected Topics in Applied Earth Observations and Remote Sensing, vol. 6, pp. 1263-1273, 2013.*

*[121] N. Anfinsen, A. P. Doulgeris, T. Eltoft, "Goodness-of-Fit Tests for Multilook Polarimetric Radar Data Based on the Mellin Transform,"[J] IEEE Transactions on Geoscience and Remote Sensing, vol. 49, pp. 2764-2781, 2011.*

*[122] F. Biondi, "Multi-chromatic analysis polarimetric interferometric synthetic aperture radar (MCA-PolInSAR) for urban classification,"[J] International journal of remote sensing, vol. 40, pp. 3721-3750, **2019**.*

*[123] V. Akbari, S. N. Anfinsen, A. P. Doulgeris, G. M. T. Eltoft, S. B. Serpico, "Polarimetric SAR Change Detection With the Complex Hotelling–Lawley Trace Statistic,"[J] IEEE Transactions on Geoscience and Remote Sensing, vol. 54, pp. 3953-3966, **2016**.*

*[124] J. Prendes, M. Chabert, F. Pascal, A. Giros, J.-Y. Tourneret, "A new multivariate statistical model for change*

*detection in images acquired by homogeneous and heterogeneous sensors,"[J] IEEE Transactions on Image Processing, vol. 24, pp. 799-812, 2014.*

*[125] N. Bouhlel, S. Méric, "Multilook Polarimetric SAR Change Detection Using Stochastic Distances Between Matrix-Variate $Gd^0$ Distributions,"[J] IEEE Transactions on Geoscience and Remote Sensing, **2020**.*

*[126] T. Liu, Z. Yang, A. Marino, G. Gao, J. Yang, "Robust CFAR Detector Based on Truncated Statistics for Polarimetric Synthetic Aperture Radar,"[J] IEEE Transactions on Geoscience and Remote Sensing, **2020**.*

*[127] A. D. Nascimento, A. C. Frery, R. J. Cintra, "Detecting changes in fully polarimetric SAR imagery with statistical information theory,"[J] IEEE Transactions on Geoscience and Remote Sensing, vol. 57, pp. 1380-1392, **2018**.*

*[128] W. Yang, X. Yang, T. Yan, H. Song, G.-S. Xia, "Region-based change detection for polarimetric SAR images using Wishart mixture models,"[J] IEEE Transactions on Geoscience and Remote Sensing, vol. 54, pp. 6746-6756, **2016**.*

*[129] A. Marino, I. Hajnsek, "Statistical Tests for a Ship Detector Based on the Polarimetric Notch Filter,"[J] IEEE Transactions on Geoscience and Remote Sensing, vol. 53, pp. 4578-4595, **2015**.*

*[130] D. Tao, A. P. Doulgeris, C. Brekke, "A Segmentation-Based CFAR Detection Algorithm Using Truncated Statistics,"[J] IEEE Transactions on Geoscience and Remote Sensing, vol. 54, pp. 2887-2898, **2016**.*

*[131] P. A. A. Penna, N. D. A. Mascarenhas, "SAR Speckle Nonlocal Filtering With Statistical Modeling of Haar Wavelet Coefficients and Stochastic Distances,"[J] IEEE Transactions on Geoscience and Remote Sensing, vol. 57, pp. 7194-7208, **2019**.*

*[132] L. Torres, S. J. S. Sant'Anna, C. C. Freitas, A. C. Frery, "Speckle Reduction in Polarimetric SAR Imagery with Stochastic Distances and Nonlocal Means,"[J] Pattern Recognition, vol. 47, pp. 141--157, 2014.*

*[133] J.-S. Lee, T. L. Ainsworth, Y. Wang, K.-S. Chen, "Polarimetric SAR Speckle Filtering and the Extended Sigma Filter,"[J] Transactions on Geoscience and Remote Sensing, vol. 53, pp. 1150--1160, **2015**.*

*[134] H. Zhong, J. Zhang, G. Liu, "Robust Polarimetric SAR Despeckling Based on Nonlocal Means and Distributed Lee Filter,"[J] IEEE Transactions on Geoscience and Remote Sensing, vol. 52, pp. 4198 - 4210 2014.*

*[135] M. A. Nielsen, I. L. Chuang, "Quantum Computation and Quantum Information: 10th Anniversary Edition,"[M], 2011.*

*[136] P. Lin, Z. Yu, C. Li, "Review and forecast of quantum radar,"[C] in 2013 Asia-Pacific Conference on Synthetic Aperture Radar (APSAR), Tsukuba, 2013, pp. 432-433.*

*[137] K. Liu, H. Xiao, H. Fan, Q. Fu, "Analysis of Quantum Radar Cross Section and Its Influence on Target Detection Performance,"[J] IEEE Photonics Technology Letters, vol. 26, pp. 1146-1149, 2014.*

*[138] C. Fang, "The Simulation and Analysis of Quantum Radar Cross Section for Three-Dimensional Convex Targets,"[J] IEEE Photonics Journal, vol. 10, pp. 1-8, **2018**.*

*[139] S. Zhao, "Quantum detection theory and optimum strategy in quantum radar system,"[J] The Journal of Engineering, vol. 11, pp. 7428-7431, **2019**.*

*[140] S. Lloyd, "Enhanced Sensitivity of Photodetection via Quantum Illumination,"[J] Science, vol. 321, pp. 1463-1465, 2008.*

*[141] Y. Li, S. Feng, X. Zhang, L. Jiao, "SAR image segmentation based on quantum-inspired multiobjective evolutionary clustering algorithm,"[J] Information Processing Letters, vol. 114, pp. 287-293, 2014.*

*[142] S. Gou, X. Zhuang, L. Jiao, "SAR image segmentation using quantum clonal selection clustering," in Asian-Pacific Conference on Synthetic Aperture Radar Xian, Shanxi, 2009, pp. 817-820.*

*[143] S. P. Gou, X. Zhuang, L. C. Jiao, "Quantum Immune Fast Spectral Clustering for SAR Image Segmentation,"[J] IEEE Geoscience and Remote Sensing Letters, vol. 9, pp. 8-12, 2012."*

# SAR Image Statistical Modeling Part I: Single-Pixel Statistical Models

Dong-Xiao Yue, *Student Member, IEEE*, Feng Xu, *Senior Member, IEEE*, Alejandro Frery, *Senior Member, IEEE*, Ya-Qiu Jin, *Fellow, IEEE*

***Abstract*—With the rapid development of spaceborne SAR technology and the acquisition of large volume of SAR images, SAR image interpretation has become an urgent and difficult research topic. SAR image statistical modeling is one of the theoretical foundations for SAR image interpretation. It is of great value for the in-depth analysis of SAR images. This paper reviews the major development of SAR image statistical modeling since the beginning, including more than 20 statistical distributions of 8 statistical models, and gives their derivations and expressions, which can be used as a basic reference for statistical modeling of SAR images.**

***Index Terms*—Synthetic Aperture Radar, Speckle, Texture, Statistical Modeling**

# 1 Introduction

## 1.1 *Background*

Synthetic Aperture Radar (SAR) has become an important tool for land survey, resource mapping, environment monitoring, disaster rescue and national security due to its all-time, all-weather, high-penetration and high-resolution imaging capability at the global scale. SAR systems have evolved from low resolution to high resolution, single polarization (single-pol) to full polarization (full-pol), single temporal to multi-temporal, and single incidence to multiple incidences, among other features. There is a huge volume of archived SAR images, constantly increasing by new observations on a daily basis. Computerized automated SAR image interpretation has become a key research direction to enhance the application-value of SAR data [1, 2].
SAR imagery contains a wealth of information about the target and scene under observation. There are many methods for analyzing SAR images. As shown in Figure 1, there are mainly two categories depending on their theoretical foundations, i.e. one is the electromagnetic (EM) physics methods based on Maxwell's equations [3], the other is the statistical method focusing on the image itself.

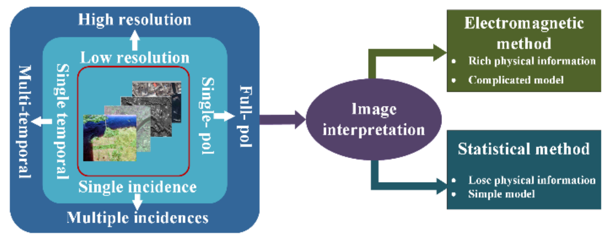


*Figure 1: SAR technological development and SAR image interpretation*

EM-based physics methods have a clear physical meaning of electromagnetic scattering. However, due to its high complexity, both theoretical and computational, only simplified or empirical models can be established for specific scenarios. The statistical method is based on the distributional characteristics of pixel values and their relationships. It only considers the high-level cognitive characteristics of the image, but does not necessary take into account the actual scattering and imaging mechanism. This approach is often easier to model and solve, but often ignores the underlying physical process that gave rise to the images.
Figure 2 lists the categories of these two main methods. The development of EM method has gone through three stages: experimental EM before 1864, classical EM from 1864 to 1950 and the computational EM after 1950. The statistical method can be summarized into two types: coherent scatterer model and empirical models.

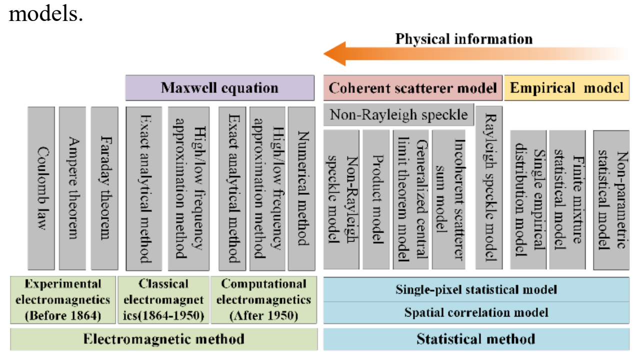


*Figure 2: Details of the two main categories of SAR image analysis*

With the newly emerging SAR technologies, SAR data are becoming high-resolution, multi-dimension and multi-modes. In order to realize automatic interpretation of new SAR data, it is desirable to

Manuscript received xxx; revised xxx...
This work was supported in part by Natural Science Foundation of China no. 61991422 and 61822107.

D.-X. Yue, F. Xu and Y.-Q. Jin are with the Key Laboratory for Information Science of Electromagnetic Waves (MoE), Fudan University, Shanghai, China 200433; A. Frery is with Universidade Federal de Alagoas, Brazil (Corresponding author: Feng Xu, fengxu@fudan.edu.cn).

combine the advantages of both EM physics and statistical method, e.g., to simplify the EM scattering model from a statistical point of view and to use image processing methods for auxiliary analysis. In view of this critical needs, this paper attempts to review the statistical modeling of SAR images with the perspective of physics modeling, including two parts: single-pixel statistical modeling, and spatial correlation statistical modeling.

Statistical analysis of SAR images can be traced back to the 1950s [4, 5]. The earliest statistical analysis was based on ocean SAR clutter. Due to the low resolution of early radar images, the Rayleigh speckle model was established under the assumption of the Central Limit Theorem, leading to the Rayleigh distribution for the amplitude of radar echoes [4, 6, 7]. However, with the improvement of SAR image resolution, the Rayleigh model became less accurate. Therefore, based on the random walk model [8], the non-Rayleigh speckle model [9] was proposed leading to more expressive models such as the K distribution [10], and the incoherent scatterer sum model [11-13], which was used in SAR clutter simulation. Also, empirical probability distributions with more parameters, such as the log-normal and Weibull distributions, were used to accurately describe non-Rayleigh clutters of some specific scenarios.

In 1981, Ward proposed the product model [14], a turning point in the study of SAR statistical modeling. The product model can be regarded as a generalization of the Rayleigh speckle model. Its derivation is much simpler than the non-Rayleigh speckle model based on the random walk model. Thus, it has been widely studied and applied, and inspired the proposal of many classical SAR statistical distribution models. The product model is still the most popular model for SAR image statistical modeling. However, with the further improvement of resolution, SAR images contain more and more details of terrain objects and manmade targets. The relatively simple statistical models are no longer capable of fully describing the data. Therefore, the finite mixture statistical model [15, 16], the non-parametric method model [17-19] and the generalized central limit theorem model [20-22] have been proposed successively. However, the modeling of SAR images from the statistical distribution of image pixel values cannot fully describe the scattering information embedded in SAR images. Such approaches ignore the EM physics, impairing limitations to SAR image interpretation. In recent years, the research on high-resolution SAR image statistical modeling has refocused on the physical process of EM scattering. As a consequence, the early non-Rayleigh speckle model based on scattering process modeling [9, 10, 23] reclaims a prominent position. Figure 3 illustrates the development of the SAR image statistical models reviewed in this paper.

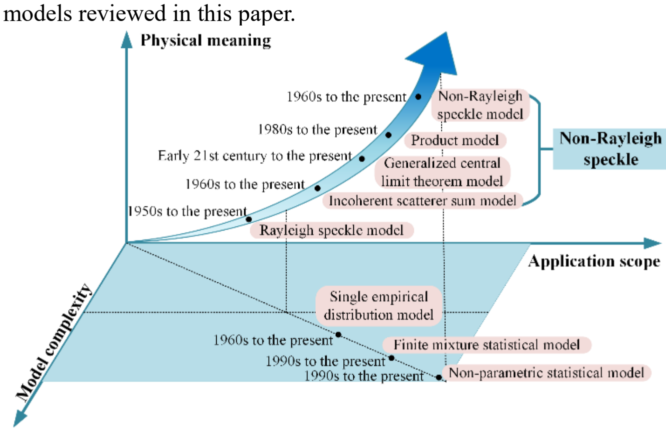


*Figure 3: Development of SAR data statistical models*

The statistical modeling for SAR image can be divided into two parts: single-pixel statistical modeling, and spatial correlation modeling. This part studies the single-pixel statistical modeling. More than 20 probability distributions of 8 statistical modeling methods are reviewed, and the methods of model selection and parameter estimation are briefly introduced. The spatial correlation modeling part introduces 3 kinds of correlation analysis of SAR images and the related clutter simulation methods [24].

The statistical modeling of single pixel can be mainly categorized into coherent scatterer model introduced in Section 2 and empirical model in Section 3. Section 4 gives several model assessment and parameter estimate methods. Section 5 comes to the conclusion.

In more detail, Figure 4 shows the various statistical models and their relationships as reviewed in this paper. The coherent scatterer model is a classical model for speckle [25], which is also referred to as "discrete scatterer model" in [1]. Here, we call it "coherent scatterer model" just to emphasize the nature of coherent superposition, as opposed to the incoherent scatterer sum model which will be introduced later. The coherent scatterer model based on random walk is reviewed in Section 2.1. It models the coherent EM field summation effect and, thus, its derived distributions are determined by the number, amplitude and phase of the scatterers located in a single resolution cell [9, 25]. If taking the assumption that 1) the number of scatterers is constant but approaches infinite, 2) the scatterer amplitude is constant, 3) the scatterer phase is uniformly distributed, and 4) there is collective independence among the random variables, then the coherent scatterer model can be simplified as the Rayleigh speckle model which is known to fit well homogeneous regions (Section 2.2) [1, 2]. For the Rayleigh speckle model, it is found that the speckle can also be seen as a multiplicative noise that is applied on the RCS of a uniform scene. The multiplicative property can be further generalized into inhomogeneous scenes, and a widely applicable product model can be obtained (Section 2.3) [2, 14].

As opposed to the Rayleigh speckle model, the original, and more general, coherent scatterer model gives rise to non-Rayleigh speckle, i.e. without taking the Rayleigh assumptions [9]. non-Rayleigh speckle covers the statistical modeling developed from the coherent scatterer model whose amplitude does not follow the Rayleigh distribution including the product model, non-Rayleigh speckle model, generalized central limit theorem model and incoherent scatterer sum model. Section 2.4 introduces the non-Rayleigh speckle model, which can be applied to heterogeneous regions. The non-Rayleigh speckle model can be degenerated into the generalized central limit theorem model under the assumption that 1) the real and imaginary components of the scattered field obey distributions with infinite variance and 2) the number of scatterers is an infinite constant [20-22, 26] (Section 2.5). In the coherent scatterer model, when the phase is uniformly distributed, the coupling term caused by the scattering phase can be neglected, then an approximate model, i.e., the incoherent scatterer sum model, can be obtained [11-13, 27, 28] (Section 2.6). The incoherent scatterer sum model can be used for correlated clutter simulation. It was once referred to as the surface model [11, 12]. Here, we do not use this convention as to avoid confusion with 'rough surface model' in EM scattering theory.

Section 3 introduces the statistical approach based on empirical models . These models no longer consider the scattering process, but only fit the statistics of the pixel. The main idea is to establish a statistical distribution that can better fit observed SAR image data. Depending on whether there exist analytical expressions and whether the model is elaborate, empirical models can be divided into single empirical distribution, finite mixture, and non-parametric. The single empirical distribution model uses one suitable probability distribution [1]. The finite mixture statistical model [29, 30] is a semi-parametric model that employs with multiple probability distributions. It involves more parameters than the single distribution model, but has a wider range of applications. Both models have analytical expressions. The non-parametric approach uses general mathematical models to fit real SAR images, such as the Parzen window method [31], neural networks [18, 32, 33], and support vector machines (SVM) [19]. The non-parametric approach is usually elaborate and has no analytical expressions.

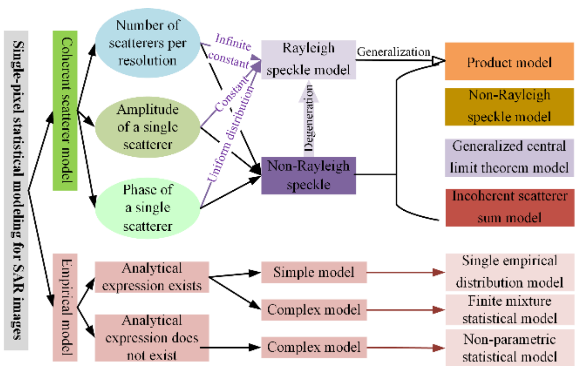


Figure 4: The framework of single-pixel statistical modeling

### 1.2 *Notation and definition*

If not otherwise specified, the notations employed in this paper are defined as follows:
$N$: the number of scatterers per resolution cell;
$\boldsymbol{E}$: complex scattered field per resolution cell;
$A$: amplitude of the scattered field $\boldsymbol{E}$;
$a$: amplitude of a single scatterer;
$\theta$: phase of the scattered field $\boldsymbol{E}$;
$\phi$: phase of a single scatterer;
$\mathfrak{R}$: the real part of the scattered field $\boldsymbol{E}$;
$\mathfrak{I}$: the imaginary part of the scattered field $\boldsymbol{E}$;
$\sigma$: for the model not taking into account the imaging function, it denotes the intensity of scattered field $\sigma = A^2$; but for the model taking into account imaging function, it denotes the radar cross section (RCS), while the intensity is denoted by $I$;
$A_n$: amplitude of the scattered field after $n$-look multilooking;
$\sigma_n$: intensity of the scattered field after $n$-look multilooking;
$Z$: SAR image pixel value, $Z_A = X_A Y_A$ denotes the pixel amplitude, $Z_I = X_I Y_I$ denotes the pixel intensity;
$X$: RCS, $X_A$ denotes amplitude of RCS, $X_I$ denotes intensity of RCS;
$Y$: speckle, $Y_A$ denotes its amplitude, $Y_I$ denotes its intensity;
$I$: intensity of image pixel for models taking into account imaging function;
$\mathrm{E}[\cdot]$ or $\langle\cdot\rangle$: expectation of a random variable;
$\mathrm{Mean}(\cdot)$: the mean of a random variable;
$\mathrm{Var}(\cdot)$: the variance of a random variable;
$C$: coefficient of variation (CV);
Note that **bold** version of these symbols denote the corresponding vector or matrix form.

# 2 Statistical modeling based on coherent scatterer model

### 2.1 *Coherent scatterer model*

Assuming $N$ discrete ideal point scatterers in a resolution cell, the backscattering field contribution of the $i$-th scatterer ($i = 1,2,\dots,N$) is [34]

$$E_i = K_i a_i cos(\omega t - 2kr_i + \theta_i), \tag{1}$$

where $K_i$ is the constant related to radar system such as free space propagation loss, antenna gain, etc.; $a_i$ denotes the $i$-th scatterer amplitude; $\theta_i$ denotes $i$-th scatterer phase; $r_i$ denotes the distance between the antenna and the scatterer; $k = 2\pi/\lambda$ is the wavenumber; $\omega$ denotes angular frequency. In free space, $k = \omega\sqrt{\mu_0\varepsilon_0} = \omega/c$, where $c$ denotes the speed of light.
The phasor-domain counterpart of Eq. (1) is:

$$\boldsymbol{E}_i = K_i a_i e^{j\phi_i}, \qquad \phi_i = \theta_i - 2kr_i, \tag{2}$$

where $\phi_i$ denotes the phase angle of $\boldsymbol{E}_i$.
Consider the following assumptions [34]:
Assumption (1): The scatterers per resolution are statistically independent, and the interaction between adjacent scatterers can be ignored. Then the total instantaneous field $\boldsymbol{E}$ can be expressed as a coherent superposition:

$$\boldsymbol{E} = \sum_{\mathrm{i}=1}^{N} K_i a_i e^{j\phi_i}. \tag{3}$$

Assumption (2): The maximum distance between targets $\Delta r = |r_i - r_j|_{\max}$ is far less than the average distance between the antenna and targets; the antenna gain is uniform across the illuminated area, e.g. $K_i = K, i = 1,2,\dots,N$. For convenience, we shall set $K = 1$, then:

$$\boldsymbol{E} = \sum_{i=1}^{N} a_i e^{j\phi_i} = Ae^{j\theta}, \tag{4}$$

where $A$ and $\theta$ are the amplitude and phase of $\boldsymbol{E}$ respectively.
As shown in Eq. (4) , if the above two assumptions are satisfied, the complex scattered field $\boldsymbol{E}$ can be modeled as a random walk model in the complex plane and it can be expressed as the summation of the scattered contributions of $N$ independent scatterers in a resolution cell. This is called "coherent scatterer model", also known as the discrete scatterer model in [1].
According to the coherent scatterer model in Eq. (4), it can be seen that the probability distribution of the observation in a resolution cell is mainly determined by four factors:
(a) The spatial fluctuation distribution of scatterer amplitude $a_i$ in a resolution cell [9]. For simplicity, it is generally assumed that such amplitudes are independent identically distributed, as 1) constant, 2) variable, or 3) a sum of a known constant and an infinite number of variables. For complex scenes, it needs to be modeled as a finite mixture of multiple scatterers [35].
(b) The number $N$ of scatterers in a resolution cell. This quantity can be either fixed across resolution cells, or a random variable. In either case, it can be finite or infinite.
(c) The distribution of scatterer phase $\phi_i$ in a resolution cell. It can be modeled as uniform distribution or non-uniform distribution.
(d) The correlation between the amplitude $a_i$ and phase $\phi_i$ and the complex correlation among the scatterers in a resolution cell also contributes to the final single-pixel probability distribution. For simplicity, it is usually assumed that the amplitudes and phases are collectively independent. This hypothesis is assumed true throughout this paper.
The single-pixel statistical modeling based on the coherent scatterer model can be classified into Rayleigh and non-Rayleigh speckle, according to these four factors. The Rayleigh speckle model can be generalized to the product model. The non-Rayleigh speckle includes the product model, non-Rayleigh speckle model, generalized central limit theorem model and incoherent scatterer sum model. The statistical modeling of SAR images under these models will be introduced in Sections 2.2 to 2.6.

## 2.2 *Statistical modeling based on Rayleigh speckle*

The Rayleigh speckle model is used to describe the scattering echoes from a uniform region [1, 2, 34]. The model simplifies the coherent scatterer model by adopting the central limit theorem. In this section, we firstly derive the Rayleigh speckle model based on the coherent scatterer model. We then introduce the statistical distribution of single-look/multi-look amplitude and intensity of the scattered field.

### 2.2.1 *Rayleigh speckle model*

The Rayleigh speckle model is established when the coherent scatterer model in Eq. (4) satisfies the following assumptions [4, 34]:

**Assumption (1)**: The amplitudes and phases $(a_1,\phi_1),(a_2,\phi_2),\dots,(a_N,\phi_N)$ are collectively independent.

**Assumption (2)**: Since $\phi_i=\theta_i-2kr_i$ is a random variable determined by $r_i$, then $a_i$ and $r_i$ are also independent; this is the same as assuming randomly positioned scatterers.

**Assumption (3)**: The scattered amplitudes $a_1,a_2,\dots$ are independently identically distributed with finite first and second moments, which ensures that there are no dominant scatterers in a resolution cell.

**Assumption (4)**: The scatterers are randomly located and the maximum distance $\Delta r$ is far greater than the wavelength, so the scatterer phase $\phi_i$ is uniformly distributed in $(-\pi,\pi]$.

**Assumption (5)**: The number $N$ of scatterers is infinitely large.

The real and imaginary components of the scattered field in Eq. (4) are expressed as:

$$\Re=\mathrm{Re}\{\boldsymbol{E}\}=\sum_{i=1}^{N}a_i\cos\phi_i\text{, and}$$
$$\Im=\mathrm{Im}\{\boldsymbol{E}\}=\sum_{i=1}^{N}a_i\sin\phi_i. \tag{5}$$

The first order moments of $\Re$ and $\Im$ can be derived using assumptions (1-4) [25, 36] :

$$\begin{aligned}\mathrm{E}[\Re]&=\mathrm{E}\left[\sum_{i=1}^{N}a_i\cos\phi_i\right]=\sum_{i=1}^{N}\mathrm{E}[a_i\cos\phi_i]\\&=\sum_{i=1}^{N}\mathrm{E}[a_i]\mathrm{E}[\cos\phi_i]=0\text{, and}\\ \mathrm{E}[\Im]&=\mathrm{E}\left[\sum_{i=1}^{N}a_i\sin\phi_i\right]=\sum_{i=1}^{N}\mathrm{E}[a_i\sin\phi_i]\\&=\sum_{i=1}^{N}\mathrm{E}[a_i]\mathrm{E}[\sin\phi_i]=0,\end{aligned} \tag{6}$$

where $\mathrm{E}[\cdot]$ denotes expectation. Similarly, the second order moments of $\Re$ and $\Im$ are [25, 36]:

$$\begin{aligned}\sigma_{\Re}^2&=\sum_{i=1}^{N}\sum_{k=1}^{N}\mathrm{E}[a_ia_k]\mathrm{E}[\cos\phi_i\cos\phi_k]\\&=\sum_{i=1}^{N}\mathrm{E}\left[a_i^2\right]\mathrm{E}[\cos^2\phi_i]\\&=\sum_{i=1}^{N}\frac{\mathrm{E}\left[a_i^2\right]}{2}\text{, and}\\ \sigma_{\Im}^2&=\sum_{i=1}^{N}\sum_{k=1}^{N}\mathrm{E}[a_ia_k]\mathrm{E}[\sin\phi_i\sin\phi_k]\\&=\sum_{i=1}^{N}\mathrm{E}\left[a_i^2\right]\mathrm{E}[\sin^2\phi_i]=\sum_{i=1}^{N}\frac{\mathrm{E}\left[a_i^2\right]}{2},\end{aligned} \tag{7}$$

where $\sigma_{\Re}$ and $\sigma_{\Im}$ denote the standard variation of $\Re$ and $\Im$, respectively.

The correlation between $\Re$ and $\Im$ is [25] :

$$\rho_{\Re,\Im}=\mathrm{E}[\Re\Im]=\sum_{i=1}^{N}\mathrm{E}\left[a_i^2\right]\mathrm{E}[\cos\phi_i\sin\phi_i]=0. \tag{8}$$

Assumption (5) allows us to use the central limit theorem, thereby $\Re$ and $\Im$ are Gaussian distributed random variables with zero mean and the same variance $\sigma/2$. Then the joint probability density function of $\Re$ and $\Im$ is [25] :

$$p_{\Re,\Im}(\Re,\Im)=\frac{1}{\pi\sigma}e^{-\frac{\Re^2+\Im^2}{\sigma}}. \tag{9}$$

### 2.2.2 *Statistical distributions*

The probability distributions of amplitude $A$ and intensity $\sigma$ then can be derived from Eq. (9) by variable substitution and integrating with respect to the phase [25]. The definition, distribution type as well as the probability density function (PDF), and the statistical characteristics of intensity image are summarized in Table 1.

The image generated by replacing $n$ pixels with a new pixel bearing their average value is called an $n$-look image. The $n$-look statistics of amplitude and intensity are also listed in Table 1. The coefficient of variation (CV), denoted as $C$, is defined as the ratio of the standard derivation to the mean [25]:

$$C=\frac{\sqrt{\text{variance}}}{\text{mean}}. \tag{10}$$

It is an important parameter that reflects the characteristics of the speckle pattern and is a measure of the intensity (or amplitude) fluctuation relative to the average intensity (or amplitude). In intensity, $C$ is a constant between $0$ and $n^{-1/2}$. If the observations are all equal, then $C=0$; as the roughness of target increases, the speckle gradually changes from partial developed to fully developed speckle, and $C$ gradually increases. If the target surface is very rough, the fluctuation of speckle is of the same order as the average value and $C=1$, which is called "fully developed speckle" [2, 25]. Notice that this discussion about $C$ is valid only on areas where the variance of the real and imaginary parts of the scattered field does not change from pixel to pixel.

## 2.3 *Statistical modeling based on the product model*

The assumptions in the Rayleigh speckle model limit the scope of application to homogenous regions but are not valid for inhomogeneous areas. The product model in this section is able to characterize inhomogeneous areas and provides a wealth of room for their statistical modeling. This section first introduces the product model, and then summaries the statistical distributions developed by the product model.

### 2.3.1 *Product model*

The product model was proposed by Ward in 1981 [14], which considers SAR image observations as the product of the RCS with uncorrelated speckle noise. It can be seen as a generalization of the Rayleigh speckle model describing a uniform scene. The Rayleigh speckle model can be seen as a multiplication of a constant RCS with a square root gamma distribution or a gamma distribution. The product model simplifies the analysis of statistical modeling of SAR images. The rationality and accuracy of the product model will be discussed in Section 2.3.3. Figure 5 shows a schematic of the product model.

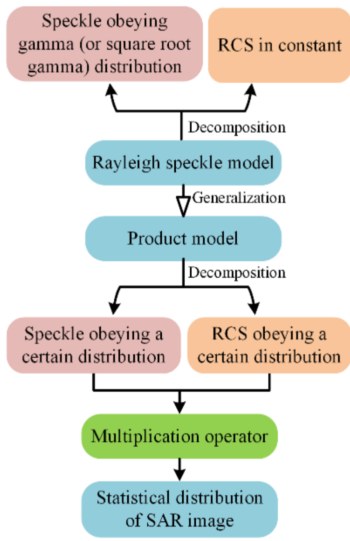


*Figure 5: Schematic of the product model*

The mathematical representation of the product model is [1, 2, 14, 37]:

$$Z = X \cdot Y, \tag{11}$$

where $Z$ denotes the observed value; $X$ denotes RCS; $Y$ denotes speckle, $X_A, X_\sigma$ denote the amplitude and intensity of RCS, respectively; and $Y_A, Y_\sigma$ denote the amplitude and intensity of speckle, respectively.

### 2.3.2 *Statistical distributions*

Figure 6 shows the modeling process of intensity statistical distributions based on the product model. The product model models the SAR image intensity as the product of speckle and RCS, therefore, the statistical distribution of intensity can be modeled by separately analyzing the statistical distribution of the speckle component and the RCS component. The "Yellow shading box with embedded product operator" in Figure 6 denotes the "Product model" which has two inputs, i.e. the statistical distribution of speckle and RCS, and outputs the distribution of SAR image intensity.

As shown in Figure 6, the speckle component can be modeled as negative exponential distribution for single-look intensity image and gamma distribution for multi-look intensity image when the central limit theorem is satisfied. The speckle component can be modeled as generalized gamma distribution when the central limit theorem is not satisfied.

The RCS component also has multiple different modeling methods depending on different physical scenarios:

(a) The RCS is considered as a constant for homogenous area. The Rayleigh speckle model can be obtained if the central limit theorem is satisfied according to the product model shown in Figure 6.

(b) For inhomogeneous area, the RCS can be modeled as generalized gamma distribution, generalized inverse Gaussian distribution, Beta distribution of the first kind and Beta distribution of the second kind [23]. And the generalized inverse Gaussian distribution can be degenerated into inverse Gaussian distribution, gamma distribution and inverse gamma distribution under certain conditions.

As shown in Figure 6, under the product model, 1) generalized compound distributed (GC distribution) SAR images can be obtained when the RCS obeys the generalized gamma distribution and the speckle obeys the generalized gamma distribution [38-40]; 2) The SAR image obeying the $G$ distribution can be obtained by the RCS obeying the generalized inverse Gaussian distribution and the speckle obeying the gamma distribution. The $G$ distribution can be degenerated into $G^h$ distribution, $K$ distribution and $G^0$ distribution under certain conditions [41]; 3) $U$-distributed SAR images can be obtained by the RCS obeying Beta distribution of the second kind and gamma-distributed speckle [23]; 4) The SAR image obeying $W$ distribution can be obtained by the RCS obeying the first kind of Beta distribution and the speckle obeying gamma distribution [23]. $K$ distribution, $G^0$ distribution, $U$ distribution and $W$ distribution are all probability distributions belonging to the Pearson system [42-44].

The distribution functions and related statistical characteristics based on the product model are summarized in Table 2 which will be introduced in the following. Since the $U$ distribution and the $W$ distribution can also be modeled under the non-Rayleigh speckle model, they will be introduced in detail in Section 2.4.2 and will not be introduced here.

*Table 1: Statistical distribution and characteristics of the Rayleigh speckle model*

| | Definition | Distribution type | Probability density function (PDF) | Mean | Variance | Coefficient of variation (CV) |
|---|---|---|---|---|---|---|
| **Intensity** | $\sigma = A^2$ | Negative exponential distribution | $p(\sigma) = \frac{1}{\sigma}\exp\left(-\frac{\sigma}{\sigma}\right)$ | $\sigma$ | $\sigma^2$ | 1 |
| $\boldsymbol{n-}$**look intensity** | $\sigma_n = \frac{1}{n}\sum_{\ell=1}^{n}\sigma(\ell)$ | Gamma distribution | $p(\sigma_n) = \frac{1}{\Gamma(n)}\left(\frac{n}{\sigma}\right)^n \sigma_n^{n-1}\exp\left(-\frac{n\sigma_n}{\sigma}\right)$ | $\sigma$ | $\frac{\sigma^2}{n}$ | $\frac{1}{\sqrt{n}}$ |

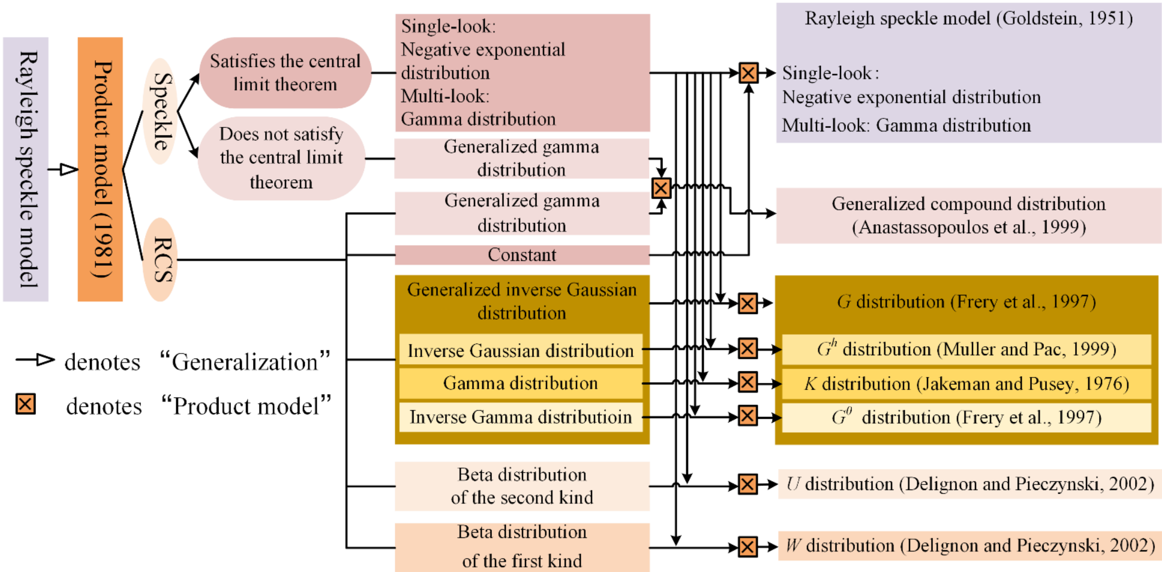


*Figure 6: Statistical distributions of scattered intensity based on product model*

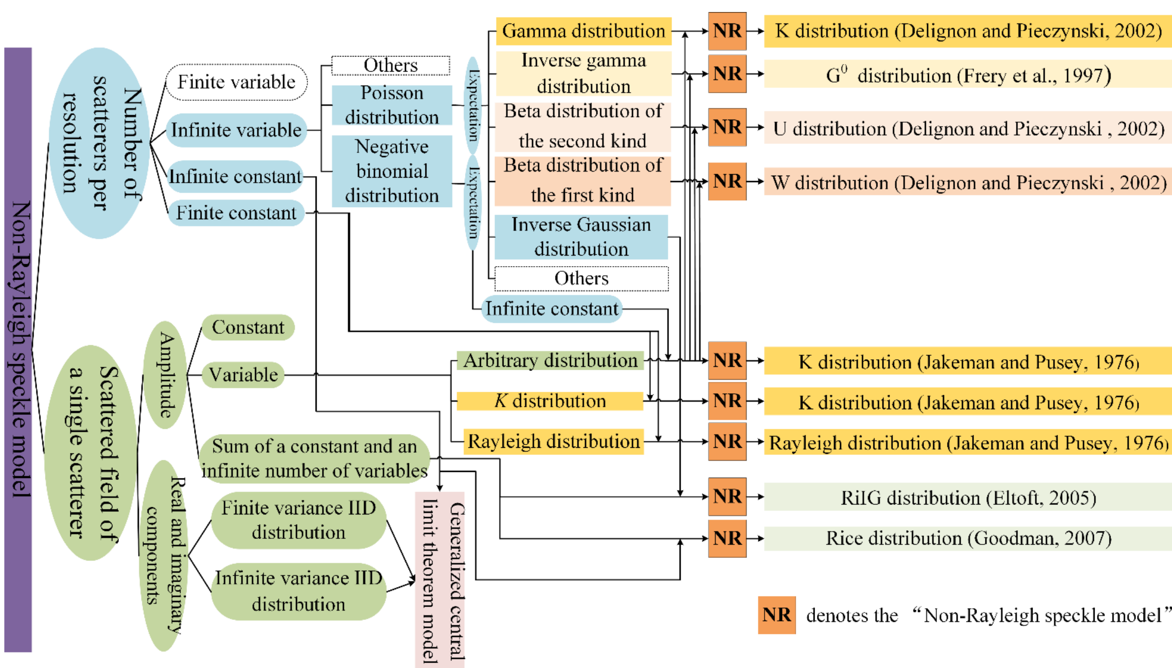


*Figure 7 Statistical distributions of scattered intensity based on non-Rayleigh speckle model*

*Table 2: Statistical distribution and characteristics of product model for intensity data*

| Distribution type | PDF of RCS $p(X_\sigma = x)$ | PDF of Speckle $p(Y_\sigma = y)$ | PDF of SAR image $p(Z_\sigma = z)$ | $r-$order moment $\mathrm{E}\{Z_\sigma^r\}$ |
|---|---|---|---|---|
| Gamma distribution [1] | $p_C$ | $p_\Gamma$ | $p_{\mathrm{Gamma}_\sigma}(Z_\sigma = z; n, \sigma) = \frac{1}{\Gamma(n)}\left(\frac{n}{\sigma}\right)^n z^{n-1}\exp\left(-\frac{nz}{\sigma}\right)$ | $\mathrm{E}\{Z_\sigma^r\} = \frac{\Gamma(n+r)}{\Gamma(n)}\left(\frac{\sigma}{n}\right)^r$ |
| $G$ distribution [43,44] | $p_{GIG}$ | | $p_{G_\sigma}(Z_\sigma = z; \beta, \gamma, \alpha, n) = \frac{n^n(\beta/\gamma)^{\alpha/2} z^{(n-1)}}{\Gamma(n)K_\alpha(2\sqrt{\beta\gamma})}\left(\frac{\gamma+nz}{\beta}\right)^{\frac{\alpha-}{2}}$ | $E\{Z_\sigma^r\} = \left(\frac{\gamma}{n^2\beta}\right)^{\frac{r}{2}}\frac{K_{\alpha+r}(2\sqrt{\beta\gamma})\Gamma(n+r)}{K_\alpha(2\sqrt{\beta\gamma})\Gamma(n)}$ |
| $K$ distribution [2,43] | $p_{\mathrm{Gamma}}$ | | $p_{K_\sigma}(Z_\sigma = z; \beta, \alpha, n) = \frac{2\beta n}{\Gamma(n)\Gamma(\alpha)}(\beta nz)^{\frac{\alpha+n}{2}-1}K_{\alpha-n}(2\cdot$ | $\mathrm{E}\{Z_\sigma^r\} = (n\beta)^{-r}\frac{\Gamma(n+r)\Gamma(\alpha+r)}{\Gamma(n)\Gamma(\alpha)}$ |
| $G^0$ distribution [43] | $p_{\mathrm{Gamma}^{-1}}$ | | $p_{G_\sigma^0}(Z_\sigma = z; \gamma, -\alpha, n) = \frac{n^n\Gamma(n-\alpha)\gamma^{-\alpha}z^{n-1}}{\Gamma(n)\Gamma(-\alpha)(\gamma+nz)^{n-\alpha}}$ | $\mathrm{E}\{Z_\sigma^r\} = (\gamma/n)^r\frac{\Gamma(n+r)\Gamma(-\alpha-r)}{\Gamma(n)\Gamma(-\alpha)}$ |
| $G^h$ distribution [43,45] | $p_{\mathrm{IG}}$ | | $p_{G_\sigma^h}(Z_\sigma = z; \lambda, \mu) = \sqrt{\frac{2\lambda}{\pi}}e^{\sqrt{\frac{\lambda^2}{\mu}}}\frac{n^n z^{n-1}}{\Gamma(n)}\left(\frac{(\lambda+2nz)\mu}{\lambda}\right. \times K_{n+\frac{1}{2}}\left(\frac{(\lambda+2nz)\lambda}{\mu}\right)$ | $E\{Z_\sigma^r\} = \sqrt{\frac{2\lambda}{\pi}}\left(\frac{\mu}{n^2}\right)^{\frac{r}{2}}e^{\sqrt{\frac{\lambda^2}{\mu}}}\mu^{-\frac{1}{4}} \times \frac{K_{r-1/2}(\lambda/\sqrt{\mu})\Gamma(n+r)}{\Gamma(n)}$ |
| GC distribution [38] | $p_{G\Gamma}$ | $p_{G\Gamma}$ | $p_{GC_\sigma}(Z_\sigma = z; a, b_1, v_1, b_2, v_2) = \frac{b_1 b_2}{2z\Gamma(v_1)\Gamma(v_2)}\frac{\sqrt{z}^{b_1 v_1}}{a^{b_2 v_2}}\int_0^\infty x^{b_2 v_2} \times \exp\left[-\left(\frac{x}{a}\right)^{b_2} - \left(\frac{\sqrt{z}}{x}\right)^{b_1}\right]dx$ | $\mathrm{E}\{Z_\sigma^r\} = a^{2r}\frac{\Gamma(\frac{2r}{b_1}+v_1)\Gamma(\frac{2r}{b_2}+v_2)}{\Gamma(v_1)\Gamma(v_2)}$ |

**Notes and Supplements**

Without special explanation, the symbols in this table above are defined as follows: $n$ is the number of look, the special function $K_n(\cdot)$ is the second type of modified Bessel function, $\Gamma(\cdot)$ is the gamma function, $X_\sigma$ denotes the RCS, and $Y_\sigma$ denotes the speckle. $Z_\sigma = X_\sigma \cdot Y_\sigma$ denotes the SAR intensity image.

(1) The detailed expressions in the second column, i.e. Probability density function (PDF) of RCS, are:

$$p_C(X_\sigma = x; \sigma) = \begin{cases} 1, x = \sigma \\ 0, \text{others} \end{cases}; \ \sigma > 0,$$

$$p_{GIG}(X_\sigma = x; \beta, \gamma, \alpha) = \frac{\left(\frac{\beta}{\gamma}\right)^{\frac{\alpha}{2}}}{2K_\alpha(2\sqrt{\beta\gamma})}x^{(\alpha-1)} \times e^{-\left(\beta x + \frac{\gamma}{x}\right)}; \alpha \in R, (\beta, \gamma) \in \Theta_\alpha; \Theta_\alpha = \begin{cases} \{(\beta,\gamma): \beta > 0, \gamma \geq 0\} & if \ \alpha > 0 \\ \{(\beta,\gamma): \beta > 0, \gamma > 0\} & if \ \alpha = 0, \\ \{(\beta,\gamma): \beta \geq 0, \gamma > 0\} & if \ \alpha < 0 \end{cases}$$

$$p_{\mathrm{Gamma}}(X_\sigma = x; \beta, \alpha) = \frac{\beta^\alpha}{\Gamma(\alpha)}x^{(\alpha-1)}e^{-\beta x}; \beta, \alpha > 0,$$

$$p_{\mathrm{Gamma}^{-1}}(X_\sigma = x; \alpha, \gamma) = \frac{\gamma^{-\alpha}}{\Gamma(-\alpha)}x^{\alpha-1}e^{-\gamma/x}; -\alpha, \gamma > 0,$$

$$p_{\mathrm{IG}}(X_\sigma = x; \mu, \lambda) = \left[\frac{\lambda}{2\pi x^3}\right]^{1/2} \times \exp\left[-\lambda\left(\frac{x}{2\mu} + \frac{1}{2x}\right)\right]; \mu \geq 0, \lambda > 0,$$

$$p_{G\Gamma}(X_\sigma = x; a, b_2, v_2) = \frac{b_2}{2\sqrt{x}a\Gamma(v_2)}\left(\frac{\sqrt{x}}{a}\right)^{b_2 v_2 - 1} \times \exp\left[-\left(\frac{\sqrt{x}}{a}\right)^{b_2}\right]; a, b_2, v_2 > 0.$$

(2) The detailed expressions in the third column, i.e. PDF of Speckle, are gamma distributed speckle $Y_\sigma \sim \mathrm{Gamma}(n, n)$, which is

$$p_\Gamma(Y_\sigma = y) = \frac{2n^n}{\Gamma(n)}y^{2n-1}\exp(-ny^2), y, n > 0,$$

and generalized gamma distributed speckle $Y_\sigma \sim \mathrm{G\Gamma}(b_1, v_1)$, which is:

$$p_{G\Gamma}(Y_\sigma = y) = \frac{b_1}{2\Gamma(v_1)}y^{\frac{b_1 v_1}{2}-1}\exp\left[-y^{\frac{b_1}{2}}\right]; b_1, v_1 > 0$$

### *a) Gamma distribution*

The square root gamma distribution is used to describe the multi-look amplitude images of homogenous areas [1], which has been derived from the Rayleigh speckle model in Section 2.2.2. It can be re-modeled as the product of the RCS and speckle under the product model. For the intensity image, if the RCS intensity is a constant $X_\sigma = \sigma$, the multi-look speckle intensity $Y_\sigma$ obeys the gamma distribution $Y_\sigma \sim \mathrm{Gamma}(n, n)$, and then the image intensity $Z_\sigma$ obeys the gamma distribution according to the product model. According to the statistical moment in the Table 2, when the number of looks $n$ is known, the second-order sample moment $\hat{m}_2$ can be used to estimate the parameter: $\hat{\sigma} = \hat{m}_2$.

### *b) $G$ distribution*

The $G$ distribution was proposed by Frery et al. in 1997 [45] using the product model to describe the statistical characteristics of inhomogeneous areas. In this model, the RCS intensity obeys the generalized inverse Gaussian distribution $X_\sigma \sim \mathrm{GIG}(\beta, \gamma, \alpha)$ [46] and the speckle obeys the gamma distribution. According to the product model, the SAR image intensity $Z_\sigma$ obey the $G_\sigma$ distribution.

*c) **K** distribution*

The $K_\sigma$ distribution is a classical statistical distribution model describing inhomogeneous regions [2, 45]. The $K_\sigma$ distribution can be derived based on several different modeling methods. The modeling under the product model is described here and other modeling methods will be detailed in Section 2.4.2. The $K_\sigma$ distribution can also be seen as a special case of the $G_\sigma$ distribution under the condition that $\gamma \to 0$ [45]. At this time, the RCS amplitude distribution is degenerated from the generalized inverse Gaussian distribution to the gamma distribution $X_\sigma \sim \mathrm{Gamma}(\beta, \alpha)$,. Then the $K_\sigma$ distribution of intensity image are obtained shown in the Table 2.

If the number of looks $n$ is known, when $r = 1/2,\ 1$, the sample moments $\widehat{m}_{1/2}, \widehat{m}_1$can be used to estimate the distribution parameters $\alpha, \beta$ by solving the following system of equations:

$$\frac{\Gamma(n+1/2)\Gamma(\hat{\alpha}+1/2)\Gamma(n)\Gamma(\hat{\alpha})}{\Gamma^2(n+1/4)\Gamma^2(\hat{\alpha}+1/4)} - \frac{\widehat{m}_1}{\widehat{m}_{\frac{1}{2}}^2} = 0,$$
$$\hat{\beta} = \frac{1}{n}\left(\frac{\Gamma(n+1/2)\Gamma(\hat{\alpha}+1/2)}{\Gamma(n)\Gamma(\hat{\alpha})\widehat{m}_1}\right)^2. \tag{12}$$

*d) **$G^0$** distribution*

The $G_\sigma^0$ distribution is also a statistical distribution describing the inhomogeneous regions [45]. When $\beta \to 0,\ \alpha < 0, \gamma > 0$, the $G_\sigma$ distribution can be degenerated into a $G_\sigma^0$ distribution. Under the product model, If the RCS intensity obeys the inverse gamma distribution $X_\sigma \sim \mathrm{Gamma}^{-1}(\alpha, \gamma)$, the speckle obeys a Gamma distribution, then the intensity $Z_\sigma$ distribution of the SAR image obey and $G_\sigma^0$ distribution. The parameters of the $G^0$ distribution include $\gamma, \alpha, n$, where $n$ is the number of look; $\alpha$ indicates the roughness, $\alpha \le -15$ represents the homogeneous area such as grassland, and $\alpha \in (-15, -5]$ represents inhomogeneous areas such as forests, and $\alpha \in (-5, 0]$ represents extremely inhomogeneous area; $\gamma$ is a scale parameter.

If the number of looks $n$ is known, when $r = 1/2,\ 1$, the sample moments $\widehat{m}_{1/2}, \widehat{m}_1$can be used to estimate the distribution parameters $\alpha, \gamma$:

$$\frac{\Gamma^2(n+1/4)\Gamma^2(-\hat{\alpha}-1/4)}{\Gamma(n+1/2)\Gamma(-\hat{\alpha}-1/2)\Gamma(n)\Gamma(-\hat{\alpha})} - \frac{\widehat{m}_{\frac{1}{2}}^2}{\widehat{m}_1} = 0,$$
$$\hat{\gamma} = n\left(\frac{\widehat{m}_1\Gamma(n)\Gamma(-\hat{\alpha})}{\Gamma(n+1/2)\Gamma(-\hat{\alpha}-1/2)}\right)^2. \tag{13}$$

The mathematical form of $G^0$ distribution is equivalent to the Fisher distribution, also called "Fisher–Snedecor", described in the Table 3 in Section 3.1. The Fisher distribution can be obtained by setting $n = L, \alpha = -M, \gamma = -\mu\alpha$.

*e) **$G^h$** distribution*

The $G_\sigma^h$ distribution is another statistical distribution for describing inhomogeneous areas [45, 47, 48]. If $\beta = \lambda/(2\mu), \gamma = \lambda/2, \alpha = -1/2$, the $G_\sigma$ distribution can be degraded to $G_\sigma^h$ distribution. Under the product model, if the RCS intensity obeys the inverse Gaussian distribution $X_\sigma \sim \mathrm{IG}(\mu, \lambda)$, and the speckle obeys the gamma distribution, then the intensity $Z_\sigma$ of the SAR image obeys a $G_\sigma^h$ distribution.

*f) **GC** distribution*

The GC (Generalized Compound) distribution is a statistical distribution proposed by Anastassopoulos et al. [40] based on the product model for describing inhomogeneous areas. Under the product model, if the RCS intensity obeys the generalized gamma distribution $X_\sigma \sim \mathrm{G}\Gamma(a, b_2, v_2)$, and the speckle obeys the generalized gamma distribution $Y_\sigma \sim \mathrm{G}\Gamma(b_1, v_1)$, then the intensity $Z_\sigma$ of the SAR image obeys a GC distribution shown in Table 2. The GC distribution has other distributions as particular cases, for example:

a) If $b_1 = b_2 = 2, v_1 = 1, v_2 = v$, then GC distribution is the $K$ distribution:

$$p_{Z_\sigma}(z; a, v) = \frac{2}{a\sqrt{z}\Gamma(v)}\left(\frac{\sqrt{z}}{a}\right)^v K_{v-1}\left(\frac{2\sqrt{z}}{a}\right), \tag{14}$$

and the corresponding $r$-order moment is:

$$\mathrm{E}\{Z_\sigma^r\} = a^r\frac{\Gamma(r+1)\Gamma(r+v)}{\Gamma(v)}. \tag{15}$$

b) If $b_1 = b_2 = 2c, v_1 = 1, v_2 = 1/2$, the GC distribution becomes a Weibull distribution：

$$p_{Z_\sigma}(z; a, c) = \frac{2c}{a\sqrt{z}\Gamma(1/2)}\left(\frac{\sqrt{z}}{a}\right)^{\frac{3c}{2}-1} K_{-1/2}\left(2\left(\frac{\sqrt{z}}{a}\right)^c\right). \tag{16}$$

If $b = a \times 2^{-1/c}$, the above equation can be transformed into $p_{WB}(z; c, b)$ in Table 3.

### 2.3.3 *Validity assessment of the product model*

Although the product model greatly simplifies the statistical modeling of SAR images, few works have dealt with the verification of its theoretical and physical foundations. Especially, whether the speckle of high-resolution SAR images still is multiplicative noise has always been controversial. Some scholars believe that the speckle should be seen as a scattering phenomenon rather than multiplicative noise [1]. This section summarizes the current assessment of the validity of the product model.

Early Tur et al. [49] studied the conditions applicable to the multiplicative speckle from the theoretical model of optical coherent imaging. The random intensity $I_{ts}$ received at a certain point $P = (x_p, y_p)$ can be expressed as:

$$I_{ts}(x_p, y_p) = \left|\iint_{R_{cell}} dx'dy' \times h(x_p - x', y_p - y')t(x', y')\exp[i\varphi(x', y')]\right|^2, \tag{17}$$

where $h(x, y)$ represents the amplitude response of the system, $\varphi(x', y')$ represents the random phase at the point $(x', y')$, $t(x', y')$ indicates the scattering contribution at the point $(x', y')$. It should be noted that the meanings of $t(x', y')$ and $\varphi(x', y')$ here correspond to the scattering amplitude and phase of a single scatterer in one resolution cell in radar imaging, respectively.

If and only if $t(x', y')$ does not change within a resolution cell, according to the Cauchy–Schwarz inequality, Eq. (17) can be expressed as [49]:

$$I_{ts}(x_p, y_p) = \left|t(x_p, y_p)\right|^2 \left|\iint_{\mathrm{R_{cell}}} dx'dy' \times h(x_p - x', y_p - y')\exp[i\varphi(x', y')]\right|^2 \tag{18}$$
$$= \alpha \cdot I_{\mathrm{inc}}(x_p, y_p) \cdot I_s(x_p, y_p),$$

$$I_{\mathrm{inc}}(x_p, y_p) = \frac{1}{\alpha}\left|t(x_p, y_p)\right|^2 \tag{19}$$

$$I_s(x_p,y_p) = \left|\iint_{\mathrm{R_{cell}}} dx'dy' \times h(x_p - x', y_p - y') \exp[i\varphi(x',y')]\right|^2,$$

where $I_{\mathrm{inc}}(x,y)$ represents the incoherent image intensity of $t$, $I_s(x,y)$ represents the intensity value at $t(x,y)=1$, and $\alpha$ is a constant depending on system parameters. Eq. (18) gives the product model in a coherent imaging system. Based on the above theoretical derivation, the literature [49] concludes that: the product model is established when $t(x',y')$ is constant in a resolution cell; the product model is no longer valid when $t(x',y')$ changes and there is detail information within a resolution cell.

In addition, Lee et al. studied the product model from the fact that the coefficient of variation of the Rayleigh speckle model should be constant for homogenous areas [2]. Suppose a product model:

$$z(k,l) = x(k,l)y(k,l), \tag{20}$$

where $z(k,l)$ is the intensity or amplitude of the $(k,l)$th pixel in the SAR image, $x(k,l)$ is the reflection coefficient, and $y(k,l)$ is the noise with mean of 1 and standard deviation $\sigma_y$.

Suppose $x(k,l)$ and $y(k,l)$ are statistically independent, according to the product model and $E[y]=1$, it can be derived that:

$$E[z] = E[x]. \tag{21}$$

Furthermore, the variance of $z$ can be derived as:

$$\mathrm{Var}\,(z) = \mathrm{E}[(z-\bar{z})^2] = (\mathrm{Var}(x) + \bar{x}^2)\sigma_y^2 + \mathrm{Var}(x), \tag{22}$$

then the coefficient of variation of $z$ can be obtained as:

$$\frac{\sqrt{\mathrm{Var}\,(z)}}{\bar{z}} = \sqrt{\frac{\mathrm{Var}(x)(1+\sigma_y^2)}{\bar{z}^2} + \sigma_y^2}. \tag{23}$$

There is no variation of the reflection coefficient over homogenous areas, therefore $\mathrm{Var}(x)=0$, and then:

$$\frac{\sqrt{\mathrm{Var}\,(z)}}{\bar{z}} = \sigma_y. \tag{24}$$

Thus, the coefficient of variation is constant in the multiplicative noise model of homogenous regions. In the literature [2], it is explained that the homogenous SAR image satisfies the product model by testing the coefficient of variation of the single/multi-look SAR amplitude/intensity image as a constant.

It can be seen that the product model is theoretically strictly established only for homogenous regions but not in the inhomogeneous case. That is, the product model based on the Rayleigh speckle model is theoretically strictly established; but there is no theoretical support for the product model to be extended to inhomogeneous regions. However, the statistical modeling based on the product model is still widely used because it is applicable to several typical distribution models for inhomogeneous regions, such as the K-distribution, and it simplifies the derivation process of statistical modeling [50].

## 2.4 *Statistical modeling based on the non-Rayleigh speckle model*

The Rayleigh speckle model is used to describe low-resolution radar images. The model assumes that there is a large number of independent scatterers in a resolution cell, the scattered amplitude of the scatterers are independently and identically distributed, and the scattering phase is uniformly distributed. Such assumptions are seldom valid in high-resolution radar imagery, though. The non-Rayleigh speckle model is developed based on the coherent scatterer model. In this model, the radar echo appears to contain "target signal" with fluctuations, and the main explanation for this phenomenon is [9]:

(1) The scattered amplitude in a resolution cell is no longer a constant but has some fluctuating characteristics. As shown in Figure 8, $a_i(\boldsymbol{r})$ represents the fluctuating characteristic of the scattered amplitude of the $i$-th scatterer at different observation positions $\boldsymbol{r}$. At a specific time $t_0$, the number of scatterers at the specified observation position $r_0$ is $N$ ($N=4$ in Figure 8,), the spatial fluctuation characteristics of the scatterer $a_i(\boldsymbol{r})$ cause the scattered field at the position $r_0$ to be determined by a few strongly contributed scatterers. Therefore, even when the number $N$ of scatterers is large, such fluctuations cause non-Rayleigh scattered echoes. This phenomenon gave birth to the concept of "equivalent number of scatterers," which will be introduced in Section 2.4.1.

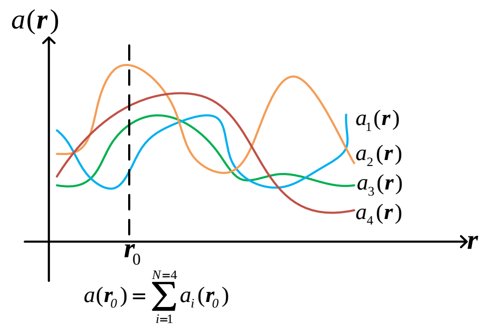


*Figure 8 Amplitude fluctuation of non-Rayleigh speckle model*

(2) The number $N$ of scatterers in a resolution cell is small and the central limit theorem is no longer satisfied. The scattering echo at this time is no longer a Rayleigh echo, and the fluctuation characteristics of the number of scatterers influence the probability distribution of a single pixel. The number of scatterers can be modeled as a random variable obeying Poisson distribution whose expectation is also a random variable obeying some distribution.

(3) The distribution of the phase of scattered field in a resolution cell is no longer uniform distributed. The discussion of phase distribution is relatively rare, since it is generally assumed that the scatterers are randomly positioned, and the maximum distance between the scatterers is much larger than the wavelength, therefore the scattered phase is usually sufficient to satisfy the uniform distribution.

This section first theoretically deduces and analyzes the probabilistic statistical model under the non-Rayleigh speckle model, and then introduces various statistical distributions based on the non-Rayleigh speckle model.

### 2.4.1 *Non-Rayleigh speckle model*

Rewrite the expression of the scattered field $E(\boldsymbol{r})$ in the coherent scatterer model (Eq. (4)) as follows:

$$E(\boldsymbol{r}) = \sum_{i=1}^{N} a_i e^{j\phi_i} = \sum_{i=1}^{N}(a_i\cos\phi_i + ja_i\sin\phi_i) = \Re + j\Im = Ae^{j\theta}. \tag{25}$$

Take the following assumptions:

(1) $a_i$, $a_j$, $\phi_i$, $\phi_j$, $(i \neq j)$ are collectively independent random variables;

(2) $\{\phi_i\}$ is uniformly distributed at $[0,2\pi)$.

The characteristic functions $M_{\Re i}(\omega)$ and $M_{\Im i}(\omega)$ of the real component $a_i\cos\phi_i$ and imaginary part $a_i\sin\phi_i$ of the $i$-th scatterer can be written as:

$$\begin{aligned} M_{\Re i}(\omega) = M_{\Im i}(\omega) &\equiv E[\exp(j\omega a_i \cos\phi_i)] \\ &= \int_{-\pi}^{\pi} p_\phi(\phi_i)\exp(j\omega a_i\cos\phi_i)\,d\phi_i \\ &= \frac{1}{2\pi}\int_{-\pi}^{\pi}\exp(j\omega a_i\cos\phi_i)\,d\phi_i \\ &= J_0(a_i\omega), \end{aligned} \tag{26}$$

where $J_0$ is the first type of zero-order Bessel function.
Assuming that the number of scatterers $N$ is a constant, then the characteristic function of the sum of $N$ independent random variables is the product of the characteristic function of each variable, and the characteristic function of the real and imaginary components of the scattered field can be written as [9, 25]:

$$\begin{aligned} M_{\Re}(\omega) = M_{\Im}(\omega) &= \prod_{i=1}^{N} M_{\Re i}(\omega) = \prod_{i=1}^{N} M_{\Im i}(\omega) \\ &= \prod_{i=1}^{N} J_0(a_i\omega). \end{aligned} \tag{27}$$

Since the phase angles of the summation of the individual components are uniformly distributed within $(-\pi,\pi]$, the joint probability density and joint characteristic function of the real and imaginary components of the summed phase vector is circularly symmetric. The two-dimensional characteristic function $M_{\Re,\Im}(\omega_\Re,\omega_\Im)$ is [9, 23]:

$$\begin{aligned} M_{\Re,\Im}(\omega_\Re,\omega_\Im) &= M_{\Re,\Im}\left(\sqrt{\omega_\Re^2+\omega_\Im^2}\right) \\ &= \prod_{i=1}^{N} J_0\left(a_i\sqrt{\omega_\Re^2+\omega_\Im^2}\right). \end{aligned} \tag{28}$$

Denoting $u=\sqrt{\omega_\Re^2+\omega_\Im^2}$ the characteristic function of the amplitude $A$ of the scattered field, $E(\boldsymbol{r})$ [9, 25] can be written as:

$$M_N(u) = \prod_{i=1}^{N} J_0(a_i u). \tag{29}$$

According to Eq. (29), using the Fourier-Bessel transform, the PDF $P_A(A)$ of the amplitude $A$ can be written as:

$$\begin{aligned} P_A(A) &= 2\pi\int_0^\infty \rho\prod_{i=1}^{N} J_0(2\pi\rho a_i)J_0(2\pi\rho A)\,d\rho \\ &= \frac{1}{2\pi}\int_0^\infty u\prod_{i=1}^{N} J_0(u a_i)J_0(uA)\,du, \end{aligned} \tag{30}$$

where $\rho = u/2\pi, A=\sqrt{\Re^2+\Im^2}$.
Define the intensity of scattered field $\sigma(\boldsymbol{r})$ as the square of the amplitude of the scattered field:

$$\sigma(\boldsymbol{r}) \equiv |E(\boldsymbol{r})|^2 = A^2. \tag{31}$$

Suppose that $\{a_i\}$ is a constant, then the probability distribution of $\sigma$ can be derived from $P_\sigma(\sigma) = P_A(\sqrt{\sigma}))/(2\sqrt{\sigma})$ [25]:

$$P_\sigma(\sigma;\boldsymbol{r};\{a_i(\boldsymbol{r})\}) = \frac{1}{2}\int_0^\infty \omega J_0(\omega\sqrt{\sigma})\prod_{i=1}^{N} J_0(\omega a_i(\boldsymbol{r}))\,d\omega. \tag{32}$$

Assuming that the elements $\{a_i\}$ are collectively independent and identically distributed, then the average of $\{a_i\}$ is:

$$P_\sigma(\sigma;\boldsymbol{r}) = \frac{1}{2}\int_0^\infty \omega J_0(\omega\sqrt{\sigma})\langle J_0[\omega a(\boldsymbol{r})]\rangle^N\,d\omega, \tag{33}$$

where $\langle\cdot\rangle$ denotes the expectation and

$$\langle J_0[\omega a(\boldsymbol{r})]\rangle = \int_0^\infty J_0(\omega a)p(a;\boldsymbol{r})\,da, \tag{34}$$

where $p(a;\boldsymbol{r})$ is the PDF of $\{a_i\}$, which is usually a function of the observed position $\boldsymbol{r}$.
Eq. (33) represents the PDF of the intensity of scattered field as a function of $p(a;\boldsymbol{r})$ and $N$. Due to the complex integral, it is difficult to derive the analytical expression when $p(a;\boldsymbol{r})$ is arbitrary, but its analytical expression can be written for specific probability distributions $p(a;\boldsymbol{r})$.
The $n$-order moment of $P_\sigma(\sigma;\boldsymbol{r})$ can be obtained by solving the $n$-order derivative of the moment generating function of $P_\sigma(\sigma;\boldsymbol{r})$ at zero, which is [9, 25]:

$$\sigma^n(\boldsymbol{r}) = (n!)^2\sum_{m_1=0}^{\infty}\sum_{m_2=0}^{\infty}\cdots\sum_{m_N=0}^{\infty}\left[\frac{\prod_{i=1}^{N}\langle a^{2m_i}(\boldsymbol{r})\rangle}{\left(\prod_{i=1}^{N} m_i!\right)^2}\right]_{\sum_{i=1}^{N} m_i = n}, \tag{35}$$

where $\langle a^{2m}(\boldsymbol{r})\rangle$ indicates the $2m$-order moment of $p(a;\boldsymbol{r})$, and the above equation satisfies $\sum_{i=1}^{N} m_i = n$. Then the mean and normalized 2-order moment can be derived as:

$$\begin{gathered} \langle\sigma(\boldsymbol{r})\rangle = N\langle a^2(\boldsymbol{r})\rangle, \\ \frac{\langle\sigma^2(\boldsymbol{r})\rangle}{\langle\sigma(\boldsymbol{r})\rangle^2} = 2\left(1-\frac{1}{N}\right)+\frac{1}{N}\frac{\langle a^4(\boldsymbol{r})\rangle}{\langle a^2(\boldsymbol{r})\rangle^2}. \end{gathered} \tag{36}$$

In particular, if $N\to\infty$, then the normalized $n$-order moment $\langle\sigma^n(\boldsymbol{r})\rangle/\langle\sigma(\boldsymbol{r})\rangle^n \to n!$, and it is equal to the normalized moment of the negative exponential distribution.
The number of equivalent scatterers $N_{\text{eff}}$ is defined by [9, 25]:

$$N_{\text{eff}}(\boldsymbol{r}) \equiv \frac{N\langle a^2(\boldsymbol{r})\rangle^2}{\langle a^4(\boldsymbol{r})\rangle}, N_{\text{eff}} < N. \tag{37}$$

It can be seen $N_{\text{eff}}$ is determined by both the number $N$ of scatterers and the normalized moment of $a(\boldsymbol{r})$. Even if $N$ is large enough, the value of $\langle a^2(\boldsymbol{r})\rangle^2/\langle a^4(\boldsymbol{r})\rangle$ may be small due to the fluctuation of $\{a_i\}$, then $N_{\text{eff}}$ is also small and eventually leads to non-Rayleigh echo. If $N_{\text{eff}} \geq 10$, the deviation of adopting Rayleigh speckle model is relatively small [9, 25, 35]; if $N_{\text{eff}} \approx 1$, Rayleigh speckle model will show significant error; if $N_{\text{eff}} \ll 1$, Rayleigh speckle model will be invalid.

### 2.4.2 *Statistical distributions*

As shown in Figure 7, this section summarizes the statistical distributions based on the non-Rayleigh speckle model starting from the modeling of the number of scatterers and the amplitude of the scatterers. The number of scatterers in a single resolution cell can typically be modeled as a constant (including infinite constant and finite constant) or a variable obeying a certain distribution (such as the Poisson and negative binomial distributions). The scattered amplitude of each scatterer can be modeled as 1) a constant, 2) a number of independent identically distributed variables (such as $K$ distribution, Rayleigh distribution, or arbitrary distribution), and 3) sum of a constant and an infinite number of variables. The "Yellow shading box with embedded 'NR'" in Figure 7 denotes the "non-Rayleigh speckle model" which inputs the statistical distribution of the number of scatterers and the amplitude of the scatterers, and outputs the distribution of SAR image intensity.
If the number of scatterers is an infinite constant and the scattered amplitude is modeled as the sum of a known constant and an infinite number of independent identically distributed (IID) variables, then the Rice (or Rician) distributed [25] scattered field can be obtained. Rician inverse Gaussian (RiIG) distributed intensity can be obtained by mixing the Rician distribution and inverse Gaussian distribution which is explained by Brownian motion with a stop time [51]. Interestingly,

RiIG distribution can also be explained using the non-Rayleigh speckle model. If the number of scatterers is modeled as Poisson distribution with its expectation obeying inverse Gaussian distribution and the amplitude is modeled as the sum of a known constant and an infinite number of IID variables, then RiIG distributed intensity is obtained [52]. If the number of scatterers is modeled as a Poisson distribution, and the expectation of the Poisson distribution is also a random variable which can be modeled as gamma distribution, inverse gamma distribution, Beta distribution of the second kind, and Beta distribution of the first kind, then the scattered intensity obeying $K$ distribution, $G^0$ distribution, $U$ distribution and $W$ distribution can be respectively obtained by combing the above different distributions of Poisson expectation and amplitude with arbitrary distribution [23].

The $K$ distribution under the product model framework has been introduced in Section 2.3.2. This section will supplement the other modeling methods of $K$ distribution. The scattered field of the $K$ distribution can also be obtained when the number of scatterers obeys the negative binomial distribution with infinite expectation and the amplitude obeys arbitrarily distribution. $K$ distributed amplitude and finite constant of the number of scatterers also lead to the $K$ distributed scattered intensity. Similarly, the scattered field obeying Rayleigh distribution can also be obtained by the Rayleigh distributed amplitude and finite constant of the number of scatterers.

In addition, when the real and imaginary components of the scattered field are IID variables with infinite variance and the number of scatterers is an infinite constant, the non-Rayleigh speckle model can be degenerated into the generalized central limit theorem model [26] which will be introduced in Section 2.5.

*a) K distribution*

The amplitude and intensity of the scattering field of the $K$ distribution have been derived from the product model in Section 2.3.2. Here, the other four ways of modeling $K$ distributions are introduced based on the non-Rayleigh speckle model which is determined by the fluctuations of the number of scatterers and scattered amplitude [9, 10, 23, 51, 53, 54].

(1) When the scattered amplitude of each scatterer is independently and identically $K$-distributed with probability distribution $p(a;\boldsymbol{r})$, and $N$ is an arbitrary finite constant, then the scattered intensity $\sigma$ is $K$-distributed [9]. The corresponding derivation process is given below. Assume that $p(a;\boldsymbol{r})$ is $K$-distributed which is:

$$p(a;\boldsymbol{r}) = \frac{2b}{\Gamma(1+v)}\left(\frac{ba}{2}\right)^{v+1} K_v(ba), \qquad v > -1. \tag{38}$$

Substituting $p(a;\boldsymbol{r})$ into Eq. (33), the scattered intensity distribution $P_\sigma(\sigma;\boldsymbol{r})$ can be derived as:

$$P_\sigma(\sigma;\boldsymbol{r}) = \frac{b/\sqrt{\sigma}}{\Gamma(M)}\left(\frac{b\sqrt{\sigma}}{2}\right)^M K_{M-1}\left(b\sqrt{\sigma}\right). \tag{39}$$

This is equivalent to the $K$-distributed intensity equation $p_{K_\sigma}(Z_\sigma = z;\beta,\alpha,n)$ in Table 2 when it satisfies that:

$$\beta = b^2/4, \alpha = M, n = 1, \tag{40}$$

where $Z_\sigma = z = \sigma$.

(2) When the number of scatterers in a resolution cell obeys the negative binomial distribution with mean $\bar{N}$ and $\bar{N} \to \infty$, then it can be deduced that the scattered amplitude and intensity obey the $K$ distribution regardless of the distribution of scattered amplitude [10, 54]. The following is the detailed derivation process.

Suppose the number $N$ of scatterers is a negative binomial distributed statistical random variable independent of $\{a_i\}$ and $\{\phi_i\}$ with PDF:

$$p(N;\bar{N},\alpha) = \binom{N+\alpha-1}{N}\frac{\left(\frac{\bar{N}}{\alpha}\right)^N}{\left(1+\frac{\bar{N}}{\alpha}\right)^{N+\alpha}}, \tag{41}$$

where $N$ could be seen as the number of failures before the $\alpha$ successes in a series of independent Bernoulli trials, and the probability of success for each trial is $\alpha/(\alpha+\bar{N})$. The corresponding mean and variance are:

$$\mathrm{Mean}(N) = \bar{N}, \mathrm{Var}(N) = \alpha^{-1} + \bar{N}^{-1}. \tag{42}$$

The characteristic function of the scattered field has been derived in Eq. (29). Now assume that the scattered amplitude $a_i$ of each scatterer is independent identically distributed, and $N$ is a statistical random variable obeying the negative binomial distribution in Eq. (41). Take the expectation of $N$, and let $a = a/\sqrt{\bar{N}}$ , then the following characteristic function could be derived:

$$M_{\bar{N}}(u) = \left[1 + (\bar{N}/\alpha)(1 - \langle J_0(au/\sqrt{\bar{N}})\rangle)\right]^{-\alpha}. \tag{43}$$

It holds that

$$\lim_{N\to\infty} M_{\bar{N}}(u) = [1 + \langle a^2\rangle u^2/4\alpha]^{-\alpha}, \tag{44}$$

which is exactly the characteristic function of the $K$ distribution:

$$p(A) = \frac{2b}{\Gamma(\alpha)}\left(\frac{bA}{2}\right)^\alpha K_{\alpha-1}(bA), \tag{45}$$

where $A$ is the scattered amplitude. Then the intensity distribution can be obtained using the transformation formula $p_{Z_\sigma}(z) = p_A\left(\sqrt{z}\right)/(2\sqrt{z})$ and it is equivalent to the $p_{K_\sigma}(Z_\sigma = z;\beta,\alpha,n)$ in Table 2 when it satisfies that $b = 2\sqrt{\beta}, n = 1$.

(3) Assuming that the number of scatterers in a single resolution cell obeys the Poisson distribution with expectation $\Omega = \bar{N}$ shown in Eq. (46), and $\Omega$ obeys the gamma distribution shown in Eq. (47), then it can be derived that this is equivalent to the negative binomial distribution in Eq. (41) according to the total probability formula in Eq. (48). Therefore, $K$-distributed SAR image in Eq. (45) can be obtained regardless of the distribution of scattered amplitude according to (2) [23, 54]

$$p(N|\Omega = \bar{N}) = \frac{\bar{N}^N}{N!}\exp(-\bar{N}), \tag{46}$$

$$p(\Omega = \omega) = \frac{1}{\Gamma(\alpha)}\left(\frac{\alpha}{\bar{N}}\right)^\alpha \omega^{\alpha-1}\exp\left(-\frac{\omega\alpha}{\bar{N}}\right), \tag{47}$$

$$p(N) = \int_0^\infty p(N|\Omega = \omega)p_\Omega(\omega)\,\mathrm{d}\omega. \tag{48}$$

(4) The $K$-distributed SAR image can also be modeled in the perspective of a random walk of Brownian motion [51]. The real component $\Re$ and imaginary $\mathfrak{I}$ component of the complex scattered field are modeled as two Wiener processes with zero mean. When the stop time $Z = z$ is given, $\Re$ and $\mathfrak{I}$ are normal distributed variables with a variance of $z/2$, then a Rayleigh distributed amplitude $A = \sqrt{\Re^2 + \mathfrak{I}^2}$ can be obtained as:

$$p(A|z) = \frac{2A}{z}e^{-\frac{A^2}{z}}. \tag{49}$$

If the stop time $Z$ obeys gamma distribution:

$$p(z) = \frac{(b/2)^{2\alpha}}{\Gamma(\alpha)}z^{\alpha-1}\exp\left(-\frac{zb^2}{4}\right), \tag{50}$$

Then, according to the Bayesian formulation:

$$p(A) = \int_0^\infty p(A|z)p(z)\,dz. \tag{51}$$

Substituting the transformation formula $p_{Z_\sigma}(z) = p_A(\sqrt{z})/(2\sqrt{z})$, it can be deduced that the scattered field intensity $\sigma$ both obey the $K$ distribution (see $p_{K_\sigma}(Z_\sigma = z; \beta, \alpha, n)$ in Table 2).

*b) Rice distribution*

The Rice (or Rician) distribution is the probability distribution of the amplitude of a circularly symmetric Gaussian random variable with a non-zero mean. In the coherent scatterer model, the Rice distribution can be obtained by assuming that the scattered field is a summation of a constant $A_0$ and an infinite number of random variables [25, 55], that is, the scattered field can be expressed as:

$$\boldsymbol{E} = A_0 + \sum_{i=1}^{N} a_i e^{j\phi_i} = A_0 + A_n e^{j\theta_n}. \tag{52}$$

The scattered intensity can be written as:

$$\sigma = |\boldsymbol{E}|^2 = A_0^2 + A_n^2 + 2A_0A_n\cos\theta_n, \tag{53}$$

Assuming that 1) the number of scatterers $N \to \infty$, 2) the amplitudes of each scatterer $\{a_i\}$ are independently identically distributed, and 3) the phase of scattered field obeys a uniform distribution in $(0, \pi]$, then it can be deduced that the scattered field intensity obeys the Rice distribution which is:

$$p_{Rice}(\sigma) = \frac{1}{2\sigma^2}\exp\left\{-\frac{\sigma + A_0^2}{2\sigma^2}\right\} I_0\left(\frac{\sqrt{\sigma}A_0}{\sigma^2}\right), \tag{54}$$

where $I_0$ is the modified zero-order Bessel function of the first kind.
When the constant $A_0$ is zero, the Rice distribution becomes the Rayleigh distribution. Because the Rice distribution stems from the central limit theorem, it is also not suitable for modeling of high-resolution SAR images.
Denote $k = \sigma_0/\overline{\sigma_n}$, where $\overline{\sigma_n} = \overline{A_n^2} = 2\sigma^2$, $\sigma_0 = A_0^2$, as the ratio of the constant intensity and the average intensity ($k$ is called "beam ratio" in holographic techniques) [25], then Eq. (54) can be written as:

$$\begin{aligned} p_{\text{Rice}}(\sigma) &= \frac{1}{\overline{\sigma_n}}\exp\left\{-\frac{\sigma + \sigma_0}{\overline{\sigma_n}}\right\} I_0\left(2\frac{\sqrt{\sigma\sigma_0}}{\overline{\sigma_n}}\right) \\ &= \frac{1}{\overline{\sigma_n}}\exp\left\{-\left(\frac{\sigma}{\overline{\sigma_n}} + k\right)\right\} I_0\left(2\sqrt{\frac{\sigma}{\overline{\sigma_n}}k}\right). \end{aligned} \tag{55}$$

Eq. (55) is also called "modified Rice distribution" and the corresponding $r$-order moment of intensity is:

$$\mathrm{E}\{\sigma^r\} = \bar{\sigma}_n^r e^{-k} r!\,{}_1^1F_1(r + 1, 1, k), \tag{56}$$

where ${}_1^1F_1$ is confluent hypergeometric function [56-58].
The corresponding mean, variance and coefficient of variation are:

$$\begin{aligned} \text{Mean}(\sigma) &= (1 + k)\overline{\sigma_n}, \\ \text{Var}(\sigma) &= \overline{\sigma_n}^2(1 + 2k), \\ C &= \frac{\sqrt{\text{Var}(\sigma)}}{\text{Mean}(\sigma)} = \frac{\sqrt{1 + 2k}}{1 + k}. \end{aligned} \tag{57}$$

*c) RiIG distribution*

When 1) the number of scatterers in a single resolution cell obeys Poisson distribution with the expectation obeying inverse Gaussian distribution or the stop time of Brownian motion obey the inverse Gaussian distribution, 2) the scattered amplitude of each scatterer is modeled as the summation of a known constant and an infinite number of independent identically distributed variables, which obey the Rice distribution, then scattered field obeys the Rician inverse Gaussian (RiIG) distribution [51]. In the following, the RiIG distribution is first derived from the two-dimensional Brownian motion, and then the scattered amplitude given the stop time can be derived to be Rice-distributed according to the Bayesian theorem.
The real component $\Re$ and the imaginary component $\Im$ of the scattered field $E$ are respectively regarded as two Brownian motions with the offsets of $\beta_\Re$, $\beta_\Im$, the stop time $z$, the diffusion coefficient $\rho = 1$ and the variance $\rho z = z$. That is, assume that $\Re$ and $\Im$ are independent Gaussian random variables with mean values $\beta_\Re z$ and $\beta_\Im z$, and variance $z$[ their joint probability density distribution is [51]:

$$\begin{aligned} p_\Re(\Re|z) &= \frac{1}{\sqrt{2\pi z}}\exp\left(-\frac{(\Re - \beta_\Re z)^2}{2z}\right), \\ p_\Im(\Im|z) &= \frac{1}{\sqrt{2\pi z}}\exp\left(-\frac{(\Im - \beta_\Im z)^2}{2z}\right). \end{aligned} \tag{58}$$

Consider $Z = z$ as a random variable, then $\Re$ and $\Im$ can be expressed as:

$$\Re = \beta_\Re Z + \sqrt{Z}\mathcal{N}_\Re,\ \ \Im = \beta_\Im Z + \sqrt{Z}\mathcal{N}_\Im, \tag{59}$$

where $\mathcal{N}_\Re$ and $\mathcal{N}_\Im$ are standard Gaussian random variables.
Describe the above conclusion in the two-dimensional form, then random vector $\boldsymbol{E} = [\Re, \Im]$ is a two-dimensional Gaussian distribution with the mean $\boldsymbol{\beta}z, \boldsymbol{\beta} = [\beta_\Re, \beta_\Im]$, and the variance $\Sigma z$, where

$$\Sigma = \begin{pmatrix} 1 & 0 \\ 0 & 1 \end{pmatrix} \tag{60}$$

Assume that the stop time $Z$ of the Brownian motion obeys the inverse Gaussian distribution, i.e. $Z \sim \mathrm{IG}(\delta, \gamma)$, $\gamma = \sqrt{\alpha^2 - (\beta_\Re^2 + \beta_\Im^2)} = \sqrt{\alpha^2 - \beta^2}$, then the two-dimensional random vector $\boldsymbol{E} = [\Re, \Im]$ obeys the normal-inverse Gaussian (NIG) distribution with the PDF:

$$p(\boldsymbol{E}) = a(\alpha, \boldsymbol{\beta}, \boldsymbol{\mu}, \delta, \Sigma)\,b(\boldsymbol{E}; \alpha, \boldsymbol{\mu}, \delta, \Sigma)\exp(\boldsymbol{\beta}\boldsymbol{E}^{\mathrm{T}}), \tag{61}$$

where

$$\begin{aligned} a(\alpha, \boldsymbol{\beta}, \boldsymbol{0}, \delta, \Sigma) &= \frac{\alpha^{3/2}}{(2\delta\pi^3)^{1/2}}\exp(\gamma\delta), \\ b(\boldsymbol{E}; \alpha, \boldsymbol{0}, \delta, \Sigma) &= \frac{\delta^{3/2}K_{3/2}(\alpha\sqrt{\Re^2 + \Im^2 + \delta^2})}{(\Re^2 + \Im^2 + \delta^2)^{3/4}}, \\ q(\boldsymbol{E}; \boldsymbol{0}, \delta, \Sigma) &= \frac{1}{\delta}\sqrt{\Re^2 + \Im^2 + \delta^2}. \end{aligned} \tag{62}$$

Converting the two-dimensional NIG distribution to polar coordinates and integrating the phase, the amplitude of the scattered field obeying the RiIG distribution can be obtained:

$$\begin{aligned} & p_{RiIG}(A; \alpha, \beta, \delta, \gamma) \\ &= \sqrt{\frac{2}{\pi}}\alpha^{\frac{3}{2}}\delta\exp(\delta\gamma)\frac{A}{(\delta^2 + A^2)^{\frac{3}{4}}}K_{\frac{3}{2}}\left(\alpha\sqrt{\delta^2 + A^2}\right)I_0(\beta A), \end{aligned} \tag{63}$$

where $I_0$ is the first-order modified zero-order Bessel function.
Accordingly, the density of the intensity $\sigma = A^2$ is:

$$p_{RiIG}(\sigma;\alpha,\beta,\delta,\gamma) = \sqrt{\frac{1}{2\pi}\alpha^{\frac{3}{2}}\delta\exp(\delta\gamma)\frac{1}{(\delta^2+\sigma)^{\frac{3}{4}}}K_{\frac{3}{2}}\left(\alpha\sqrt{\delta^2+\sigma}\right)I_0\left(\beta\sqrt{\sigma}\right)}. \quad (64)$$

Furthermore, it can be deduced that the conditional probability $p(\sigma|z)$ of the scattered intensity field at $Z=z$ obeys the Rice distribution:

$$p(\sigma|z) = \frac{1}{2z}\exp\left\{-\frac{\sigma+\beta^2z^2}{2z}\right\}I_0\left(\beta\sqrt{\sigma}\right). \quad (65)$$

The above equation is equivalent to Eq. (54) by substituting $z=\sigma/2, \beta=A_0/z$. If $\beta=0$, it becomes a Rayleigh distribution.
The $r$-order and second-order moments of the RiIG distribution defined in Eq. (63) are:

$$\mathrm{E}\{A^r\} = \int_0^\infty (2z)^{\frac{r}{2}}\Gamma\left(\frac{r}{2}+1\right){}_1^0F_1\left(-\frac{r}{2},1,-\frac{\beta^2z}{2}\right), \frac{\delta}{\sqrt{2\pi}}x^{-3/2}\exp(\delta\gamma)\exp\left(-\frac{1}{2}\left(\frac{\delta^2}{x}+\gamma^2x\right)\right)dz, \quad (66)$$

$$\mathrm{E}\{A^2\} = 2\frac{\delta}{\gamma}+\frac{\beta^2\delta^2}{\gamma^2}+\frac{\beta^2\delta}{\gamma^3}, \quad (67)$$

where ${}_1^1F_1$ is the confluent hypergeometric function [56].

*d) $\boldsymbol{G^0}$ distribution*

The scattered amplitude and intensity obeying the $G^0$ distribution [45] have been obtained based on the product model in Section 2.3.2. The $G^0$ distributed scattered field based on the non-Rayleigh speckle model is described here. Considering the number $N$ of scatterers as a random variable obeying the Poisson distribution [23] , the mean $\lambda$ of the Poisson distribution is a random variable $\bar{N}$. If $\bar{N}$ obeys the inverse gamma distribution:

$$f(\bar{N};-\alpha,\gamma) = \frac{\gamma^{-\alpha}}{\Gamma(-\alpha)}\bar{N}^{\alpha-1}e^{-\gamma/\bar{N}},\ \ \bar{N},-\alpha,\gamma>0. \quad (68)$$

Then the scattered intensity obeys $G^0$ distribution (or denoted as $B$ distribution in [23]):

$$g(\sigma;-\alpha,\gamma) = \frac{-\alpha\gamma^{-\alpha}}{(\sigma+\gamma)^{-\alpha+1}}, \qquad \sigma,-\alpha,\gamma>0. \quad (69)$$

*e) W distribution*

Similar to the $G^0$ distribution, the number $N$ of scatterers obeys Poisson distribution, and the mean value $\lambda$ of $N$ is a random variable $\bar{N}$. If the mean $\bar{N}$ obeys Beta distribution of the first kind [23]:

$$f(\bar{N};\beta,p,q) = \frac{\beta^q}{\mathrm{B}(p,q)}\frac{\bar{N}^{p-1}}{(\beta-\bar{N})^{q-1}},\ \ p,q\geq 0,\ \ \beta>0,\ \ 0\leq\bar{N}\leq\beta, \quad (70)$$

where $\mathrm{B}(p,q)$ is Beta function:

$$\mathrm{B}(p,q) = \frac{\Gamma(p)\Gamma(q)}{\Gamma(p+q)}, \quad (71)$$

then $W$ distributed scattered intensity can be obtained [23]:

$$p_W(\sigma;\beta,p,q) = \frac{\Gamma(p+q)}{s^2\beta\Gamma(p)}\left(\frac{\sigma}{s^2\beta}\right)^{\frac{p}{2}-1}\exp\left(-\frac{\sigma}{2s^2\beta}\right) \times W_{(-p-2q+2)/2,(p-1)/2}\left(\frac{\sigma}{s^2\beta}\right), \quad (72)$$

where $W_n(\cdot)$ is Whittaker function.
The $n$-look $W$ distribution is:

$$p_W(\sigma;\beta,p,q,n) = \frac{\Gamma(q)}{s^2\beta\Gamma(n)\mathrm{B}(p,q)}\left(\frac{\sigma}{s^2\beta}\right)^{\frac{p+n-3}{2}}\exp\left(-\frac{\sigma}{2s^2\beta}\right)W_{(-p-2q+n+1)/} \quad (73)$$

Substituting $\beta=s^2\beta, n=1$, it is:

$$p_W(\sigma;\beta,p,q) = \frac{\Gamma(p+q)}{\beta\Gamma(p)}\left(\frac{\sigma}{\beta}\right)^{\frac{p}{2}-1}\exp\left(-\frac{\sigma}{2\beta}\right)W_{(-p-2q+2)/2,(p-1)/2}\left(\frac{\sigma}{\beta}\right). \quad (74)$$

*f) U distribution*

Similarly to previous distributions, consider the case where the number $N$ of scatterers obeys a Poisson distribution, and the mean value $\bar{N}$ of the Poisson distribution obeys a Beta distribution of the second kind [23]:

$$f(\bar{N};\beta,p,q) = \frac{\beta^q}{\mathrm{B}(p,q)}\frac{\bar{N}^{p-1}}{(\bar{N}+\beta)^{p+q}}, \bar{N}>0. \quad (75)$$

Then $U$ distributed scattered intensity can be obtained [23]:

$$p_U(\sigma;\beta,p,q) = \frac{q\Gamma(p+q)}{s^2\beta\Gamma(p)}U_{q+1,2-p}\left(\frac{\sigma}{s^2\beta}\right), \quad (76)$$

where $U_{q+1,2-p}$ is degenerate hypergeometric function [23, 56].
The $n$-look $U$ distribution is:

$$p_U(\sigma;\beta,p,q,n) = \frac{\Gamma(n+q)}{s^2\beta\Gamma(n)B(p,q)}\left(\frac{\sigma}{s^2\beta}\right)^{n-1}U_{q+n,1+n-p}\left(\frac{\sigma}{s^2\beta}\right). \quad (77)$$

Substituting $\beta=s^2\beta, n=1$, it becomes:

$$p_U(\sigma) = \frac{q\Gamma(p+q)}{\beta\Gamma(p)}U_{q+1,2-p}\left(\frac{\sigma}{\beta}\right). \quad (78)$$

### 2.5 *Statistical modeling based on generalized central limit theorem*

It has been mentioned in Section 2.4 that when the real and imaginary components of the scattered field obey a distribution with an infinite variance and the number of scatterers is infinite , then the non-Rayleigh speckle model may be described with the generalized central limit theorem [26]. We first introduce this theorem, and then discuss some of the statistical distributions emerging from this model.

#### 2.5.1 *Generalized central limit theorem*

The generalized central limit theorem model can be regarded as a special case of the non-Rayleigh speckle model, or it can be seen as a generalization of the Rayleigh speckle model based on the central limit theorem. The central limit theorem [59] points out that the sum of $N$ independent identically distributed random variables with finite mean and finite variance tends to be Gaussian when $N\to\infty$. The generalized central limit theorem shows that for a set of independent identically distributed random variables, with either finite or infinite variance, the summation will converge to an $\alpha$-stable distribution [60, 61].
The $\alpha$-stable distribution was introduced by Levy in 1925 [60]. It is a generalization of the Gaussian distribution and is a widely representative random distribution model. It can well describe the characteristics of spikes and heavy tailes. The most important motivation for the development of the $\alpha$-stable distribution is because it is the only type of distribution that satisfies the generalized central limit theorem. Secondly, the linear combination of $\alpha$-stable random variables with the same characteristic parameter is still $\alpha$-stable.

Therefore, for a linear system with $\alpha$-stable distributed input, its output still follows an $\alpha$-stable distribution. Additionally, many aspects of the linear system theory for Gaussian signals can be directly extended to the $\alpha$-stable distribution [60]. With few exceptions, the PDF of an $\alpha$-stable distribution does not have an explicit expression, but its characteristic function is:

$$\varphi(s) = \exp\left[i\delta s - |\gamma s|^{\alpha} B_{s,\alpha}\right], \tag{79}$$

where

$$B_{s,\alpha} = \begin{cases} 1 - i\beta \operatorname{sgn}(s) \tan\left(\frac{\pi\alpha}{2}\right), \alpha \neq 1 \\ 1 + i\beta \operatorname{sgn}(s) \frac{2}{\pi} \log|s|, \alpha = 1 \end{cases}, \tag{80}$$

in which $-\infty < \delta < \infty$, $\gamma > 0$, $0 < \alpha \leq 2$, $-1 \leq \beta \leq 1$.
The characteristic parameter is $\alpha (0 < \alpha \leq 2)$. It controls the pulse intensity of a random process. The smaller $\alpha$ is, the stronger is the impulsivity and the heavier is the tail, which means that the probability of a random variable far from the center is larger; the larger $\alpha$ is, the more "plumpy" the probability density distribution curve is, and the lighter the tail is. If $\alpha = 2$, the $\alpha$-stable distribution becomes the Gaussian distribution. If $\alpha = 1$ and $\beta = 0$, the $\alpha$-stable distribution is the Cauchy distribution.
The scale parameter is $\gamma$, which is similar to the variance of a Gaussian distribution, and its value must be positive. It characterizes the degree of data concentration. The larger $\gamma$ is, the greater is the degree of dispersion of the data around the mean.
The symmetry parameter is $\beta$; it determines the slope of the distribution. If $\beta = 0$, it yields the symmetric $\alpha$-stable distribution ($S\alpha S$ distribution). The configurations $\alpha \neq 1$, $\beta > 0$ and $\beta < 0$ corresponds to distributions inclined to the right and to the left, respectively. However, when $\alpha = 1$, the situation is reversed.
The location parameter is $\delta$, which corresponds to the mean and median of the $\alpha$-stable distribution. It can be any real number, and it determines the position of the PDF.
When $\delta = 0$ and $\beta = 0$, one has the zero mean $S\alpha S$ distribution, and its characteristic function is:

$$\varphi(s) = \exp[|\gamma s|^{\alpha}]. \tag{81}$$

### 2.5.2 *Statistical distributions*

We present in this section statistical distributions of SAR images based on the generalized central limit theorem. They are built on the different distribution models for the real and imaginary components. As shown in Figure 9, the "Yellow shading box with embedded 'GCL'" denotes the "Generalized central limit theorem model" which inputs the statistical distribution of the real and imaginary components, and outputs the distribution of SAR image intensity. If the real and imaginary components of the scattered field obey an infinite variance distribution, and assume the number of scatterers $N \to \infty$, then the real and imaginary components of the scattered field obey an $S\alpha S$ distribution according to the generalized central limit theorem, and the scattered amplitude follows a heavy-tailed Generalized Rayleigh distribution ($S\alpha SGR$ distribution) [20]. It has been introduced in Section 2.2, the Gaussian distributed real and imaginary components produce the Rayleigh speckle model based on the central limit theorem. Generalizing Gaussian distribution to the generalized gamma or the generalized Gaussian distribution would give rise to the Generalized Gaussian Rayleigh distribution (GGR distribution) [21] and Generalized Gamma Rayleigh distribution ($G\Gamma R$ distribution) [22] for the scattered amplitude. The density expressions are given below.

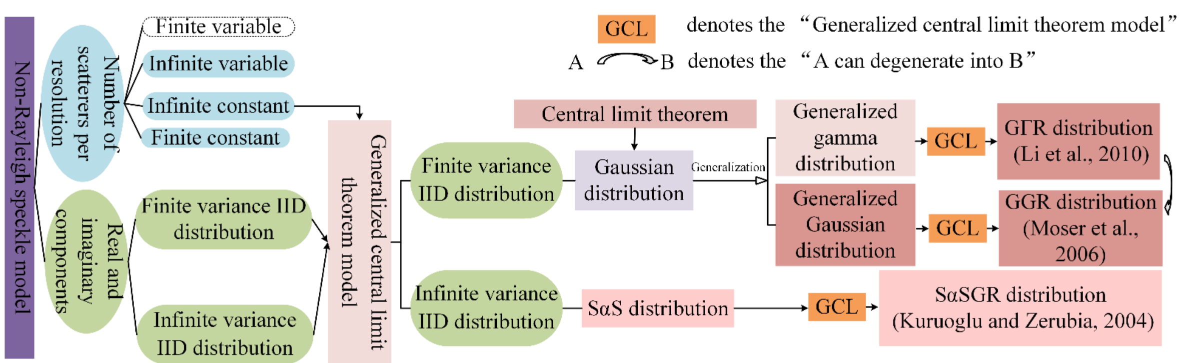


*Figure 9 Statistical distributions of scattered intensity based on generalized central limit theorem model*

a) ***SαSGR* distribution**

The $S\alpha SGR$ distribution is derived from the assumption that the real and imaginary components of the scattered field obey the joint $S\alpha S$ distribution based on the generalized central limit theorem. The characteristic function of the joint $S\alpha S$ distribution is [20]:

$$\psi(t_1, t_2) = \exp(-\gamma |\boldsymbol{t}|^{\alpha}), \tag{82}$$

where $\boldsymbol{t} = [t_1, t_2]$, $|\boldsymbol{t}| = \sqrt{t_1^2 + t_2^2}$.
The $S\alpha SGR$ distribution of scattered amplitude is [20]:

$$p_{S\alpha SGR}(A; \gamma, \alpha) = A \int_0^{\infty} s \exp(-\gamma s^{\alpha}) J_0(sA) ds, \tag{83}$$

where $J_0(\cdot)$ is the first-order zero-order Bessel function.
The corresponding $r$-order moment is [20]:

$$\mathrm{E}\{A^r\} = \frac{2^{r+1}\Gamma(\frac{r}{2}+1)}{\Gamma(-\frac{r}{2})} \frac{\gamma^{r/\alpha}\Gamma(-\frac{r}{\alpha})}{\alpha}, -2 < r < -\frac{1}{2}. \tag{84}$$

If $\alpha = 2$, the $S\alpha SGR$ distribution becomes the Rayleigh distribution:

$$p(A; \gamma) = \frac{A}{2\gamma} \exp\left(-\frac{A^2}{4\gamma}\right). \tag{85}$$

b) *GGR distribution*

The central limit theorem assumes that the real and imaginary parts of

the scattered field obey the Gaussian distribution. This model has a limited scope of application. In order to be applicable to more scenarios, the Gaussian distribution can be generalized to the generalized Gaussian distribution. Then it can be derived that the amplitude of scattered field obeys the GGR distribution [21].
The PDF of generalized Gaussian distribution is:

$$p(u;\gamma,c,m)=\frac{\gamma c}{2\Gamma\left(\frac{1}{c}\right)}\exp[-|\gamma(u-m)|^{c}],\quad c,\gamma>0,m\in R. \tag{86}$$

If $c=2$, the generalized Gaussian distribution becomes a Gaussian distribution.
The PDF of GGR distribution is [21]:

$$p_{\mathrm{GGR}}(A)=\frac{\gamma^{2}c^{2}A}{\Gamma^{2}(\frac{1}{c})}\int_{0}^{\frac{\pi}{2}}\exp\{-(\gamma A)^{c}(|\cos\theta|^{c}+|\sin\theta|^{c})\}\,d\theta. \tag{87}$$

If $c=2$, the GGR distribution becomes a Rayleigh distribution.

*c) **GΓR** distribution*

Assuming that the real and imaginary parts of the scattered field obey the two-sided generalized gamma distribution (GΓD), respectively, then it can be deduced that the amplitude of scattered field obeys the generalized Gamma Rayleigh distribution (GΓR distribution) [22, 62].
The PDF of the two-sided GΓD is [22]:

$$p(u)=\frac{\nu}{2\eta\Gamma(\kappa)}\left(\frac{|u|}{\eta}\right)^{\kappa\nu-1}\exp\left\{-\left(\frac{|u|}{\eta}\right)^{\nu}\right\},\quad \nu>0,\kappa>0,\eta>0. \tag{88}$$

If $\kappa\nu=1$, the two-sided GΓD becomes a generalized Gaussian distribution. If $\nu=2$, $\kappa=1/2$, the two-sided GΓD becomes a Gaussian distribution. If $\nu=1,\kappa=1$, the two-sided GΓD becomes a Laplacian distribution.
The PDF of the GΓR distribution is:

$$p_{\mathrm{G\Gamma R}}(A)=\left[\frac{\nu}{\eta^{\kappa\nu}\Gamma(\kappa)}\right]^{2}A^{2\kappa\nu-1}\int_{0}^{\frac{\pi}{2}}|\cos\theta\sin\theta|^{\kappa\nu-1}\exp\left\{-\left(\frac{A}{\eta}\right)^{\nu}(|\cos\theta|^{\nu}+|\sin\theta|^{\nu})\right\}d\theta. \tag{89}$$

If $\nu=2,\kappa=1/2$, the GΓR distribution becomes a Rayleigh distribution. If $\kappa\nu=1$, the GΓR distribution becomes a GGR distribution.

## 2.6 *Statistical modeling based on incoherent scatterer sum model*

### 2.6.1 *Incoherent scatterer sum model*

The incoherent scatterer sum model, called "the surface model" in [11, 12], is an approximate model which is more commonly used in clutter simulation [13]. For low-resolution SAR images, the scattered field can be modeled as the sum of a large number of randomly distributed scattered components. In this case, phase coherence has been lost between different scatterers, therefore, the scattered intensity $\sigma$ is approximated as multiple non-coherent summation of point scatterers [10-12]:

$$\sigma=\sum_{i=1}^{N}a_{i}^{2}. \tag{90}$$

The Laplace transform of the scattered intensity is [10]:

$$Q_{N}(s)=\langle\exp(-s\sigma)\rangle=\langle\exp(-sa^{2})\rangle^{N}. \tag{91}$$

### 2.6.2 *Statistical distributions*

As shown in Figure 10, the "Yellow shading box with embedded 'ISS'" denotes the "Incoherent scatterer model" which inputs the statistical distribution of the number of scatterers, and outputs the distribution of SAR image intensity. Under the incoherent scatterer sum model, when the number of scatterers $N$ in a single resolution cell is infinite, the intensity distribution of scattered field is an impulse function [10]; when $N$ is a variable that obeys the negative binomial distribution with an infinite mean, the intensity of the scattered field obeys a gamma distribution [10, 63]. The statistical distributions under the incoherent scatterer sum model is given below.

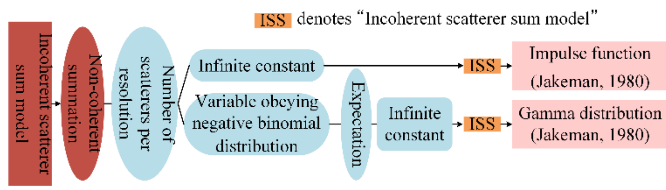


*Figure 10 Statistical distributions of scattered intensity based on incoherent scatterer sum model*

*a) Impulse function*

When the number $N$ of scatterers in a resolution cell is an infinite constant, the distribution of scattered intensity is an impulse function. Dividing $a$ by $\sqrt{N}$ in the Laplace transform $Q_N(s)$ of the scattered intensity in Eq. (91), if $N\to\infty$, the Laplace transform $Q_N(s)$ and corresponding PDF by inverse Laplace transform is[63]:

$$\lim_{N\to\infty}Q_{N}(s)=\exp(-s\langle b^{2}\rangle), \tag{92}$$

$$p(\sigma)=\delta(\sigma-\langle\sigma\rangle), \tag{93}$$

where $\delta(\cdot)$ denotes impulse function.
The scattered intensity is therefore a constant in this limit.

*b) Gamma distribution*

Section 2.2 introduces the modeling of the gamma distribution based on the Rayleigh speckle model. This section will give the other two modeling processes for the gamma distribution: 1) the gamma distribution under the incoherent scatterer sum model; 2) the gamma distribution by solving the rate equation which describes the continuous fluctuations of birth-and-death immigration model.
1) When the number of scatterers in a resolution cell obeys the negative binomial distribution with an infinite mean $\bar{N}$ as shown in Eq. (41), then the scattered intensity obeys the gamma distribution [10, 63]. The derivation process is given below.
Dividing $a$ by $\sqrt{\bar{N}}$ for $Q_N(s)$ as shown in Eq. (91), the average form of $Q_N(s)$ can be written as:

$$Q_{\bar{N}}(s)=[1+(\bar{N}/\alpha)(1-\langle\exp(-sa^{2}/\bar{N})\rangle)]^{-\alpha}. \tag{94}$$

where $\langle\cdot\rangle$ denotes the expectation.
If $\bar{N}\to\infty$, the limit form of Eq. (94) is:

$$\lim_{\bar{N}\to\infty}Q_{\bar{N}}(s)=(1+s\langle\sigma\rangle/\alpha)^{-\alpha}, \tag{95}$$

then the gamma distributed scattered intensity can be obtained using the inverse transform on Eq. (95):

$$p(\sigma)=\left(\frac{\alpha}{\langle\sigma\rangle}\right)^{\alpha}\frac{\sigma^{\alpha-1}}{\Gamma(\alpha)}\exp\left(-\frac{\alpha\sigma}{\langle\sigma\rangle}\right). \tag{96}$$

2) The scattered intensity $\sigma$ is considered as a continuous fluctuation controlled by the process of birth-and-death immigration model. The solution of the rate equation will produce a scattered intensity of gamma distribution [63].
Gamma distributed intensity is generated by the following rate equation which is a continuum analogue of birth-and-death immigration model:

$$\frac{\partial P}{\partial t}=\lambda\sigma\frac{\partial^2 P}{\partial\sigma^2}+\left[2\lambda-\nu+(\mu-\lambda)\sigma\right]\frac{\partial P}{\partial\sigma}+(\mu-\lambda)P, \tag{97}$$

where $\lambda$ is birth rate, $\mu$ is death rate, $\nu$ is immigration rate.
The solution of Eq. (97) is most readily accomplished in terms of the generating function of $P(\sigma,t)$ by Laplace transform:

$$Q(s,t)=\langle\exp(-s\sigma)\rangle, \tag{98}$$

which satisfies the partial differential equation:

$$\frac{\partial Q}{\partial t}=-s\left[\nu+(\mu-\lambda+\lambda s)\frac{\partial}{\partial s}\right]Q. \tag{99}$$

Assume the initial intensity is $\sigma_0$, and the boundary conditions on $Q$ are:

$$Q(0,t)=1;\ Q(s,0)=\exp(-s\sigma_0), \tag{100}$$

and then the solution can be obtained as:

$$Q(s,t)=\left(\frac{\lambda-\mu}{\lambda-\mu+\lambda(\theta-1)s}\right)^{\nu/\lambda}\exp\left[\frac{\sigma_0(\mu-\lambda)\theta s}{\lambda-\mu+\lambda(\theta-1)s}\right], \tag{101}$$

where

$$\theta(t)=\exp[(\lambda-\mu)t]. \tag{102}$$

If $\mu>\lambda$ and $t\to\infty$, then the equilibrium distribution is:

$$Q(s)=\left(\frac{\lambda-\mu}{\lambda-\mu-\lambda s}\right)^{\nu/\lambda}. \tag{103}$$

The inverse Laplace transformation of Eq. (103) gives the following gamma distribution:

$$p(\sigma)=\left[\frac{(\mu-\lambda)}{\lambda}\right]^{\nu/\lambda}\frac{\sigma^{\nu/\lambda-1}}{\Gamma(\nu/\lambda)}\exp\left[-\frac{(\mu-\lambda)\sigma}{\lambda}\right]. \tag{104}$$

Take $n=\nu/\lambda$, $\sigma=\nu/(\mu-\lambda)$, the above expression is equivalent to $p_{\mathrm{Gamma}_\sigma}$ in Table 2.

# 3 Statistical modeling based on empirical model

Differently from the statistical modeling based on the coherent scatterer model defined earlier, the statistical modeling based on the empirical model no longer considers the scattering process, but starts directly from the image itself. The main target of this approach is to find a tractable distribution that is consistent with the actual SAR images.
As shown in Figure 11, according to the presence of analytical expressions and the complexity of the model, the empirical statistical modeling can be classified into three categories: (i) single distribution, (ii) finite mixture, and (iii) non-parametric model.
The single distribution approach adopts only one certain mathematical distribution to model the image; this is usually suitable for relatively simple and uniform regions. Finite mixtures describe SAR images using a linear combination of one kind of distribution, or a combination of multiple distributions; the added complexity is suitable for relatively complex scenes. The non-parametric approach consists in choosing a model with more parameters to closely fit actual data; it is usually suitable for very complicated scenes. This kind of model is complex and there is no analytic expression, unlike the first two approaches.

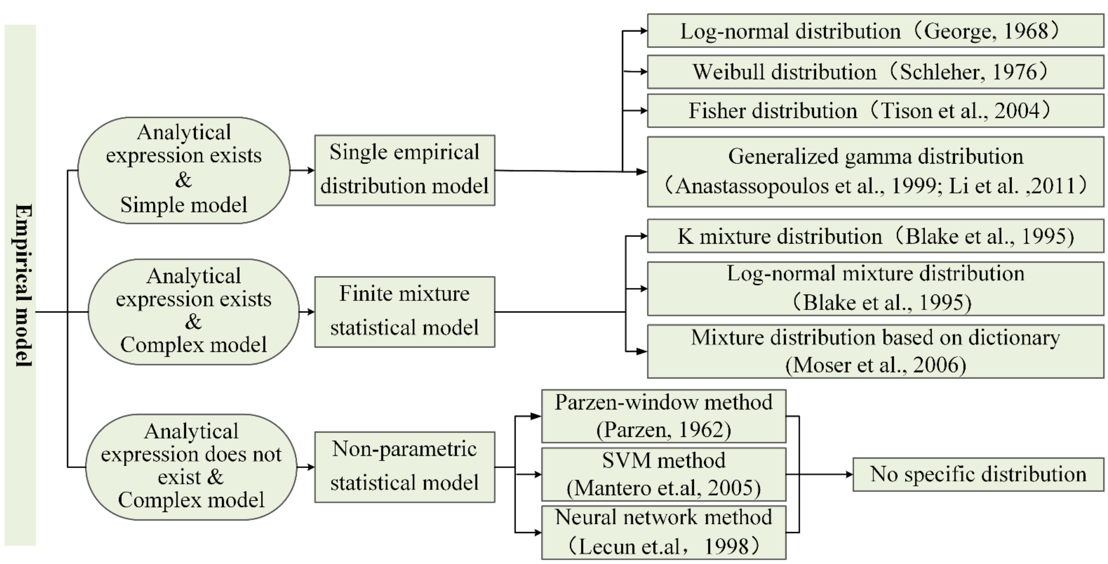


*Figure 11 Statistical distributions of scattered intensity based on empirical model*

*Table 3: Statistical distribution and characteristics of single empirical distribution model*

| Distribution type | Probability density function (PDF) | Mean | Variance | $r$-order moment |
|---|---|---|---|---|
| Log-normal distribution | $p_{LN}(z;\beta,V)=\frac{1}{z\sqrt{2\pi V}}\exp\left[-\frac{(\ln z-\beta)^2}{2V}\right]$ | $\exp\left[\beta+\frac{V}{2}\right]$ | $\exp(2\beta+V)\,(\exp(V)-1)$ | $E\{Z^r\}=\exp\left[r\beta+\frac{r^2V}{2}\right]$ |
| Weibull distribution | $p_{WB}(z;c,b)=\frac{cz^{c-1}}{b^c}\exp\left[-\left(\frac{z}{b}\right)^c\right]$ | $b\Gamma\left(1+\frac{1}{c}\right)$ | $b^2\left[\Gamma\left(\frac{2}{c}+1\right)-\Gamma^2(\frac{1}{c}+1)\right]$ | $\mathrm{E}\{Z^r\}=b^r\Gamma(\frac{r}{c}+1)$ |
| Fisher distribution | $p_F(z;L,M,\mu)=\frac{\Gamma(L+M)}{\Gamma(L)\Gamma(M)}\frac{L}{M\mu}\frac{\left(\frac{Lz}{M\mu}\right)^{L-1}}{\left(1+\frac{Lz}{M\mu}\right)^{L+M}},$ $L>0,M>0$ | $\frac{M}{M-1}\mu$ | $\frac{M^2\mu^2(L+M-1)}{L(M-1)^2(M-2)}$ | —— |
| Generalized gamma distribution (ΓΓD − 1) | $p_{G\Gamma D1}(z;a,b,v)=\frac{b}{a\Gamma(v)}\left(\frac{z}{a}\right)^{bv-1}\exp\left[-\left(\frac{z}{a}\right)^b\right]$ | $a\frac{\Gamma(\frac{1}{b}+v)}{\Gamma(v)}$ | $\frac{a^2}{\Gamma^2(v)}\left[\Gamma\left(\frac{2}{b}+v\right)\Gamma(v)-\Gamma^2\left(\frac{1}{b}+v\right)\right]$ | $\mathrm{E}\{x^r\}=a^r\frac{\Gamma(\frac{r}{b}+v)}{\Gamma(v)}$ |
| Generalized gamma distribution (GΓD − 2) | $p_{G\Gamma D2}(z;v,\kappa,\eta)=\frac{\lvert v\rvert\kappa^\kappa}{\eta\Gamma(\kappa)}\left(\frac{z}{\eta}\right)^{\kappa v-1}\exp\left[-\kappa\left(\frac{z}{\eta}\right)^v\right],$ $v\neq 0,\kappa>0,\eta>0$ | $\begin{cases}\frac{\eta}{\kappa^{1/v}}\frac{\Gamma(\kappa+\frac{1}{v})}{\Gamma(\kappa)}, & \frac{1}{v}>-\kappa\\ \infty, & \text{otherwise}\end{cases}$ | $\frac{\eta^2}{\Gamma^2(\kappa)\kappa^{\frac{2}{v}}}[\Gamma\left(\kappa+\frac{2}{v}\right)\Gamma(\kappa)-\Gamma^2\left(\kappa+\frac{1}{v}\right)],$ $\frac{1}{v}>-\kappa,\quad \frac{2}{v}>-\kappa$ | $\mathrm{E}\{x^r\}=\begin{cases}\frac{\eta^r}{\kappa^{r/v}}\frac{\Gamma(\kappa+\frac{r}{v})}{\Gamma(\kappa)}, & \frac{r}{v}>-\kappa\\ \infty, & \text{otherwise}\end{cases}$ |

*Table 4: Parameter estimation formulas of MoLC method for amplitude distributions*

| Distribution type | Probability density function (PDF) | Parameters | Estimation formula of MoLC |
|---|---|---|---|
| Rayleigh distribution | $p(A)=\frac{2A}{\sigma}e^{-\frac{A^2}{\sigma}}$ | $\sigma$ | $k_1=\frac{(\ln\sigma+\Psi(1))}{2}$ |
| Square root gamma distribution | $p(A)=\frac{2}{\Gamma(n)}\left(\frac{n}{\sigma}\right)^n A^{2n-1}e^{-nA^2/\sigma}$ | $n,$ $\sigma$ | $2k_1=\ln\sigma+\Psi(n)-\ln n$ <br> $4k_2=\Psi(1,L)$ |
| K distribution | $p(A;\beta,\alpha,n)=\frac{4\beta nA}{\Gamma(n)\Gamma(\alpha)}(\beta nA^2)^{(\alpha+n)/2-1}K_{\alpha-n}(2A\sqrt{\beta n})$ | $\beta,$ $\alpha,$ $n$ | $2k_1=\ln\beta+\Psi(n)-\ln n+\Psi(\alpha)$ <br> $4k_2=\Psi(1,n)+\Psi(1,\alpha)$ <br> $8k_3=\Psi(2,n)+\Psi(2,\alpha)$ |
| SαSGR distribution | $p_A(A;\gamma,\alpha)=A\int_0^\infty s\exp(-\gamma s^\alpha)J_0(sA)ds$ | $\gamma,$ $\alpha$ | $\alpha k_1=\Psi(1)(\alpha-1)+\alpha\ln 2+\ln\gamma$ <br> $k_2=\Psi(1,1)\alpha^{-2}$ |
| GGR distribution | $p_A(A;\gamma,c)=\frac{\gamma^2c^2A}{\Gamma^2(\frac{1}{c})}\int_0^{\frac{\pi}{2}}\exp\{-(\gamma A)^c(\lvert\cos\theta\rvert^c+\lvert\sin\theta\rvert^c)\}\,d\theta$ | $\gamma,$ $c$ | $k_1=\frac{1}{c}\Psi\left(\frac{2}{c}\right)-\ln\gamma-\frac{1}{c}\mathrm{G}_1\left(\frac{1}{c}\right)\mathrm{G}_0\left(\frac{1}{c}\right)^{-1}$ <br> $k_2=\frac{1}{c^2}\Psi\left(1,\frac{2}{c}\right)+\frac{1}{c^2}\mathrm{G}_2\left(\frac{1}{c}\right)\mathrm{G}_0\left(\frac{1}{c}\right)^{-1}-\frac{1}{c^2}\mathrm{G}_1\left(\frac{1}{c}\right)^2\mathrm{G}_0\left(\frac{1}{c}\right)^{-2}$ |
| GΓR distribution | $p_A(A;\nu,\eta,\kappa)=\left[\frac{\nu}{\eta^{\kappa\nu}\Gamma(\kappa)}\right]^2A^{2\kappa\nu-1}\cdot\int_0^{\frac{\pi}{2}}\lvert\cos\theta\sin\theta\rvert^{\kappa\nu-1}\exp\left\{-\left(\frac{A}{\eta}\right)^\nu(\lvert\cos\theta\rvert^\nu+\lvert\sin\theta\rvert^\nu)\right\}d\theta,\nu=\frac{1}{\varpi}$ | $\nu,$ $\eta,$ $\kappa$ | $k_1=\ln\eta+\varpi\Psi(2\kappa)-\varpi\frac{\mathrm{G}_1(\kappa,\varpi)}{\mathrm{G}_0(\kappa,\varpi)}$ <br> $k_2=\varpi^2\left[\Psi(1,2\kappa)+\frac{\mathrm{G}_2(\kappa,\varpi)}{\mathrm{G}_0(\kappa,\varpi)}-\frac{\mathrm{G}_1^2(\kappa,\varpi)}{\mathrm{G}_0^2(\kappa,\varpi)}\right]$ <br> $k_3=\varpi^3\left[\Psi(2,2\kappa)-\frac{\mathrm{G}_3(\kappa,\varpi)}{\mathrm{G}_0(\kappa,\varpi)}+3\frac{\mathrm{G}_2(\kappa,\varpi)\mathrm{G}_1(\kappa,\varpi)}{\mathrm{G}_0^2(\kappa,\varpi)}-2\frac{\mathrm{G}_1^3(\kappa,\varpi)}{\mathrm{G}_0^3(\kappa,\varpi)}\right]$ |
| Log-normal distribution | $p(A;V,\beta)=\frac{1}{A\sqrt{2\pi V}}\exp\left[-\frac{(\ln A-\beta)^2}{2V}\right]$ | $V,$ $\beta$ | $k_1=\beta$ <br> $k_2=V$ |
| Weibull distribution | $p(A;b,c)=\frac{cA^{c-1}}{b^c}\exp\left[-\left(\frac{A}{b}\right)^c\right]$ | $b,$ $c$ | $k_1=\ln b+\Psi(1)c^{-1}$ <br> $k_2=\Psi(1,1)c^{-2}$ |
| Fisher distribution | $p(A;L,M,\mu)=\frac{\Gamma(L+M)}{\Gamma(L)\Gamma(M)}\frac{L}{M\mu}\frac{\left(\frac{LA}{M\mu}\right)^{L-1}}{\left(1+\frac{LA}{M\mu}\right)^{L+M}}$ | $L,$ $M,$ $\mu$ | $k_1=\ln\mu+(\Psi(L)-\ln L)-(\Psi(M)-\ln M)$ <br> $k_2=\Psi(1,L)+\Psi(1,M)$ <br> $k_3=\Psi(2,L)-\Psi(2,M)$ |
| Generalized gamma distribution | $f(A;a,b,v)=\frac{b}{a\Gamma(v)}\left(\frac{A}{a}\right)^{bv-1}\exp\left[-\left(\frac{A}{a}\right)^b\right]$ | $a,$ $b,$ $v$ | $k_1=\Psi(v)/b+\ln a$ <br> $k_2=\Psi(1,v)/b^2$ <br> $k_3=\Psi(2,v)/b^3$ |

**Note: $K_v(\cdot)$ is the second type of modified Bessel function, $\Psi(\cdot)$ denotes the digamma function, $\Psi(i,\cdot)$ represents the $i$-order polygamma function, $\mathrm{G}_v(\lambda)$ is an integral function introduced in [21]:**

$$\mathrm{G}_v(\lambda)=\int_0^{\pi/2}\frac{\ln^v A(\theta,\lambda)}{A(\theta,\lambda)^{2\lambda}}\mathrm{d}\theta\,,v=0,1,2;\ A(\theta,\lambda)=\lvert\cos\theta\rvert^{1/\lambda}+\lvert\sin\theta\rvert^{1/\lambda}$$

**$\mathrm{G}_i(k,\varpi)$ is an integral function introduced in [22]:**

$$\mathrm{G}_i(k,\varpi)=\int_0^{\pi/2}\lvert\cos\theta\sin\theta\rvert^{\frac{k}{\varpi}-1}\frac{\log^i A(\theta,\lambda)}{A(\theta,\lambda)^{2k}}\mathrm{d}\theta\,;\ A(\theta,\lambda)=\lvert\cos\theta\rvert^{1/\lambda}+\lvert\sin\theta\rvert^{1/\lambda}$$

*Table 5: Summary of single-pixel statistical modeling*

| Models | Model complexity & physical meaning | Distributions | Existence of analytical PDF | Application scope |
|---|---|---|---|---|
| **Rayleigh speckle model** | Low model complexity & weak physical meaning | Negative exponential distribution | Yes | Widely used in single-look intensity image of homogenous area |
| | | Rayleigh distribution | Yes | Widely used in single-look amplitude image of homogenous area |
| | | Gamma distribution | Yes | Widely used in multi-look intensity image of homogenous area |
| | | Square root gamma distribution | Yes | Widely used in multi-look amplitude image of homogenous area |
| **Product model** | Less high model complexity & Less strong physical meaning | $G$ distribution | Yes | Used in homogenous, inhomogeneous, extremely inhomogeneous areas; suitable for single/multi-look intensity or amplitude image |
| | | $G^h$ distribution | Yes | Used in extremely inhomogeneous urban areas and mixed terrain areas; |
| | | $GC$ distribution | Yes | Used in sea and land areas of medium-resolution (15m$^2$/30 m$^2$) |
| **Non-Rayleigh speckle model** | High model complexity & strong physical significance | $G^0$ distribution | Yes | Used in homogenous, inhomogeneous, extremely inhomogeneous areas; suitable for single/multi-look intensity or amplitude image |
| | | $K$ distribution | Yes | Widely used in medium inhomogeneous area; suitable for single/multi-look intensity or amplitude image |
| | | $W$ distribution | Yes | Used in medium inhomogeneous area; suitable for single/multi-look intensity or amplitude image |
| | | $U$ distribution | Yes | Used in medium inhomogeneous area; suitable for single/multi-look intensity or amplitude image |
| | | Rice distribution | Yes | Used in low-resolution images with targets in weak clutter |
| | | RiIG distribution | Yes | Used in SAR amplitude image or ultrasound image |
| **Generalized central limit theorem model** | Less high model complexity & Less strong physical meaning | $GGR$ distribution | No | Used for multiple types of terrains (such as urban areas, farmland, lakes, mountains) in multi-polarized channels |
| | | $G\Gamma R$ distribution | No | Used for homogenous or inhomogeneous SAR amplitude image with multiple types of terrains (such as urban areas, farmland, and mountains) |
| | | $S\alpha SGR$ distribution | No | Used for Long-tailed amplitude image of urban area |
| **Single empirical distribution model** | Low model complexity & no clear physical meaning | Log-normal distribution | Yes | Used for medium-resolution amplitude images for sea clutter and homogenous urban |
| | | Weibull distribution | Yes | Used for medium-resolution amplitude or intensity images |
| | | Fisher distribution | Yes | Used in homogenous, inhomogeneous, extremely inhomogeneous areas; suitable for single/multi-look intensity or amplitude image |
| | | Generalized gamma distribution | Yes | Used for homogenous or inhomogeneous SAR amplitude/intensity image with multiple types of terrains (such as urban areas, farmland, and mountains) |
| **Finite mixture statistical model** | High model complexity & weak physical significance | Mixed $K$-distribution or mixed log-normal distribution | Yes | Used for homogenous or inhomogeneous high-resolution SAR images |
| | | Dictionary-based mixture distribution model | Yes | Used for complex scenes composed by multiple types of terrains with medium, high or ultra-high resolution. |
| **Non-parametric statistical model** | High model complexity & no clear physical meaning | Parzen-window method | No | Used for complex scenes composed by multiple types of terrains |
| | | SVM method | No | Used for complex scenes composed by multiple types of terrains |
| | | Neural network method | No | Used for complex scenes composed by multiple types of terrains |

*Figure 12 Overall framework of single-pixel statistical modeling*

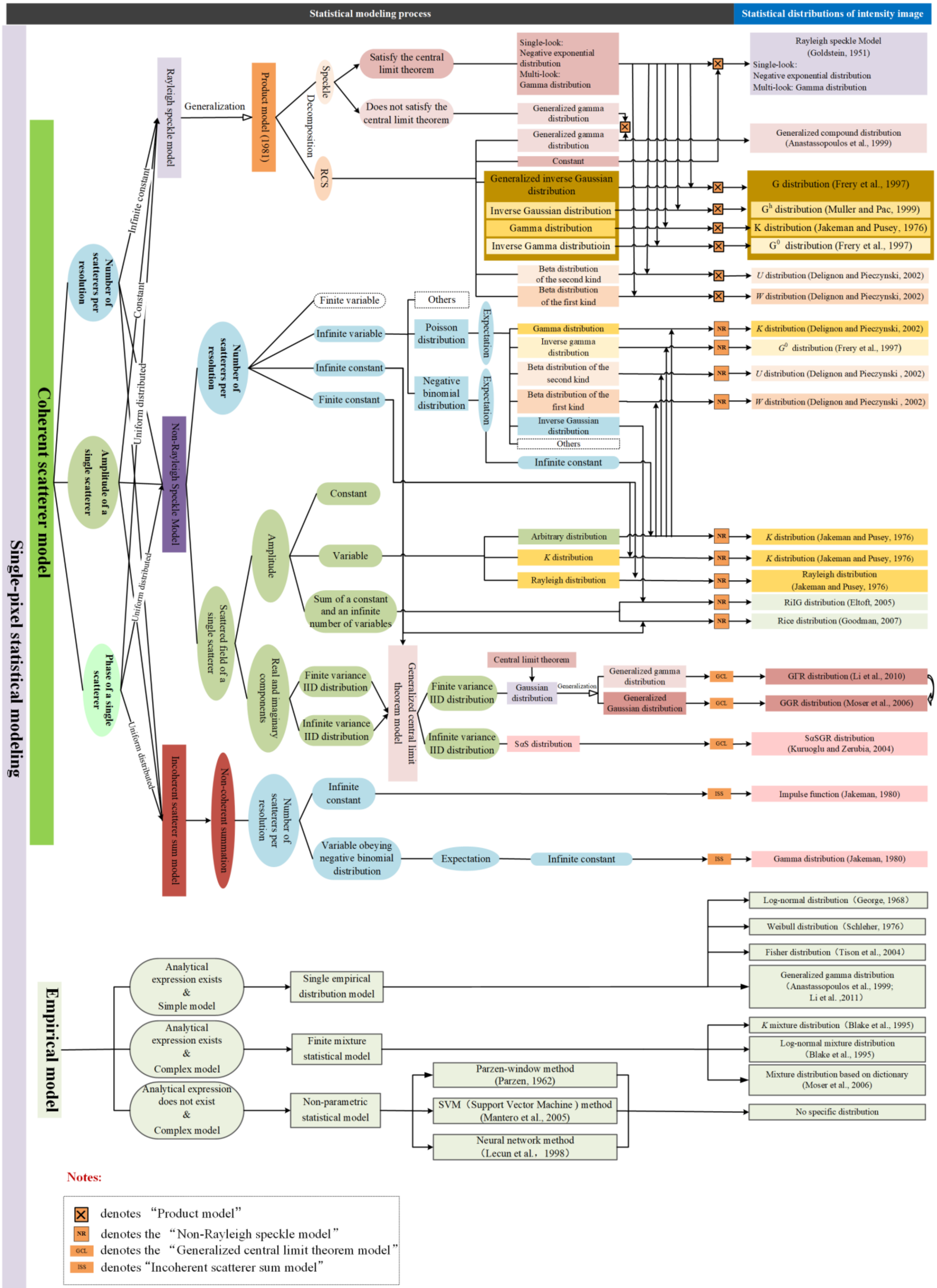

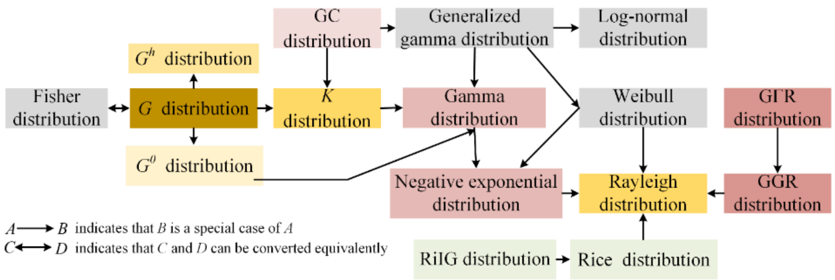


*Figure 13 Relationship between the major statistical distributions*

### 3.1 *Single empirical distribution model*

The most commonly used single empirical models include: the lognormal, Weibull, Fisher, and GΓD (generalized gamma) distributions. These laws are suitable for both amplitude and intensity data. The PDF and statistical characteristics of these distributions are summarized in Table 3. These empirical distributions only fit the SAR image mathematically and the parameters of empirical distributions do not necessarily have interpretability in terms of the physics of image formation. For example, there is no "number of looks", and no "texture parameter". The Log-normal distribution is mainly used for sea clutter of high-resolution radar [64-66]. It also can be used to describe areas with drastic spatial variation, such as urban areas [1]. The Weibull distribution can be used to describe land [67], weather [68] and sea-ice [1, 69] clutter. The Fisher distribution [70] is used to describe non-uniform SAR images of high-resolution [21]; it is a reparametrization of the $G^0$ distribution.

The generalized gamma distribution (GΓD) was first proposed by Stacy [71, 72] denoted as "$\mathrm{G\Gamma D}-1$" in Table 3. It can flexibly degenerate into multiple distributions under certain conditions, such as the Rayleigh, exponential, Nakagami, gamma, Weibull, and log-normal distributions. The flexibility of the GΓD make it widely used. Anastassopoulos et al. [40] used the GΓD to describe the speckle and RCS components of the SAR clutter to derive the GC distribution which has been introduced in Section 2.3.2. Li et al. [62] gave another expression to characterize the GΓD, denoted "$\mathrm{G\Gamma D}-2$" in Table 3, and it is experimentally verified that GΓD can be applied to many types of land-cover.

For the PDF of $\mathrm{G\Gamma D}-1$ in Table 3, if $b=1, v=1$, the GΓD becomes the exponential distribution. If $b=c/2, v=1$, the GΓD is the Weibull distribution. If $b=1$, the GΓD becomes the gamma distribution. If $b=2, v=1$, the GΓD becomes the Rayleigh distribution. If $b=1, v\rightarrow\infty$, the GΓD degrades into the log-normal distribution. If $b=2$, the GΓD degenerates to Nakagami distribution.

For the PDF of $\mathrm{G\Gamma D}-2$ in Table 3, if $v=2, \kappa=1$, GΓD degenerates to a Rayleigh distribution. If $v=1, \kappa=1$, GΓD becomes the exponential distribution. If $v=2$, GΓD degrades into Nakagami distribution. If $v=1$, GΓD degenerates to the gamma distribution. If $v=-1$, GΓD becomes the inverse gamma distribution. If $\kappa\rightarrow\infty$, GΓD degrades into log-normal distribution. If $\kappa=1$, GΓD is a Weibull distribution.

### 3.2 Finite mixtures

All the statistical distributions mentioned above belong to the parametric method [1, 26], and each is usually applicable for a specific applicable scene. However, usually there are usually multiple types of targets in a remote sensing image. Also, with the acquisition of high-resolution and ultra-high resolution SAR images, more details are highlighted, making it difficult to model SAR images with only one kind of statistical distribution [1].

To solve this problem, the Finite mixture model (FMM) [29, 73] has attracted the attention of scholars. The high flexibility of the FMM model makes it widely used in the fields of pattern recognition [74, 75], signal and image analysis [76-78], machine learning [79, 80], and remote sensing [78, 81-83]. The FMM is a semi-parametric method which models the unknown probability distribution as a linear combination of parameterized mixture components, each mixture component belonging to a dictionary of SAR-specific distributions [29].

The FMM models the PDF of the SAR amplitude image $z$ as a linear combination of $k$ mixture components [29, 30]:

$$f_z(z|M)=\sum_{i=1}^{k}\alpha_i f_i(z|m_i), \tag{105}$$

where $f_i(\cdot|m_i)$, $i=1,2,\ldots,k$ represents the probability distribution of the mixture component with parameters $m_i$, and $\{\alpha_1,\ldots,\alpha_k\}$ is a set of mixing proportions such that:

$$\sum_{i=1}^{k}\alpha_i=1,\quad 0\le\alpha_i\le 1, \tag{106}$$

where $M$ is a set collecting all the parameters of FMM, which is

$$M=\{m_1,\ldots,m_k,\alpha_1,\ldots,\alpha_k\}.$$

The distribution of each mixture component can be selected from the statistical distributions introduced earlier. The selected $R$ types of mixture components $f_j(\cdot|\xi_j)$, $j=1,2,\ldots,R$ make up a dictionary $\mathcal{D}=\{f_1,f_2,\ldots,f_k\}$, where $\xi_j$ represents the parameter of each mixture component distribution [30].

Consider the $k$ independent random variables $\{A_1,\ldots,A_k\}$ with distributions characterized by the densities $\{f_1,\ldots,f_k\}$. Assume that the observation of the experiment consists in first choosing one of these random variables with probability $\{\alpha_1,\ldots,\alpha_k\}$, and then sampling from it. In other words,

$$A=\begin{cases}A_1 \text{ with probability } \alpha_1,\\ \vdots\\ A_k \text{ with probability } \alpha_k.\end{cases}$$

The resulting random variable $A$ obeys the mixture distribution characterized by the $k$ laws $\{f_1,\ldots,f_k\}$ with proportions $\{\alpha_1,\ldots,\alpha_k\}$.

Given a SAR image and a dictionary, it is necessary to use an optimization method to determine the optimal number $k$ of mixed components, the mixing proportion $\alpha_k$ and the distribution parameter $m_i$ of each mixture component.

Blake et al. [14, 15] experimentally verified that using only a single probability distribution, such as the K, log-normal, Weibull, gamma, exponential distribution, etc., it is not possible to accurately model high-resolution SAR images. The authors' experiments show that the mixed distribution composed by two K-distributions or two log-normal distributions can be used to describe high-resolution SAR clutter. It is because the model is expanded from a single two-parameter probability distribution to the double five-parameter probability distribution which can better describe the complexity of high-resolution images. Blacknell [84, 85] proposed a correlated Gaussian mixture distribution (GMD) model to approximate the correlated K-clutter image in the logarithmic domain, and the model is applied to target detection which shows that the GMD model realizes better detection result compared with a single Gaussian distribution. At the same time, it is easier for the GMD model to introduce correlation information than other distributions. The introduction of correlation information can also significantly improve the performance of target detection.

Moser et al. [30] used a FMM to model medium resolution SAR amplitude images. Each mixture component is selected from a dictionary of six specific distributions including: log-normal, Nakagami, GGR, SαSGR, Weibull and K. The authors proposed a DSEM ('dictionary-based' stochastic expectation maximization method). It can automatically estimate parameters of the optimal mixture model combined with MoLC (method-of-log-cumulants) method and the parameters includes the number, the type as well as the distribution parameters of the mixed components. Furthermore, EDSEM (enhanced DSEM) is proposed in [83] which can more quickly estimate the number of mixed components. EDSEM further extended the DSEM algorithm for medium-resolution SAR images to very high-resolution image, and the dictionary is extended to eight probability distributions by adding the Fisher and $G\Gamma D$ laws.

## 3.3 *Non-parametric modeling*

The statistical modeling distributions reviewed previously are based on parametric or semi-parametric methods. This section introduces statistical modeling based on non-parametric methods. Non-parametric methods do not assume any analytical expression for the probability distribution governing the process, therefore they are more flexible, but there are some hyper-parameters need to be set [26, 30]. Typical non-parametric methods mainly include the Parzen-window [17, 86], support vector machines (SVM) [19, 87], ANN (artificial neural networks) [18, 88], and deep neural networks [32, 33, 89-91]. These methods adopt complex techniques to estimate statistical properties of the data based on a large number of sample data. They are mainly applied in despeckling [32, 33, 90, 91], image classification [18, 92], and ship detection [93, 94].

### *a) Parzen-Rosenblatt window*

The Parzen-window method [17, 86], also known as the Parzen-Rosenblatt window method and kernel density estimation, was proposed by Parzen and Rosenblatt. It is a widely used non-parametric approach to estimate the PDF based on a sample. Two-dimensional Parzen-window can be written as [17]:

$$p(z) = \frac{1}{n}\sum_{i=1}^{n}\frac{1}{h^2}\phi\left(\frac{z_i - z}{h}\right), \tag{107}$$

where $z_i, i = 1,2,\ldots,n$ are samples, $\phi(\cdot)$ is the window function of size $h$:

$$\phi\left(\frac{z_i - z}{h}\right) = \begin{cases} 1 & \left|\frac{z_i - z}{h}\right| \le \frac{1}{2}, \\ 0 & \text{otherwise.} \end{cases} \tag{108}$$

There are many other choices for $\phi(\cdot)$ such as the square, Gaussian, and hyper-spherical windows [86].

### *b) SVM method*

The SVM [87] method is used to estimate the PDF for the supervised classification of SAR images in [19]. The estimated cumulative distribution function (CDF) $\hat{P}(x)$ and PDF $\hat{p}(x)$ are expressed as:

$$\hat{P}(x) = \sum_{i=1}^{n}\beta_i K(x_i, x), \hat{p}(x) = \sum_{i=1}^{n}\beta_i \widetilde{K}(x_i, x), \tag{109}$$

where $\{\beta_i : i = 1,2,\ldots,n\}$ is the set of weight coefficients, $K(\cdot,\cdot)$ denotes the kernel function and $\widetilde{K}(\cdot,\cdot)$ is the cross-kernel function which are related by:

$$K(x, z) = \int_0^z \widetilde{K}(x, \zeta)\mathrm{d}\zeta\,,\quad 0 \le x, z \le 1. \tag{110}$$

A variety of estimation algorithms for support vector (SV) regression are given in [87]. Here, the specific algorithm process of a generalized square loss SV regression with dictionary of kernels is given. Select a Gaussian cross-kernel function with variance $\sigma^2$:

$$\widetilde{K}(x, z) = \frac{1}{\sigma\sqrt{2\pi}}\exp\left[-\frac{(x - z)^2}{2\sigma^2}\right], \tag{111}$$

and given a dictionary composed by cross-kernels $\{\widetilde{K}_1(\cdot,\cdot), \widetilde{K}_2(\cdot,\cdot), \ldots, \widetilde{K}_\kappa(\cdot,\cdot)\}$ with $\kappa$ parameters $\{\sigma_1, \ldots, \sigma_\kappa\}$, the estimated PDF can be written as:

$$\hat{p}(x) = \sum_{i=1}^{l}\sum_{j=1}^{\kappa}\beta_i^j \widetilde{K}_j(x_i, x), \tag{112}$$

where $\beta_i^j (i = 1,2,\ldots,l; j = 1,2,\ldots,\kappa)$ are the weight coefficient which satisfy:

$$\sum_{i=1}^{l}\sum_{j=1}^{\kappa}\beta_i^j = 1, \beta_i^j \ge 0. \tag{113}$$

The optimization goal of the algorithm is [19]:

$$\begin{cases} \min\limits_{\{\beta_i^j, \xi_i\}}\left[\sum_{i=1}^{l}\xi_i^2 + C\sum_{i=1}^{l}\sum_{j=1}^{\kappa}\frac{\beta_i^j}{\sigma_j}\right] \\ \sum_{i=1}^{l}\sum_{j=1}^{\kappa}\beta_i^j K_j(x_i, x_r) + \xi_r = P_l(x_r),\ \ r = 1,\cdots,l \\ \sum_{i=1}^{l}\sum_{j=1}^{\kappa}\beta_i^j = 1 \\ \beta_i^j \ge 0,\ \ (i = 1,2,\cdots,l; j = 1,2,\cdots,\kappa) \end{cases}, \tag{114}$$

where $\{\xi_i : i = 1,2,\ldots,l\}$ is the relaxation vector, and $C$ is a given empirical parameter.

### *c) Neural networks*

Statistical modeling based on neural network methods are usually combined with applications such as image despeckling [32, 33, 90, 91], and image classification [18, 92], among other applications. Neural networks can be regarded as a non-linear model with a large number of parameters.

This approach had two stages of development: artificial neural networks (ANN), and deep neural networks. The ANN proposed in 1943 are shallow networks mainly comprised of two key steps: feature extraction, and classification [18]. They are limited by the choice of features and the computational burden. Deep neural networks [95], as proposed in 2006, built on a many-layer structure which can automatically extract the statistical features of images based on a large number of training samples and classify them [89].

As the most representative deep neural network, convolutional neural networks (CNN) [96] have achieved such good results in image processing that they became a research focus in recent years [97]. It is totally data-driven which is difficult to be analyzed from a physical perspective.

# 4 Model assessment and parameter estimation

We have already reviewed various statistical distributions based on different models, and every statistical distribution has its own applicable scenarios. The next step is choosing a model, and performing parameter estimation according to the specific application. This section will introduce several model assessment and parameter estimation methods.

The main statistical model assessment tests are based distances or divergences: $\chi^2$ [98, 99], Kolmogorov-Smirnov [99, 100], Kullback-Leibler (K-L) [101], and D' Agostino-Pearson [99], among others. The parameter estimation methods mainly include: Method of Moments (MoM) [98], Maximum Likelihood (ML) method [98], and Method of Logarithmic Cumulants (MoLC) [102]. Most of the model assessment and parameter estimation methods are classical methods which could be learned in specific references. Due to space limitations, they will not be described in detail here. In particular, we review the widely used MoLC method [22, 62, 103], and Table 4 summarizes the parameter estimation formulas of MoLC method for 10 amplitude distributions [30, 62, 83].

The MoLC method is a parameter estimation method based on the Mellin transform of the PDF, proposed by Nicolas et al. [102] in 2002. Compared with MoM, MoLC has higher parameter estimation accuracy [104].

The first characteristic function of the second kind is defined as the Mellin transform of a function $p(x)$ with the domain $R^+$ [105]:

$$\phi(s) = \mathrm{MT}[p(x)](s) = \int_0^\infty x^{s-1} p(x)\mathrm{d}x. \tag{115}$$

The second kind moments called log-moments, are the derivative of the first characteristic function of the second kind evaluated at $s = 1$. Such moments can be written in two ways by virtue of a fundamental property of the Mellin transform:

$$\tilde{m}_r = \left.\frac{\mathrm{d}^r \phi(s)}{\mathrm{d}s^r}\right|_{s=1} = \int_0^\infty (\ln x)^r p(x)\mathrm{d}x\ , \quad r = 1,2, \ldots. \tag{116}$$

For discrete cases, the log-moments can be written as:

$$\tilde{m}_r = \frac{1}{N}\sum_{i=1}^{N} (\ln x_i)^r\ , \quad r = 1,2, \ldots. \tag{117}$$

The second characteristic function of the second kind is defined as the natural logarithm of the first characteristic function of the second kind:

$$\xi(s) = \ln \phi(s). \tag{118}$$

The derivative of the second characteristic function of the second kind, evaluated at $s = 1$, defines second kind cumulants, called log-cumulants [102, 106]:

$$\tilde{k}_r = \left.\frac{\mathrm{d}^r \xi(s)}{\mathrm{d}s^r}\right|_{s=1}. \tag{119}$$

The relationships between the log-moments and log-cumulants and the first three log-cumulants can be written as:

$$\begin{aligned} \tilde{k}_r &= \tilde{m}_r - \sum_{i=1}^{r-1} \binom{r-1}{i-1} \tilde{k}_i \tilde{m}_{r-i}, \\ \tilde{k}_1 &= \tilde{m}_1, \\ \tilde{k}_2 &= \tilde{m}_2 - \tilde{m}_1^2, \\ \tilde{k}_3 &= \tilde{m}_3 - 3\tilde{m}_1\tilde{m}_2 + 2\tilde{m}_1^3. \end{aligned} \tag{120}$$

Given $N$ samples $x_i (i = 1,2, \ldots, N)$, the estimation of the log-cumulants of the first three orders is given by the solution of:

$$\begin{aligned} \hat{k}_1 &= \frac{1}{N}\sum_{i=1}^{N} [\ln x_i], \\ \hat{k}_2 &= \frac{1}{N}\sum_{i=1}^{N} \left[\left(\ln x_i - \hat{k}_1\right)^2\right], \\ \hat{k}_3 &= \frac{1}{N}\sum_{i=1}^{N} \left[\left(\ln x_i - \hat{k}_1\right)^3\right]. \end{aligned} \tag{121}$$

# 5 Conclusion

## 5.1 *Summary of single-pixel statistical modeling*

Table 5 summarizes all statistical distribution models reviewed in this paper in terms of the complexity, the physical meaning, the existence of analytical expression of the PDF, and the scope of application. Figure 12 presents the whole view of the relationships among different models. Figure 13 summarizes the relationship between the major statistical distributions. It shows that:

- except for the lognormal distribution, all the distributions shown here can be degenerated into Rayleigh distributions;
- the Fisher distribution and the $G$ distribution can be equivalently transformed;
- the K, $G^h$, $G^0$ distributions are special cases of $G$ distribution;
- the Gamma distribution could be degenerated from the K distribution, the generalized Gamma distribution or the $G^0$ distribution;
- the log-normal distribution and the Weibull distribution can be degenerated from the generalized Gamma distribution;
- the negative exponential distribution can be degenerated from either the Gamma distribution or the Weibull distribution;
- the Rice distribution is a special case of RiIG distribution;
- the GGR distribution can be degenerated from the GΓR distribution.

The parameter relationships of these distribution conversions and degenerations can be found in the previous sections.

## 5.2 *Outlook*

The statistical modeling of SAR images is an important means of extracting information from the data. Intended as a comprehensive reference for further development in the field, this paper reviews the development of the single-pixel statistical modeling of SAR image.

It categorized the most important models into two main types, i.e. the coherent scatterer model based on random walk model, and the empirical model. The coherent scatterer model describes the scattered field of a resolution cell as a coherent superposition of multiple scatterers. It is more physically plausible. Under different conditions, five types of statistical models can be developed based on the coherent scatterer model, i.e. the Rayleigh speckle model, the product model, the non-Rayleigh speckle model, the generalized central limit theorem model, and the incoherent scatterer sum model. Based on these five types of statistical models, we reviewed seventeen statistical distributions (see Figure 12). Empirical models can be divided into three types: single empirical distribution model, finite mixture statistical model and non-parametric statistical model. We recalled seven statistical distributions based on these models (see Figure 12). Empirical models are easy to apply, they do not involve specific scattering processes, but they are not physically explainable. The source code for the for the PDFs and plots is available at https://github.com/dxyue/StatisticalModeling.git .

The rapid development of radar system technologies lead to the emergence of new types of SAR images, including polarimetric SAR (PolSAR) [2], interferometric SAR [107], bistatic and multistatic constellation SAR [108-112] and quantum radar [113]. For example, the advanced non-interrupted synchronization scheme for spaceborne bistatic SAR in [108] demonstrates superiority over techniques of existing systems such as TanDEM-X and is promising in the future spaceborne bistatic and multistatic systems. Another example is quantum radar which may greatly enhance receiver sensitivity. These new types of SAR data have brought higher requirements and more opportunities to the task of image interpretation. For the outlook, five aspects are discussed as follows:

(1) To fit different scenarios and different users, various statistical models have been developed. However, they mainly come from the approximation or improvement of classical physical models. It is better to build these statistical models under a unified framework. The most suitable model can be selected for a specific scenario. It can also lower the threshold for beginners to understand the statistical modeling of SAR images. Therefore, a general statistical framework for SAR images stems as an important research topic. This paper provides an important reference for future study of a generalized statistical framework.

(2) Existing statistical modeling of SAR images is mainly for single-pixel statistical modeling, which is not sufficient for mining 2D image information. Two-pixel statistical features such as correlation functions can further describe SAR texture features. However, research on correlated textures is far less ubiquitous than single-pixel statistical modeling, and the existing texture representation models are either too complex or purely empirical. Therefore, simple but effective textures characterization is another important research direction.

(3) Existing statistical models of SAR images mainly describe the homogenous clutter texture, and do not involve the position or boundary of textures. However, actual SAR images are often composed of a variety of terrain surfaces with relatively clear boundaries. Therefore, further inclusion of boundaries of homogenous clutter texture to form a two-layer semantic map is also a valuable research topic.

(4) PolSAR images contain richer scene information compared with the single-channel SAR data [2]. The statistical analysis [114, 115] of PolSAR images plays an important role for its interpretation such as image segmentation [116, 117] and classification [118-122], change detection [123-128], target detection [129, 130] and despeckling [131-134]. Many statistical distributions for PolSAR data can be seen as an extension of single-channel statistical modeling reviewed in this paper. The scaled complex Wishart distribution is employed as a statistical model for homogeneous regions in PolSAR images [115]. And the product model has developed many statistical distributions to describe the nonhomogeneous regions in PolSAR images such as the polarimetric $G_P$ distribution, $K_P$ distribution, $G_P^0$ distribution, $U$ distribution and so on [114, 120]. The expansion from single-channel statistical modeling to polarimetric statistical modeling and the study of polarimetric statistical modeling will provide an important research foundation for the wide application of PolSAR images.

(5) Quantum technology [135] may bring change to both radar systems and image interpretation.

On the one hand, the development of quantum device in quantum radar [113] is based on the mechanisms of quantum physics. Quantum radar has been proved to have the potential to break the limit of conventional radar detection performance such as system sensitivity [136] and target detection capability [137]. Several quantum radar concepts such as quantum radar equation, quantum radar cross section (QRCS) and quantum detection theory have been researched recently [137-139]. Quantum entanglement is a quantum phenomenon where multiple particles are linked together in a way such that the measurement of one particle's quantum state determines the possible quantum states of the other particles [113]. It leads to correlations between observable physical properties of the systems [113, 136]. It has been shown the resolution of quantum radar systems using entangled photons is higher then that of non-entangled quantum radar [140]. As the further development of quantum radar theory and core techniques, the corresponding statistical modeling should be a studied.

On the other hand, the principles of quantum computing [135], such as uncertainty, superposition, interference and implicit parallelism, make it have better diversity and better trade-off between the exploration and the exploitation than common evolutionary algorithms [141]. These principles have inspired many evolutionary computing algorithms to solve the optimization problem in SAR image segmentation, such as quantum clonal selection clustering (QCSC) algorithm [142], quantum immune fast spectral clustering (QIFSC) approach [143] and quantum-inspired multiobjective evolutionary clustering (QMEC) algorithm [141]. These research results demonstrate the application value of quantum computing in the field of SAR image modeling and data processing.

# References

[1] C. Oliver, S. Quegan, "Understanding Synthetic Aperture Radar Images,"[M]. Raleigh,USA: SciTech Publishing, Inc., 2004.

[2] J. S. Lee, E. Pottier, "Polarimetric Radar Imaging: From Basics to Applications," Baton Rouge, United States.: CRC press-Taylor & Francis Group, 2009.

[3] J. A. Kong, "Electromagnetic Wave Theory,"[M]: Wiley-Interscience, 1990.

[4] H. Goldstein, "Sea echo,"[M]. New York: McGraw-Hill: Propagation of Short Radio Wave, 1951.

[5] K. D. Ward, R. J. A. Tough, S. Watts, "Sea clutter: Scattering, the K distribution and radar performance,"[M]. Stevenage, UK: IET, 2002.

[6] F. T. Ulaby, T. F. Haddock, R. T. Austin, "Fluctuation statistics of millimeter-wave scattering from distributed targets,"[J] IEEE Trans.geosci.remote Sensing, vol. 26, pp. 268-281, 1988.

[7] H. H. Arsenault, G. April, "Properties of speckle integrated with a finite aperture and logarithmically transformed,"[J] Journal of the Optical Society of America, vol. 66, pp. 1160-1163, 1976.

[8] F. Spitzer, "Principles of Random Walk,"[M]: World Publishing Co., 1964.

[9] E. Jakeman, P. N. Pusey, "A model for non-Rayleigh sea echo,"[J] IEEE Trans. Antennas Propagat., vol. 24, pp. 806-814, 1976.

[10] E. Jakeman, "On the statistics of K-distributed noise,"[J] J. Phys. A, Math. Gen., vol. 13, pp. 31--48, 1980.

[11] C. J. Oliver, "Correlated K-distributed Clutter Models,"[J] Optica Acta International Journal of Optics, vol. 32, pp. 1515-1547, 1985.
[12] C. J. Oliver, "A Model for Non-Rayleigh Scattering Statistics,"[J] Optica Acta International Journal of Optics, vol. 31, pp. 701-722, 1984.
[13] M. J. Collins, J. M. Allan, "Modeling and Simulation of SAR Image Texture,"[J] IEEE Transactions on Geoscience & Remote Sensing, vol. 47, pp. 3530-3546, 2009.
[14] K. D. Ward, "Compound representation of high resolution sea clutter,"[J] Electronics Letters, vol. 17, pp. 561-563, 1981.
[15] A. P. Blake, D. Blacknell, C. J. Oliver, "High resolution SAR clutter textural analysis,"[C], 1995, pp. 10/1-10/9.
[16] A. P. Blake, D. Blacknell, C. J. Oliver, "High-resolution SAR clutter textural analysis and simulation,"[J] Proceedings of SPIE - The International Society for Optical Engineering, pp. 101-109, 1995.
[17] P. E, "On estimation of a probability density function and mode,"[J] Ann. Math. Statis, vol. 33(3), pp. 1065-1076, 1962.
[18] L. Bruzzone, M. Marconcini, U. Wegmuller, A. Wiesmann, "An Advanced System for Automatic Classification of Multitemporal SAR Images,"[J] IEEE Transactions on Geoscience & Remote Sensing, vol. 42, pp. 1321-1334, 2004.
[19] P. Mantero, G. Moser, S. B. Serpico, "Partially supervised classification of remote sensing images using SVM-based probability density estimation,"[J] IEEE Transactions on Geoscience & Remote Sensing, vol. 43, pp. 559-570, 2005.
[20] E. E. Kuruoglu, J. Zerubia, "Modeling SAR images with a generalization of the Rayleigh distribution,"[J] IEEE Transactions on Image Processing A Publication of the IEEE Signal Processing Society, vol. 13, pp. 527-533, 2004.
[21] G. Moser, J. Zerubia, S. B. Serpico, "SAR amplitude probability density function estimation based on a generalized Gaussian model,"[M]: IEEE Press, 2006.
[22] H.-C. Li, W. Hong, Y.-R. Wu, P.-Z. Fan, "An Efficient and Flexible Statistical Model Based on Generalized Gamma Distribution for Amplitude SAR Images,"[J] IEEE Transactions on Geoscience & Remote Sensing, vol. 48(6), pp. 2711-2722, 2010.
[23] Y. Delignon, W. Pieczynski, "Modeling non-Rayleigh speckle distribution in SAR images,"[J] IEEE Trans.geosci.remote Sens, vol. 40, pp. 1430-1435, 2002.
[24] D.-X. Yue, F. Xu, A. C. Frery, Y.-Q. Jin, "SAR Image Statistical Modeling Part II：Spatial Correlation Model,"[J] IEEE Geoscience and Remote Sensing Magazine, submitted, 2020.
[25] J. W. Goodman, "Speckle Phenomena in Optics: Theory and Applications,"[M]: Ben Roberts & Company, 2007.
[26] G. Gui, "Statistical modeling of SAR images: a survey,"[J] Sensors, vol. 10, pp. 775-795, 2010.
[27] C. J. Oliver, R. J. A. Tough, "On the Simulation of Correlated K-distributed Random Clutter,"[J] Optica Acta International Journal of Optics, vol. 33, pp. 223-250, 1986.
[28] C. J. Oliver, "The interpretation and simulation of clutter textures in coherent images,"[J] Inverse Problems, vol. 2, p. 481, 1986.
[29] M. A. T. F. a. A. K. Jain, "Unsupervised learning of finite mixture models,"[J] IEEE Transactions on Pattern Analysis and Machine Intelligence, vol. 24, pp. 381-396, March 2002.
[30] G. Moser, J. Zerubia, S. B. Serpico, "Dictionary-based stochastic expectation-maximization for SAR amplitude probability density function estimation,"[J] IEEE Transactions on Geoscience & Remote Sensing, vol. 44, pp. 188-200, 2006.
[31] Z. Du, R. Liu, L. Nan, C. Peng, "A New Method for Ship Detection in SAR Imagery Based on Combinatorial PNN Model,"[C] in First International Conference on Intelligent Networks & Intelligent Systems, 2008.
[32] P. Wang, H. Zhang, V. M. Patel, "SAR Image Despeckling Using a Convolutional Neural Network,"[J] IEEE Signal Processing Letters, vol. 24, pp. 1763-1767, 2017.
[33] D. X. Yue, F. Xu, Y. Q. Jin, "SAR despeckling neural network with logarithmic convolutional product model,"[J] International Journal of Remote Sensing, vol. 39, pp. 1-23, 2018.
[34] F. T. Ulaby, D. G. Long, "Microwave Radar and Radiometric Remote Sensing,"[M]. United States of America: The University of Michigan Press, 2014.
[35] X. Deng, C. López-Martínez, E. M. Varona, "A Physical Analysis of Polarimetric SAR Data Statistical Models,"[J] IEEE Transactions on Geoscience and Remote Sensing, vol. 54, pp. 3035-3048, 2016.
[36] J. W. Goodman, "Statistical properties of laser speckle patterns,"[J] Laser Speckle & Related Phenomena, vol. 9, pp. 9-75, 1975.
[37] F. T. Ulaby, F. Kouyate, B. Brisco, T. H. L. Williams, "Textural Information in SAR Images,"[J] IEEE Trans.geosci.remote Sens, vol. 24, pp. 235-245, 1986.
[38] V. Anastassopoulos, G. A. Lampropoulos, "A generalized compound model for radar clutter,"[C] in IEEE National Radar Conference, 1994., 1994, pp. 41-45.
[39] V. Anastassopoulos, G. A. Lampropoulos, "High resolution radar clutter classification,"[C] in IEEE International Radar Conference, 1995. , 1995, pp. 662-667.
[40] V. Anastassopoulos, G. A. Lampropoulos, A. Drosopoulos, M. Rey, "High resolution radar clutter statistics,"[J] Aerospace & Electronic Systems IEEE Transactions on, vol. 35, pp. 43-60, 1999.
[41] A. C. Frery, H. J. Muller, C. D. C. F. Yanasse, S. J. S. Sant'Anna, "A model for extremely heterogeneous clutter,"[J] IEEE Transactions on Geoscience & Remote Sensing, vol. 35, pp. 648-659, 1997.
[42] M. Abramowitz, I. A. Stegun, J. E. Romain, "Handbook of Mathematical Functions, with Formulas, Graphs, and Mathematical Tables,"[M]: Dover Publications, 1970.
[43] N. L. Johnson, S. Kotz, "Distributions in Statistics: Discrete Distributions,"[J] American Sociological Review, 1971.
[44] N. L. Johnson, S. Kotz, "Distributions in statistics. Continuous univariate distributions. I,"[M]: New York: Wiley, 1969.
[45] A. C. Frery, H. J. Muller, C. C. F. Yanasse, S. J. S. Sant'Anna, "A model for extremely heterogeneous clutter,"[J] IEEE Transactions on Geoscience & Remote Sensing, vol. 35, pp. 648-659, 1997.
[46] B. Jørgensen, "Statistical properties of the generalized inverse Gaussian distribution,"[J] vol. 80, pp. 1998-2005, 1982.
[47] H. J. Muller, R. Pac, "G-statistics for scaled SAR data,"[C] in IEEE Geoscience and Remote Sensing Symposium, 1999, pp. 1297-1299.
[48] A. C. Frery, J. Jacobo-Berlles, J. Gambini, M. Mejail, "Polarimetric SAR Image Segmentation with B-Splines and a New Statistical Model,"[J] Multidimensional Systems and Signal Processing, vol. 21, pp. 319--342, 2010.
[49] M. Tur, K. C. Chin, J. W. Goodman, "When is speckle noise multiplicative?,"[J] Applied Optics, vol. 21, p. 1157, 1982.
[50] G. Gui, Z. Jun, L. Xin-ming, Z. Die-fei, H. Ji-jun, J. Yong-mei, "Analysis of Multiplicative Noise Models in SAR Imagery,"[J] Signal Processing, pp. 1-167, 2008.
[51] T. Eltoft, "The Rician inverse Gaussian distribution: a new model for non-Rayleigh signal amplitude statistics,"[J] IEEE Transactions on Image Processing A Publication of the IEEE Signal Processing Society, vol. 14, pp. 1722-1735, 2005.
[52] D.-X. Yue, F. Xu, A. C. Frery, Y.-Q. Jin, "A generalized Gaussian coherent scatterer model for correlated SAR texture,"[J] IEEE Trans. Geosci. Remote Sensing, 2019.
[53] E. Jakeman, "K-distributed noise,"[J] Journal of Optics A Pure & Applied Optics, vol. 1, p. 784, 1999.
[54] E. Jakeman, R. J. A. Tough, "Generalized K distribution: a statistical model for weak scattering,"[J] Journal of the Optical Society of America A, vol. 4, pp. 1764-1772, 1987.
[55] S. O. Rice, "Mathematical analysis of random noise,"[J] The Bell System Technical Journal, vol. 23, pp. 282-332, 1944.
[56] [Z. X. Wang, D. R. Guo, "Special functions,"[M]: Singapore World Scientific Publishing, 1989.
[57] G. E. Andrews, R. Askey, R. Roy, "Special functions,"[J] Nature, vol. 221, pp. 99-103, 2006.
[58] F. W. Olver, D. W. Lozier, R. F. Boisvert, C. W. Clark, "NIST Handbook of Mathematical Functions,"[M]: Cambridge University Press, 2010.
[59] A. Papoulis, H. Saunders, "Probability, Random Variables and Stochastic Processes (2nd Edition),"[J] Journal of Vibration & Acoustics, vol. 111, 1989.
[60] [60] Z. Tao, W. Jia, "Overview of α-stable Distribution,"[J] Audio Engineering, 2011.
[61] [61] ChrysostomosL, "Signal processing with alpha-stable distributions and applications,"[M]: John Wiley & Sons,Inc, 1995.

[62] H.-C. Li, W. Hong, Y.-R. Wu, P.-Z. Fan, "On the Empirical-Statistical Modeling of SAR Images With Generalized Gamma Distribution,"[J] IEEE Journal of Selected Topics in Signal Processing, vol. 5, pp. 386-397, 2011.
[63] E. Jakeman, "Statistics of Integrated Gamma-lorentzian Intensity Fluctuations,"[J] Optica Acta International Journal of Optics, vol. 27, pp. 735-741, 1980.
[64] S. F. George, "The Detection of Nonfluctuating Targets in Log-Normal Clutter,"[J] 1968.
[65] A. Farina, A. Russo, F. A. Studer, "Coherent radar detection in log-normal clutter,"[J] Communications Radar & Signal Processing Iee Proceedings F, vol. 133, pp. 39-53, 1986.
[66] G. V. Trunk, "Radar Properties of Non-Rayleigh Sea Clutter,"[J] IEEE Transactions on Aerospace & Electronic Systems, vol. AES-8, pp. 196-204, 1972.
[67] M. Sekine, S. Ohtani, T. Musha, T. Irabu, E. Kiuchi, T. Hagisawa, Y. Tomita, "Weibull-Distributed Ground Clutter,"[J] IEEE Transactions on Aerospace & Electronic Systems, vol. AES-17, pp. 596-598, 2007.
[68] M. Sekine, T. Musha, Y. Tomita, T. Hagisawa, T. Irabu, E. Kiuchi, "On Weibull-Distributed Weather Clutter,"[J] IEEE Transactions on Aerospace & Electronic Systems, vol. AES-15, pp. 824-830, 1979.
[69] D. C. Schleher, "Radar Detection in Weibull Clutter,"[J] IEEE Transactions on Aerospace & Electronic Systems, vol. AES-12, pp. 736-743, 1976.
[70] C. Tison, J. M. Nicolas, F. Tupin, H. Maître, "A new statistical model for Markovian classification of Urban areas in high-Resolution SAR images,"[J] Geoscience & Remote Sensing IEEE Transactions on, vol. 42, pp. 2046-2057, 2004.
[71] E. W. Stacy, "A Generalization of the Gamma Distribution,"[J] Annals of Mathematical Statistics, vol. 33, pp. 1187-1192, 1962.
[72] E. W. S. a. G. A. Mihram, "Parameter estimation for a generalized gamma distribution,"[J] Technometrics, vol. 7, pp. 349–358, 1965.
[73] G. J. McLachlan, D. Peel, NetLibrary, "Finite mixture models,"[M]. Wiley series in probability and statistics. Applied probability and statistics section New York : Wiley, 2000
[74] B. C, "Assessing a mixture model for clustering with the integrated completed like-lihood,"[J] IEEE Trans. Pattern Anal. Machine Intell, vol. 22(7), pp. 719-725, 2000.
[75] R. A. Redner, H. F. Walker, "Mixture densities, maximum likelihood and the EM algorithm. SIAM Rev,"[J] Siam Review, vol. 26, pp. 195-239, 1984.
[76] B. Nizar, "Count data modeling and classification using finite mixtures of distributions,"[J] IEEE Transactions on Neural Networks, vol. 22, pp. 186-198, 2011.
[77] B. Nizar, Z. Djemel, "High-dimensional unsupervised selection and estimation of a finite generalized Dirichlet mixture model based on minimum message length,"[J] IEEE Transactions on Pattern Analysis & Machine Intelligence, vol. 29, p. 1716, 2007.
[78] D. Y, M. A, P. W, "Estimation of Generalized Mixtures and Its Application in Image Segmentation,"[J] IEEE Transactions on Image Processing, vol. 6(10), pp. 1364-1375, 1997.
[79] N. Greggio, A. Bernardino, C. Laschi, P. Dario, J. Santosvictor, "Unsupervised Greedy Learning of Finite Mixture Models,"[C] in IEEE International Conference on Tools with Artificial Intelligence, 2010.
[80] L. R. Acharya, D. Zhu, "Estimating an Optimal Correlation Structure from Replicated Molecular Profiling Data Using Finite Mixture Models,"[C] in International Conference on Machine Learning & Applications, 2009.
[81] D. A. Landgrebe, "Signal Theory Methods in Multispectral Remote Sensing,"[M]. New York: Wiley, 2003.
[82] G. Moser, J. Zerubia, S. B. Serpico, "Dictionary-Based Stochastic Expectation–Maximization for SAR Amplitude Probability Density Function Estimation,"[J] IEEE Transactions on Geoscience & Remote Sensing, vol. 44, pp. 188-200, 2006.
[83] V. A. Krylov, G. Moser, S. B. Serpico, J. Zerubia, "Enhanced Dictionary-Based SAR Amplitude Distribution Estimation and Its Validation With Very High-Resolution Data,"[J] IEEE Geoscience & Remote Sensing Letters, vol. 8, pp. 148-152, 2011.
[84] D. Blacknell, "Mixture distribution model for correlated SAR clutter,"[J] Proceedings of SPIE - The International Society for Optical Engineering, vol. 2958, pp. 38-49, 1996.
[85] D. Blacknell, "Target detection in correlated SAR clutter,"[J] IEE Proceedings - Radar, Sonar and Navigation, vol. 147, pp. 9-16, 2000.
[86] R. O. Duda, P. E. Hart, D. G. Stork, "Pattern classification,"[M]: Wiley: New York,NY,USA, 2001.
[87] J. Weston, A. Gammerman, M. O. Stitson, V. Vapnik, V. Vovk, C. Watkins, "Support Vector Density Estimation,"[J] Advances in Kernel Methods, 1999.
[88] C. M. Bishop, "Neural Networks for Pattern Recognition,"[M] 2nd ed.: Oxford University Press: Oxford,UK, 1996.
[89] Y. Lecun, L. Bottou, Y. Bengio, P. Haffner, "Gradient-based learning applied to document recognition,"[J] Proceedings of the IEEE, vol. 86, pp. 2278-2324, 1998.
[90] G. Chierchia, D. Cozzolino, G. Poggi, L. Verdoliva, "SAR image despeckling through convolutional neural networks,"[J] 2017.
[91] Z. Qiang, Q. Yuan, L. Jie, Y. Zhen, L. Zhang, "Learning a Dilated Residual Network for SAR Image Despeckling,"[J] Remote Sensing, vol. 10, pp. 1-18, 2018.
[92] P. Mantero, G. Moser, S. B. Serpico, "Partially supervised classification of remote sensing images using SVM-based probability density estimation,"[C] in IEEE Workshop on Advances in Techniques for Analysis of Remotely Sensed Data, 2003.
[93] J. Q, "Ship detection in RADARSAT SAR imageryusingPNN-model," in Proceedings of ADRO Symposium'98 Montreal,Canada, 1998.
[94] X. Y. Hou, W. Ao, Q. Song, J. Lai, H. P. Wang, F. Xu, "FUSAR-Ship: building a high-resolution SAR-AIS matchup dataset of Gaofen-3 for ship detection and recognition,"[J] Sci China Inf Sci, vol. 63, p. 140303, 2020.
[95] Y. Lecun, Y. Bengio, G. Hinton, "Deep learning,"[J] Nature, vol. 521, pp. 436-444, 2015.
[96] A. Krizhevsky, I. Sutskever, G. E. Hinton, "ImageNet classification with deep convolutional neural networks,"[C] in International Conference on Neural Information Processing Systems, 2012, pp. 1097-1105.
[97] F. Xu, C. Hu, J. Li, A. Plaza, M. Datcu, "Special focus on deep learning in remote sensing image processing,"[J] Sci China Inf Sci, vol. 63, p. 140300, 2020.
[98] A. Papoulis, S. U. Pillai, "Probability, Random Variables, and Stochastic Processes, Fourth Edition,"[M]. New York, USA: McGraw-Hill Education, 2002.
[99] M. D. Devore, J. A. O'Sullivan, "Quantitative statistical assessment of conditional models for synthetic aperture radar,"[J] IEEE Transactions on Image Processing A Publication of the IEEE Signal Processing Society, vol. 13, pp. 113-25, 2004.
[100] M. D. Devore, J. A. O'Sullivan, "Statistical assessment of model fit for synthetic aperture radar data,"[J] Proceedings of SPIE - The International Society for Optical Engineering, pp. 379-388, 2001.
[101] S. Kullback, " Information Theory and Statistics,"[M]: Dover Publications, 1959.
[102] J. M. Nicolas, "Introduction to second kind statistics: application of Log-moments and Log-cumulants to SAR image law analysis,"[J] Traitement Du Signal, vol. 19, pp. 139-167, 2002.
[103] X. Deng, C. López-Martínez, "Higher Order Statistics for Texture Analysis and Physical Interpretation of Polarimetric SAR Data,"[J] IEEE Geoscience & Remote Sensing Letters, vol. 13, pp. 912-916, 2016.
[104] V. A. Krylov, M. Gabriele, S. B. Serpico, Z. Josiane, "On the method of logarithmic cumulants for parametric probability density function estimation,"[J] IEEE Trans Image Process, vol. 22, pp. 3791-3806, 2013.
[105] F. Oberhettinger, "Tables of Mellin transforms,"[M]: Springer, Berlin, Heidelberg, 1974.
[106] G.-T. Shi, L.-J. Zhao, J. Lu, Y.-M. Yong, G.-Y. Kuang, "A Novel Parameter Estimation Method for the K Distribution Based on the Mellin Transform,"[J] ACTA ELECTRONICA SINICA, vol. 38, pp. 2083-2089, 2010.
[107] S. R. Cloude, K. P. Papathanassiou, "Polarimetric SAR interferometry,"[J] IEEE Transactions on Geoscience and Remote Sensing, vol. 36, pp. 1551-1565, 1998.
[108] D. Liang, K. Liu, H. Yue, Y. Chen, Y. Deng, H. Zhang, G. J. C. Li, R. Wang, "An Advanced Non-Interrupted Synchronization Scheme for Bistatic Synthetic Aperture Radar," in 2019 IEEE International Geoscience and Remote Sensing Symposium Yokohama, Japan, 2019, pp. 1116-1119.

[109] H. Zhang, Y. Deng, R. Wang, N. Li, S. Zhao, F. Hong, L. Wu, O. Lofeld, "Spaceborne/Stationary Bistatic SAR Imaging With TerraSAR-X as an Illuminator in Staring-Spotlight Mode,"[J] IEEE Transactions on Geoscience and Remote Sensing, vol. 54, pp. 5203-5216, 2016.

[110] M. Zhang, R. Wang, Y. Deng, L. Wu, Z. Zhang, H. Zhang, N. Li, Y. Liu, X. Luo, "A Synchronization Algorithm for Spaceborne/Stationary BiSAR Imaging Based on Contrast Optimization With Direct Signal From Radar Satellite,"[J] IEEE Transactions on Geoscience and Remote Sensing, vol. 54, pp. 1977-1989, 2016.

[111] R. Wang, W. Wang, Y. Shao, F. Hong, P. Wang, Y. Deng, Z. Zhang, O. Loffeld, "First Bistatic Demonstration of Digital Beamforming in Elevation With TerraSAR-X as an Illuminator,"[J] IEEE Transactions on Geoscience and Remote Sensing, vol. 54, pp. 842-849, 2016.

[112] Z. Li, Z. Bao, H. Wang, G. Liao, "Performance improvement for constellation SAR using signal processing techniques,"[J] IEEE Transactions on Aerospace and Electronic Systems, vol. 42, pp. 436-452, 2006.

[113] M. Lanzagorta, "Quantum Radar,"[M]: Morgan & Claypool, 2011.

[114] X. Deng, C. López-Martínez, J. Chen, P. Han, "Statistical modeling of polarimetric SAR data: A survey and challenges,"[J] Remote Sensing, vol. 9, p. 348, 2017.

[115] A. C. Frery, R. J. Cintra, A. D. C. Nascimento, "Entropy-based Statistical Analysis of PolSAR Data,"[J] IEEE Transactions on Geoscience & Remote Sensing, vol. 51, pp. 3733-3743, 2012.

[116] F. Lang, J. Yang, D. Li, L. Zhao, L. Shi, "Polarimetric SAR image segmentation using statistical region merging,"[J] IEEE geoscience and remote sensing letters, vol. 11, pp. 509-513, 2013.

[117] N. Bouhlel, S. Méric, "Unsupervised Segmentation of Multilook Polarimetric Synthetic Aperture Radar Images,"[J] IEEE Transactions on Geoscience and Remote Sensing, vol. 57, pp. 6104-6118, 2019.

[118] S.-W. Chen, C.-S. Tao, "PolSAR image classification using polarimetric-feature-driven deep convolutional neural network,"[J] IEEE Geoscience and Remote Sensing Letters, vol. 15, pp. 627-631, 2018.

[119] A. Masjedi, M. J. V. Zoej, Y. Maghsoudi, "Classification of polarimetric SAR images based on modeling contextual information and using texture features,"[J] IEEE Transactions on Geoscience and Remote Sensing, vol. 54, pp. 932-943, 2015.

[120] W. B. Silva, C. C. Freitas, S. J. Sant'Anna, A. C. Frery, "Classification of segments in PolSAR imagery by minimum stochastic distances between Wishart distributions,"[J] IEEE Journal of Selected Topics in Applied Earth Observations and Remote Sensing, vol. 6, pp. 1263-1273, 2013.

[121] N. Anfinsen, A. P. Doulgeris, T. Eltoft, "Goodness-of-Fit Tests for Multilook Polarimetric Radar Data Based on the Mellin Transform,"[J] IEEE Transactions on Geoscience and Remote Sensing, vol. 49, pp. 2764-2781, 2011.

[122] F. Biondi, "Multi-chromatic analysis polarimetric interferometric synthetic aperture radar (MCA-PolInSAR) for urban classification,"[J] International journal of remote sensing, vol. 40, pp. 3721-3750, 2019.

[123] V. Akbari, S. N. Anfinsen, A. P. Doulgeris, G. M. T. Eltoft, S. B. Serpico, "Polarimetric SAR Change Detection With the Complex Hotelling–Lawley Trace Statistic,"[J] IEEE Transactions on Geoscience and Remote Sensing, vol. 54, pp. 3953-3966, 2016.

[124] J. Prendes, M. Chabert, F. Pascal, A. Giros, J.-Y. Tourneret, "A new multivariate statistical model for change detection in images acquired by homogeneous and heterogeneous sensors,"[J] IEEE Transactions on Image Processing, vol. 24, pp. 799-812, 2014.

[125] N. Bouhlel, S. Méric, "Multilook Polarimetric SAR Change Detection Using Stochastic Distances Between Matrix-Variate $Gd^0$ Distributions,"[J] IEEE Transactions on Geoscience and Remote Sensing, 2020.

[126] T. Liu, Z. Yang, A. Marino, G. Gao, J. Yang, "Robust CFAR Detector Based on Truncated Statistics for Polarimetric Synthetic Aperture Radar,"[J] IEEE Transactions on Geoscience and Remote Sensing, 2020.

[127] A. D. Nascimento, A. C. Frery, R. J. Cintra, "Detecting changes in fully polarimetric SAR imagery with statistical information theory,"[J] IEEE Transactions on Geoscience and Remote Sensing, vol. 57, pp. 1380-1392, 2018.

[128] W. Yang, X. Yang, T. Yan, H. Song, G.-S. Xia, "Region-based change detection for polarimetric SAR images using Wishart mixture models,"[J] IEEE Transactions on Geoscience and Remote Sensing, vol. 54, pp. 6746-6756, 2016.

[129] A. Marino, I. Hajnsek, "Statistical Tests for a Ship Detector Based on the Polarimetric Notch Filter,"[J] IEEE Transactions on Geoscience and Remote Sensing, vol. 53, pp. 4578-4595, 2015.

[130] D. Tao, A. P. Doulgeris, C. Brekke, "A Segmentation-Based CFAR Detection Algorithm Using Truncated Statistics,"[J] IEEE Transactions on Geoscience and Remote Sensing, vol. 54, pp. 2887-2898, 2016.

[131] P. A. A. Penna, N. D. A. Mascarenhas, "SAR Speckle Nonlocal Filtering With Statistical Modeling of Haar Wavelet Coefficients and Stochastic Distances,"[J] IEEE Transactions on Geoscience and Remote Sensing, vol. 57, pp. 7194-7208, 2019.

[132] L. Torres, S. J. S. Sant'Anna, C. C. Freitas, A. C. Frery, "Speckle Reduction in Polarimetric SAR Imagery with Stochastic Distances and Nonlocal Means,"[J] Pattern Recognition, vol. 47, pp. 141--157, 2014.

[133] J.-S. Lee, T. L. Ainsworth, Y. Wang, K.-S. Chen, "Polarimetric SAR Speckle Filtering and the Extended Sigma Filter,"[J] Transactions on Geoscience and Remote Sensing, vol. 53, pp. 1150--1160, 2015.

[134] H. Zhong, J. Zhang, G. Liu, "Robust Polarimetric SAR Despeckling Based on Nonlocal Means and Distributed Lee Filter,"[J] IEEE Transactions on Geoscience and Remote Sensing, vol. 52, pp. 4198 - 4210 2014.

[135] M. A. Nielsen, I. L. Chuang, "Quantum Computation and Quantum Information: 10th Anniversary Edition,"[M], 2011.

[136] P. Lin, Z. Yu, C. Li, "Review and forecast of quantum radar,"[C] in 2013 Asia-Pacific Conference on Synthetic Aperture Radar (APSAR), Tsukuba, 2013, pp. 432-433.

[137] K. Liu, H. Xiao, H. Fan, Q. Fu, "Analysis of Quantum Radar Cross Section and Its Influence on Target Detection Performance,"[J] IEEE Photonics Technology Letters, vol. 26, pp. 1146-1149, 2014.

[138] C. Fang, "The Simulation and Analysis of Quantum Radar Cross Section for Three-Dimensional Convex Targets,"[J] IEEE Photonics Journal, vol. 10, pp. 1-8, 2018.

[139] S. Zhao, "Quantum detection theory and optimum strategy in quantum radar system,"[J] The Journal of Engineering, vol. 11, pp. 7428-7431, 2019.

[140] S. Lloyd, "Enhanced Sensitivity of Photodetection via Quantum Illumination,"[J] Science, vol. 321, pp. 1463-1465, 2008.

[141] Y. Li, S. Feng, X. Zhang, L. Jiao, "SAR image segmentation based on quantum-inspired multiobjective evolutionary clustering algorithm,"[J] Information Processing Letters, vol. 114, pp. 287-293, 2014.

[142] S. Gou, X. Zhuang, L. Jiao, "SAR image segmentation using quantum clonal selection clustering," in Asian-Pacific Conference on Synthetic Aperture Radar Xian, Shanxi, 2009, pp. 817-820.

[143] S. P. Gou, X. Zhuang, L. C. Jiao, "Quantum Immune Fast Spectral Clustering for SAR Image Segmentation,"[J] IEEE Geoscience and Remote Sensing Letters, vol. 9, pp. 8-12, 2012.